A MOLECULAR COMMUNICATION FRAMEWORK FOR MODELING TARGETED DRUG DELIVERY SYSTEMS

A Dissertation
Presented to
The Academic Faculty

By

Youssef Chahibi

In Partial Fulfillment
of the Requirements for the Degree
Doctor of Philosophy
in
Electrical and Computer Engineering

School of Electrical and Computer Engineering
Georgia Institute of Technology
August 2016

A MOLECULAR COMMUNICATION FRAMEWORK FOR MODELING TARGETED DRUG DELIVERY SYSTEMS

Approved by:

Dr. Ian F. Akyildiz, Advisor
Key Byers Chair Professor in Telecommunications, School of ECE
Georgia Institute of Technology

Dr. Mary Ann Weitnauer
Professor, School of Electrical and Computer Engineering
Georgia Institute of Technology

Dr. Raghupathy Sivakumar
Wayne J. Holman Chair Professor in Telecommunications
Georgia Institute of Technology

Dr. Massimiliano Pierobon
Assistant Professor, Department of Computer Science & Engineering
University of Nebraska-Lincoln

Dr. Geoffrey Y. Li
Professor, School of Electrical and Computer Engineering
Georgia Institute of Technology

Date Approved: July 25, 2016

To my grandfather, for being my role model and source of inspiration.

ACKNOWLEDGMENTS

I am extremely grateful to Prof. Ian F. Akyildiz for helping me define my thesis objectives with groundbreaking ideas. His visionary insights, inspiring decisiveness, and continuous support have been essential to complete this piece of work. Prof. Ian F. Akyildiz has been present in every critical moment I have experienced during my Ph. D to instill more energy in me.

I am also deeply indebted to the Georgia Tech School of ECE, School of Biology, School of Biomedical Engineering and others, for their unique approaches to shape the future of cross-disciplinary research for future biomedial applications. I would also like to thank my mentor at the Broadband Wireless Networking Laboratory, Massimiliano Pierobon, for sharing his expertise, thorough guidance, and unceasing encouragement. I would also like to extend my thanks to international collaborators, Yevgeni Koucheryavy and Sasitharan Balasubramaniam at the Nano Communications Center in Tampere University of Technology, Finland, as well as Ilangko Balasingham at the Oslo University Hospital and Norwegian University of Science and Technology, Norway, for the valuable exchanges of know-how in their respective disciplines. I sincerely thank Prof. Sivakumar Raghupathy, Prof. Geoffrey Ye Li, Prof. Mary Ann Weitnauer, and Prof. Massimiliano Pierobon for serving in my Ph. D Defense committee.

I deeply appreciate the sponsorship of the Samsung Advanced Institute of Technology, Academy of Finland and the Research Council of Norway for providing material support and encouraging the dissemination of my work.

I would like to thank all the members of Broadband Wireless Networking Laboratory for the active atmosphere they create, my girlfriend for her boundless love and support, my family, and closest friends, without whom, none of this would have been possible.

TABLE OF CONTENTS

LIST OF TABLES

LIST OF FIGURES

SUMMARY

The goal of a *Drug Delivery System (DDS)* is to provide a localized drug presence where the medication is needed, while, at the same time, preventing the drug from affecting other healthy parts of the body. Amongst others, the most advanced solutions use drugs composed of nano-sized particles for *Particulate Drug Delivery Systems (PDDS)* or antibody fragments for *Antibody-mediated Drug Delivery Systems (ADDS). Molecular Communication (MC)* is a new paradigm in communication research where the exchange of information is achieved through the propagation of molecules.

The objective of the proposed research is to develop an analytical framework for the modeling, performance analysis, and optimization of DDS through the MC paradigm. First, a fundamental analytical model of the drug particle propagation through the cardiovascular system is presented, comprised of the blood velocity network, using transmission line theory, and the drug propagation network, using harmonic matrices theory. The outcomes of the analytical model are validated by comparing them with physiological measurements as well as comprehensive simulations of drug propagation in the cardiovascular system using COMSOL finite-element simulation and kinetic Monte-Carlo simulations. Second, the MC-PDDS model is developed to take into account the biochemical interactions between the nanoparticles and the body. The performance and optimization of the MC-PDDS is studied through delay, path loss, noise, and capacity. Third, the MC-ADDS model is derived to capture the peculiarities of antibody-antigen transport and interactions. The effect of the shape and electrochemical structure of the ADDS molecules is reflected on the delay, path loss, and noise. The MC-DDS system modeling is shown to be a full-fledged and novel framework for the design and optimization of targeted DDS.

CHAPTER 1

INTRODUCTION

Targeted *Drug Delivery Systems (DDS)* are nowadays under intensive study as they are at the cutting edge of modern medical therapeutics [1]. In particular, the goal of DDS is to provide a localized drug presence where the medication is needed, while, at the same time, preventing the drug from affecting other healthy parts of the body. For this, the design of a DDS involves the joint optimization of the drug chemical behavior and the transport process from the point where the drug enters the body until reaching the targeted site.

In a DDS, the drug must be efficiently delivered in the desired concentrations where it is needed. The understanding of how the drug molecules diffuse in the body and the evolution of their distribution over time is of primary importance for the design of a DDS. The delivery of drug molecules can be viewed as a communication mechanism, where the drug molecules are information carriers, which propagate messages (drug chemical properties) from the location of transmission (intravascular injection) until the location of reception (targeted site). We advocate for the Molecular Communication (MC) paradigm [2] as a straightforward and efficient abstraction of DDS.

The *Molecular Communication (MC)* paradigm abstracts the propagation of information between a sender and a receiver realized through mass transport phenomena, since information-bearing molecules have to physically cover the distance from one location to the other. MC is increasingly attracting the interest of the research community working in the field of nanonetworking [2]. MC is a bio-inspired paradigm that, amongst others, has been developed by nature for communication among living organisms, such as cells for intracellular and intercellular signaling [3]. In MC, information is exchanged by the release, the propagation and the reception of molecules.

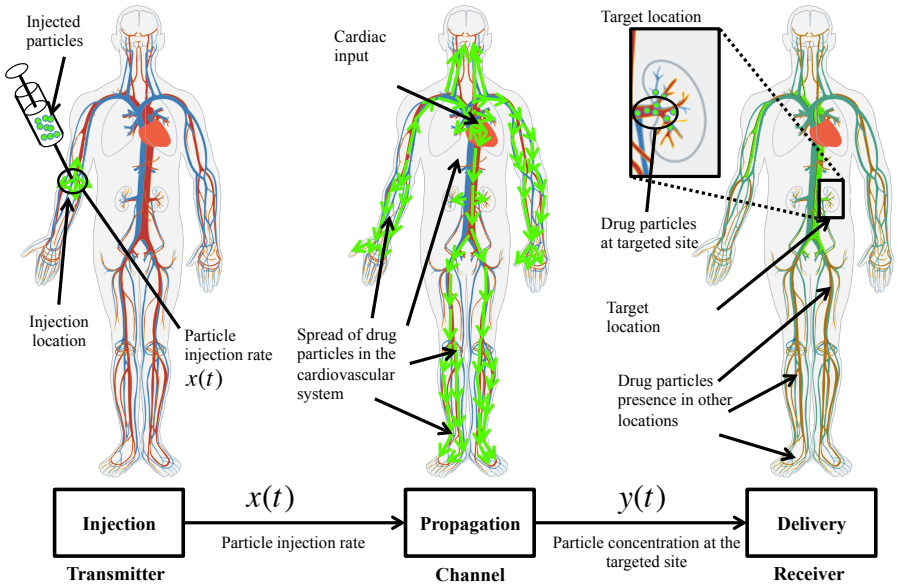

Figure 1. Molecular communication abstraction of PDDS.

1.1 Particulate Drug Delivery Systems

The study of a *Particulate Drug Delivery System (PDDS)* is especially suited to the MC abstraction. As shown in Figure 1, PDDS takes advantage of the blood distribution network for the propagation of drug particles from a location where they are injected into the blood flow to a targeted site within the reach of the cardiovascular system. The cardiovascular system is an intricate network of vessels which distribute the blood throughout the body, while the blood flow is generated by rhythmic contractions of the heart. In particular, the mass transport phenomena operated by the cardiovascular system for the propagation of the drug particles are two, namely, diffusion and advection. As a result of *diffusion*, the drug particles in suspension in the blood are subject to the Brownian motion spread from a region of higher concentration to a region of lower concentration. As a result of *advection*, the drug particles are subject to translation by the blood flow in the vessels of the cardiovascular system. The combination of these two phenomena can be interpreted and modeled as an MC channel. This abstraction should comprise a complete analytical model of the drug particle propagation through the cardiovascular system. The interactions of nanoparticles

with the blood, their adhesion and absorption by tissues and biological fluids, should be reflected by the model with greater accuracy than existing multi-compartmental models [4]. Also, the time-varying characteristics of the blood flow, which significantly affect the drug propagation, should be considered in the new MC model. The effect of the noise and the capacity of the MC model of DDS could be studied to evaluate the performance of DDS from a communication point of view. The MC paradigm has the potential to provide a highly precise, realistic, and flexible framework for the design and optimization of PDDS.

1.2 Antibody-mediated Drug Delivery Systems

Antibody-mediated Drug Delivery Systems (ADDS) are one of the most advanced therapeutic methods [5]. ADDS uses artificial molecules that are constructed from biological materials to build and engineer drug delivery systems. They are inspired by the naturally occurring autoimmune mechanisms that enable the human body to diagnose itself and destroy the exact source of the disease, in an adaptive and constructive fashion. The versatility in engineering ADDS and their attested clinical success open up the possibility to develop sophisticated therapeutic strategies to effectively target diseases. As shown in Figure 2, the drug injection of the antibody molecules propagates and diffuses through the network of blood vessels, where they are also transported through the tissue. Upon entering the tissue, the antibodies specifically bind to the diseased cells because they express unique antigens not found in healthy cells and match to the antibody. The binding triggers a therapeutic effect to the cells through a special case of the ligand-binding process, called the antibody-antigen mechanism. The MC-ADDS modeling could provide a clearer understanding of the mode of operation of antibodies, and enable the development of innovative methods to guide the engineering of verifiable and safe antibody mediated therapies. This includes the design and engineering of the drug structure, mode of administration, and dosage optimization [6].

We propose to use the MC paradigm to model the ADDS while taking into account

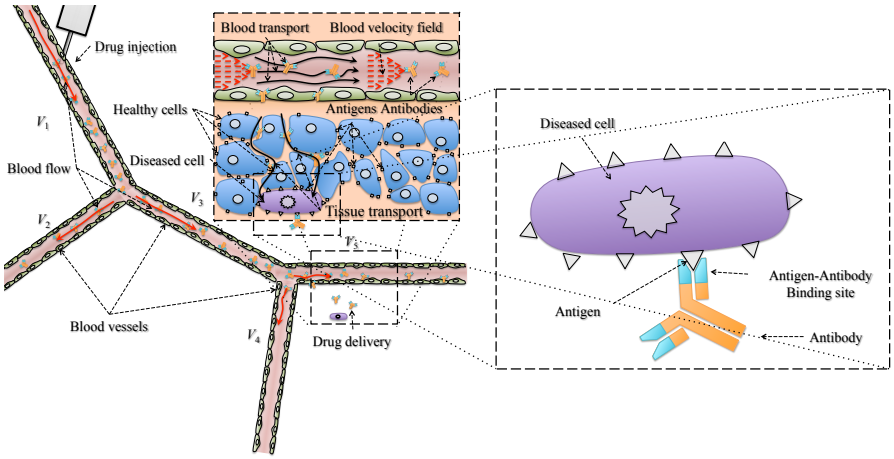

Figure 2. Molecular communication abstraction of ADDS.

the unique features of the antibodies and the new possibilities that are offered through them. Based on the sequential stages of antigen delivery to the target diseased cells, certain aspects of the MC modeling for PDDS are similar to ADDS. However, the transport and mechanism of action of ADDS is more complex and advanced than PDDS because of the complexity in the shape and biochemistry of the antibody and the antigen. In fact, the efficiency of the ADDS depends on the shape, electric charges, and the ability of the ADDS molecule to recognize the target antigen. In PDDS, the degrees of freedom in designing the nanoparticle are limited in terms of shape and surface chemistry due to their size, while in ADDS, the antibody-antigen recognition mechanism allows for more specific targeting of the diseased cells by allowing the design of ADDS molecules to bind exactly to a certain biomolecule. Also, the diffusion parameters of the ADDS molecules in the blood and through tissues depend significantly on their shape.

MC-ADDS opens up the possibility to optimize the properties of the ADDS to achieve a desired therapeutic effect, by determining the personalized optimal injection pattern in terms of frequency, concentration level, and mode of administration, thus maximizing the safety and success of ADDS and minimizing the costs [7]. The second motivation behind the use of MC-ADDS modeling, is to understand the physicochemical interactions between

ADDS and the body, which are more complex than in PDDS. For example, ADDS undergo electrostatic forces within the *Extracellular Matrix* (ECM) due to negatively charged proteins [8]. These electric forces significantly affect the intercellular transport, antigen binding, and the absorption of the ADDS by the cells.

1.3 Organization of the Thesis

The thesis focuses on developing an analytical framework for the modeling, performance analysis, and optimization of DDS through the MC paradigm. The selection of the MC paradigm is motivated by a literature survey, contained in Chapter 2, which identifies the state-of-the-art in modeling DDS from the biomedical engineering field and reviews the different MC modeling approaches initiated from the communication field that are translatable to DDS. Chapter 3 presents as system model of particulate drug delivery systems based on molecular communication. Chapter 4 contains the molecular communication analysis of noise and information theoretical capacity in a particulate drug delivery systems. In Chapter 5, the molecular communication modeling is applied to derive the pharmacokinetics and biodistribution properties of a DDS. In Chapter 6, the molecular communication modeling is tailored to enable the study of antibody-mediated drug delivery systems. Finally, Chapter 7 concludes the thesis dissertation.

CHAPTER 2

PREVIOUS WORK

In this chapter, we review the state-of-the-art in two areas covered by this proposal, namely MC and DDS. On the one hand, the previous work in MC has focused on diffusion-based channel and ligand-binding kinetics, in idealized environments. We show here that these models are not readily applicable to the human body, and need to be extended to account for realistic propagation environments. On the other hand, the DDS research has addressed many issues in tracking the time and space evolution of the drug concentration in the body but lacks in terms of the level of detail and versatility in capturing individual specificities and the peculiarities of the DDS molecules.

2.1 Molecular Communication

MC is a bio-inspired paradigm that, amongst others, has been developed by nature for communication among living organisms, such as cells for intracellular and intercellular signaling [3]. In MC, information is exchanged by the release, the propagation and the reception of molecules [9]. Due to its inherent bio-compatibility, MC is a competitive solution to the problem of communication in nanonetworks [10], especially for bio-nano-medical applications. MC is increasingly attracting the interest of the research community working in the field of nanonetworking [2]. Targeted DDS has been envisioned as one of the most important applications of the MC paradigm. In the context of targeted DDS, the information conveyed by the the particles is the therapeutic action.

The channel model of molecular communication by diffusion has been analyzed theoretically in relation to the underlying physical processes [11]. Also, the stochastic effects in the ligand-receptor binding kinetics have been modeled through a molecular communication framework [12]. The maximum achievable information rates in diffusion-based

molecular communication under the constraints of Brownian motion noise have been derived in [13] using an novel thermodynamic information theoretical framework. Many different types of MC have been studied so far, which involve either passive transport of molecules (diffusion-based architectures [14]) or active transport (molecular motors [15], bacteria chemotaxis [16]).

These existing models rigorously reflect unique channel effects in molecular communication, but they cannot be directly applied for DDS in the complex human body, because they assume linear time-invariant channel models for the propagation medium, which is not reasonable to assume in the cardiovascular system where the blood flow is highly time-varying, and they suppose a free space geometry, while the molecular communication in the cardiovascular system is confined to the complex topology of blood vessels. The molecular communication reception of nanoparticles is also heavily affected by the blood flow that interferes with the chemical interactions between ligands and receptors [17].

2.2 Targeted Drug Delivery Systems

The so-called multi-compartmental approach [18] are the most successful computational models of drug propagation for conventional targeted DDS. Multi-compartmental models consider large portions of the human body as a single compartment, which is supposed to be homogeneous. The time and space evolution of the drug molecules in one compartment is commonly described through first-order differential equation, and is obtained for a large timescale in the order of hours. These multi-compartmental models for DDS are categorized as follows:

- *TMDD (Target-Mediated Drug Disposition)* [19] [20], which uses first-order linear differential equations, with a limited number of parameters (around five), and takes into account non-linearity in the case of saturation. TMDD is empirical.

- *PK/PD (Pharmacokinetics and Pharmacodynamics)* [21] [22], which is a model that also takes into non-linearity in case of saturation and of second-order kinetics. The

parameters of the model are statistically derived from experimental work, and it gives the pharmacokinetics in the spatial scale of a cell. PK/PD only gives information on a local level, and does not reflect the global effect of drug injection.

- *PBPK (physiologically-based pharmacokinetics)* [18] [23], which are based on the division of the human body in several compartments, each representing an individual organ. Unike PK/PD, this model gives results on the global level of the body.

The aforementioned models are limited because their parameter values are empirically obtained. This makes the study of patient variability in drug disposition particularly difficult. Also, many assumptions simplify the scenario in these models, such as the ones regarding mixing, time-invariance, and convection. The mixing is assumed perfect in one organ, the blood convection is assumed constant and uniform in one organ. Also, these methods focus more on the chemical kinetics than the mass transport.

Another issue with existing DDS models is that they are not easy to optimize. We need models for which the optimization problems can have an explicit solution, especially given the high number of parameters that affect the design and propagation of drug nanoparticles. The existing models are not sufficiently detailed and flexible to study advanced drug delivery systems. Nanomedicine-enabled methods such as PDDS require new computational models where the drug interactions with the body are described with great precision at a much smaller time and space resolution and in a tractable manner.

The most promising of the aforementioned models, namely PBPK, suffers from many limitations that make them inapplicable to advancing the current state-of-the-art in nanomedicine [24] [25]. The issue with the PBPK model is that the diseases that are meant to be targeted, such as tumors, are highly localized and grow quickly, and this model does not provide enough spatial and temporal accuracy to assess the efficiency of a DDS. Novel modeling and optimization approaches are needed for DDS design. The MC paradigm is well-equipped for achieving a physiologically-based analytical framework for DDS.

CHAPTER 3

MOLECULAR COMMUNICATION SYSTEM MODEL FOR PARTICULATE DRUG DELIVERY SYSTEMS

3.1 Motivation and Related Work

Targeted Drug Delivery Systems (DDS) are nowadays under intensive study as they are at the cutting edge of modern medical therapeutics [1]. In particular, the goal of DDS is to provide a localized drug presence where the medication is needed, while, at the same time, preventing the drug from affecting other healthy parts of the body. The most advanced solutions use drugs composed of micro or nano-sized particles (particulate DDS), which are able to diffuse into the blood stream to be transported into arteries, veins and capillaries and to cross barriers that prevent large particles and organisms from escaping the bloodstream.

The transport of drug particles in the human body can be viewed as a communication system using the Molecular Communication (MC) paradigm where information is conveyed through the transport of molecules. The MC paradigm will give us a clear understanding of how the drug particles diffuse in the body and the evolution of their distribution over time, which is of primary importance for the design of a particulate DDS. In the past literature, statistical modeling methods, such as the first reaction method based on dynamic Monte Carlo [26,27], have been often used to solve for this purpose. In this chapter, we proposed an analytical approach based on the abstraction of a particulate DDSs as a communication mechanism, where the drug particles are information carriers, which propagate messages (drug chemical properties) from the location of transmission (intravascular injection) until the location of reception (targeted site).

Targeted DDS has been envisioned as one of the most important applications of the Molecular Communication (MC) paradigm [2]. MC abstracts the propagation of information between a sender and a receiver realized through mass transport phenomena. In the context of targeted DDS, the information conveyed by the the particles is the therapeutic

action. MC is increasingly attracting the interest of the research community working in the field of nanonetworking [2]. MC is a bio-inspired paradigm that, amongst others, has been developed by nature for communication among living organisms, such as cells for intracellular and intercellular signaling [3]. In MC, information is exchanged by the release, the propagation and the reception of molecules [9]. Due to its inherent bio-compatibility, MC is a competitive solution to the problem of communication in nanonetworks [10], especially for bio-nano-medical applications. Many different types of MC have been studied so far, which involve either passive transport of molecules (diffusion-based architectures [14] [28]) or active transport (molecular motors [15], bacteria chemotaxis [16]). The MC paradigm can pave the way for new approaches to the analysis of immune system attacks from a security and safety perspective in analogy with telecommunication security techniques.

A particulate Drug Delivery System (DDS) takes advantage of the blood distribution network for the propagation of drug particles from a location where they are injected into the blood flow to a targeted site within the reach of the cardiovascular system. The mass transport phenomena operated by the cardiovascular system for the propagation of the drug particles are two, namely, advection and diffusion. As a consequence of advection, the drug particles are subject to their translation while in suspension in the blood, which flows at different velocities in different locations of the cardiovascular system. The blood velocity profile follows the laws of fluid dynamics and, in particular, the Navier-Stokes equation [29]. On top of this, as a result of diffusion, the drug particles are subject to the Brownian motion spread in the blood from a region of higher concentration to a region of lower concentration. This is interpreted by the laws of particle diffusion and, in particular, by the diffusion-advection equation [26]. In this chapter, we realized the molecular communication abstraction of a particulate DDS by developing a MC channel model of the drug particle propagation through the cardiovascular system. For this, we identified two separate contributions within the model, namely, the cardiovascular network model and the

drug propagation network model.

The cardiovascular network model is developed in this chapter as a solution to the Navier-Stokes equation [29] in the cardiovascular system, and it is based on the application of the transmission line theory [30]. We have restricted our model of the cardiovascular network to the blood arteries, which are the network of blood vessels that provide organs and tissues with oxygen and nutrients, because it is the best medical administration to provide targeted drug delivery to these organs. Our objective is to administer a drug dose to a target location in the extremity. Systemic arteries are the best candidate route of administration for targeted drug delivery systems because they allow delivering a localized drug dose to the periphery without affecting healthy organs and tissues [31]. On the contrary, veins are more appropriate in the case when the drug must be evenly distributed to the extremities of the cardiovascular network. By mapping the fluidic parameters of each artery to electrical circuit components, the cardiovascular network model allows to analytically compute the blood velocity profile in every artery of the cardiovascular system given the blood flow input from the heart. A similar approach has been suggested in [30], where, differently from our work, a bulk section of the arterial system is modeled with one circuit component and does not allow obtaining the blood velocity profile at every possible location. In [32], a complete fluid dynamic analysis of a pressure pulse propagation in the cardiovascular system is performed, but without the flexibility and clarity of a circuit analogue of the blood flow dynamics in the transmission line model we developed. In [33], a transmission line model is developed which takes into account only the blood dynamics in the large systemic artery tree, while our model covers in detail both large and small artery trees. In [34], the lumped model of any artery is developed, but without taking into account their bifurcations and the transmission line network solution of an artery tree.

The drug propagation network model is developed in this chapter as a solution to the advection-diffusion equation [26], and it stems from the knowledge of the blood velocity profile computed through the cardiovascular network model. Through the application of the

Harmonic Transfer Matrix (HTM) theory [35] to the drug particle transport in the arteries and their bifurcations, the drug propagation network allows the analytical expression of the drug delivery rate at the targeted site given the drug location of injection and injection rate profile. The derived model takes into account also the individual specificities in the physiological parameters of the cardiovascular system, such as the compliance of the arteries, the heartbeat rate profile and the heartbeat stroke volume. Molecular mass transport over a network has been very recently approached from the point of view of complex system theory in [26]. While this method takes into account the time-variance of the flow, the algorithm couples a graph-based approach and numerical resolution of partial-differential equations for every vessel, which are not required in our HTM-based approach. Such method implies a high computation and memory cost. Also, this model does not yield analytical expressions that can be of practical use to solve problems such as the optimization of the drug delivery. The rest of this chapter is organized as follows. In Sec. 3.2 the main processes that compose a particulate DDS and their abstractions as the components of an MC system are introduced, together with the main objective of this work. In Sec. 3.3, the scheme of the MC channel model of a particulate DDS is detailed into two main contributions, namely, the cardiovascular network model and the drug propagation network model. Sec. 3.4 details the cardiovascular network model, while Sec. 3.5 describes the drug propagation network model. Sec. 3.6 analyzes the numerical results stemming from the proposed solution. Finally, Sec. 3.7 concludes the chapter.

3.2 Molecular Communication Abstraction of a Particulate DDS

A particulate Drug Delivery System (DDS) takes advantage of the blood circulation in the cardiovascular system for the propagation of drug particles from a location where they are injected into the blood flow until they reach a targeted site. We describe a particulate DDS as composed of three main processes, namely, **Injection**, **Propagation**, and **Delivery**, as shown in Fig. 3. The Molecular Communication (MC) paradigm abstracts the exchange

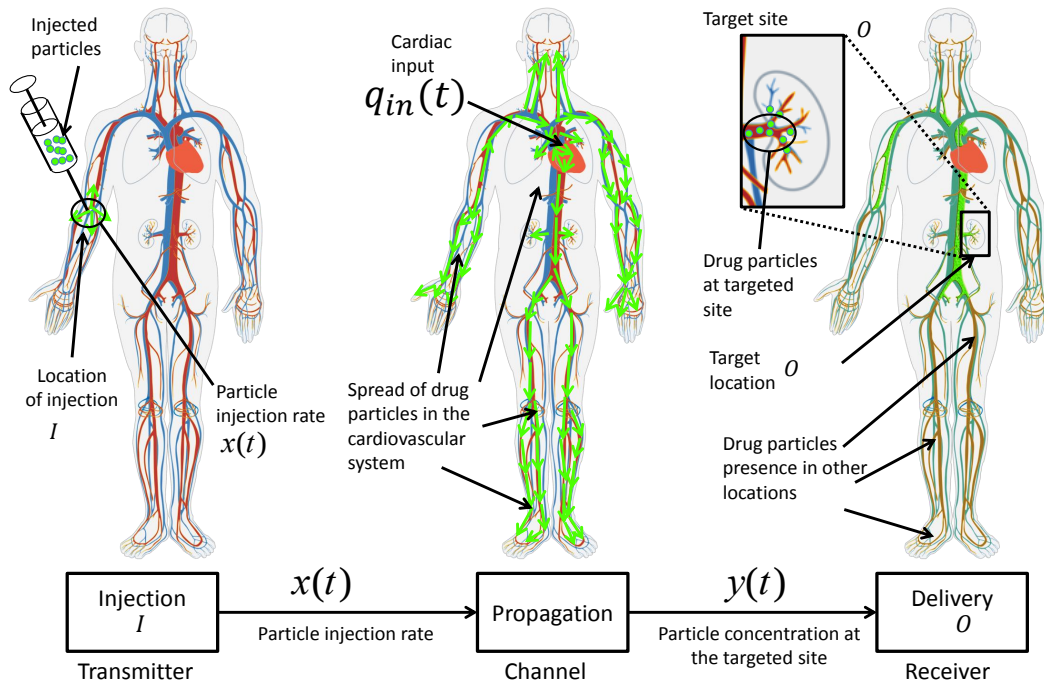

Figure 3. Graphical sketch of the main processes in a particulate DDS and their MC abstractions.

of information through the emission of particles from a **Transmitter**, their propagation through mass transport phenomena in the **Channel**, and their reception at the destination by a **Receiver**. We define the particulate DDS processes and their MC abstractions as follows:

- The **Injection** process is the introduction of the drug particles in the blood flowing in the cardiovascular system at a predefined *location of injection* I. The injection is performed according to a *particle injection rate* $x(t)$ defined as the first derivative with respect to the volume v in the number of injected particles in the location of injection as the function of the time t:

$$x(t) = \frac{\partial \{\#\text{ injected particles}\}\,(t)}{\partial v}\,. \tag{1}$$

  We abstract the injection process as the MC **Transmitter** where I is the transmitter location and $x(t)$ is the transmitted molecular signal.

- The **Propagation** process is the spread of the drug particles throughout the cardiovascular system. The cardiovascular system shows a topology of interconnected *blood vessels* where the blood flows due to the heart pumping action, which is expressed as the *cardiac input* $q_{in}(t)$, defined as the blood flow input to the cardiovascular cardiovascular system as function of the time t. Drug particles propagate through the blood vessels according to the superposition of two physical phenomena, namely, advection and diffusion. *Advection* is the transport of particles suspended in a fluid due to the fluid's bulk motion. *Diffusion* is the spontaneous spread of particles suspended in a fluid from a space region where they are in a higher concentration to another region where they are in a lower concentration. We abstract the propagation process as the MC **Channel**, where the transmitted molecular signal is propagated via advection-diffusion through the blood flow in the cardiovascular system.

- The **Delivery** process is the arrival of the drug particles at the *targeted site O*, where they are expected to perform their healing action. The drug delivery process is characterized by the *particle delivery rate* $y(t)$ at the targeted site, defined as the first derivative with respect to the volume v in the number of particles present at the targeted site as function of the time t:

$$y(t) = \frac{\partial \{\text{\# particles at targeted site}\}\,(t)}{\partial v}\,. \tag{2}$$

  We abstract the delivery process as the MC **Receiver** where O is the receiver location and $y(t)$ is the received molecular signal.

One of the main objectives in the study of a particulate DDS is to develop a model to analytically compute the particle delivery rate $y(t)$ at the targeted site as function of the time t from the knowledge of the location of injection I, the particle injection rate $x(t)$, the cardiac input $q_{in}(t)$ and the targeted site O. This is expressed as follows:

$$y(t) = f(I, x(t), q_{in}(t), O)\,, \tag{3}$$

where the function $f(.)$ represents the analytical model. *We abstract this objective as the modeling of the MC channel between the MC transmitter located at I and the MC receiver located at O, where the input transmitted molecular signal $x(t)$ is propagated by advection and diffusion in the blood flowing through the cardiovascular system as function of the cardiac input $q_{in}(t)$. The output of this MC channel is the received molecular signal $y(t)$.*

The outcome of the model expressed in (2) through the MC abstraction is twofold:

- To study optimization techniques for particulate DDSs which could allow a careful selection of the location of injection I and a definition of the particle injection rate $x(t)$ as function of the time t with the goal of obtaining a desired particle delivery rate $y(t)$ as function of the time t at a targeted site O, while minimizing the drug spread in the rest of the cardiovascular system [1].

- To develop a novel MC technique to realize Intra-Body Communication (IBC) networks [36] by modulating at the transmitter the injection of particles in the blood according to the signal to be transmitted, and, upon their propagation through the cardiovascular system, by demodulating the received signal from the delivery rate of incoming particles at the receiver.

3.3 Scheme of the MC Channel Model of a Particulate DDS

The MC channel model of a particulate DDS developed in this chapter is divided into two main contributions, namely, the **Cardiovascular Network Model** and the **Drug Propagation Network Model**, as shown in Fig. 4. These two contributions are summarized as follows:

- The **Cardiovascular Network Model** is developed as a solution to the *Navier-Stokes* equation [29], which relates the blood velocity vector $u_l(r,t)$, function of the radial coordinate r and the time variable t, in every location of the cardiovascular system to

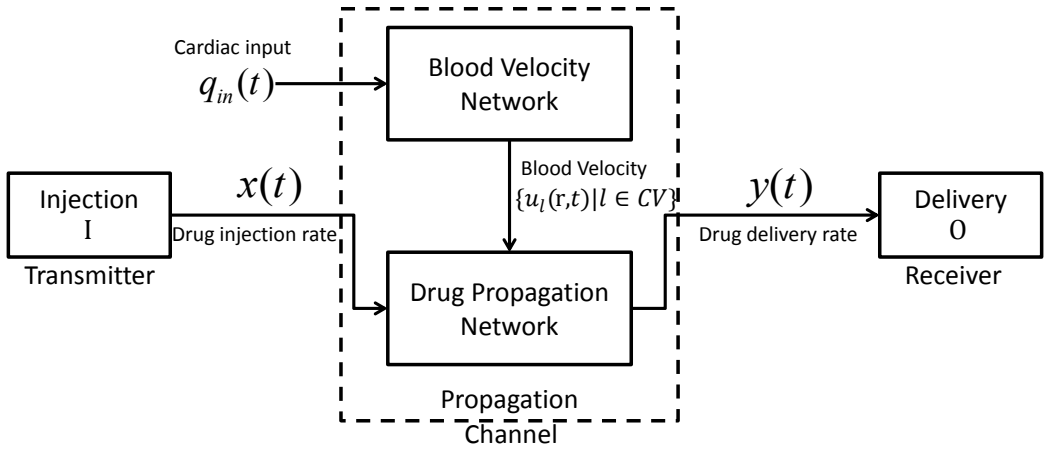

Figure 4. Scheme of the MC channel model of a particulate DDS with the two contributions.

the blood pressure $p(t)$ as functions of the time t. This is expressed as follows:

$$\rho\left(\frac{\partial u_l(r,t)}{\partial t} + u_l(r,t)\cdot\nabla u_l(r,t)\right) = -\nabla p(t) + \mu\nabla^2 u_l(r,t) + \mathbf{f}\,, \tag{4}$$

where ρ is the blood density, which we assume homogeneous, ∇ is the Nabla vector differential operator, μ is the blood viscosity, and $\mathbf{f}$ represents the contribution of blood vessel wall properties [37]. As detailed in Sec. 3.4, the cardiovascular network model allows to compute the blood velocity $u_l(r,t)$ as function of the time t in every artery l of the cardiovascular system CV from the knowledge of the cardiac input $q_{in}(t)$, expressed as follows:

$$q_{in}(t) \xrightarrow{\text{Cardiovascular Network Model}} \{u_l(r,t)|l \in CV\}\,, \tag{5}$$

where $q_{in}(t)$ is the blood flow input to the cardiovascular system, $\{.\}$ is the set symbol and CV denotes the set of all the arteries included in the cardiovascular system. As explained in Sec. 3.4, the cardiovascular network model is developed through the application of the **transmission line theory** [30] to the modeling of the interconnection of the arteries in the cardiovascular network.

- The **Drug Propagation Network Model** is developed as a solution to the *advection-diffusion* equation [38], which relates the drug concentration $c(t)$ in every location of

the cardiovascular system to the blood velocity vector $u_l(r,t)$ as functions of the time t. It is expressed as follows:

$$\frac{\partial c(t)}{\partial t} = -\nabla.\left[-D\nabla c(t) + u_l(r,t)c(t)\right] , \tag{6}$$

where ∇ is the Nabla vector differential operator, and D is the particle diffusion coefficient. As detailed in Sec. 3.5, the drug propagation network model allows to compute the particle delivery rate $y(t)$ at the targeted site as function of the time t from the knowledge of the location of injection I, the particle injection rate $x(t)$, the blood velocity $u_l(r,t)$ as function of the time t in every artery l of the cardiovascular system CV, and the targeted site O, expressed as follows:

$$I, x(t), \{u_l(r,t)|l \in CV\}, O \xrightarrow[\text{Network Model}]{\text{Drug Propagation}} y(t) , \tag{7}$$

where $\{.\}$ is the set symbol and CV denotes all the arteries included in the cardiovascular system. The drug propagation network model is developed by applying the **Harmonic Transfer Matrix (HTM)** theory [35] to express the transfer function of each artery and bifurcation in the cardiovascular system CV, as explained in Sec. 3.5.

The MC channel model, composed by the two aforementioned contributions, allows to find the analytical solution to the objective expressed in (2) by using the particulate DDS MC abstraction. The cardiovascular network and drug propagation network models are detailed in Sec. 3.4 and 3.5, respectively.

3.4 Cardiovascular Network Model

The cardiovascular network model allows to compute for every artery l the blood velocity $u_l(r,t)$ as function of the distance r from the blood vessel axis and the time t, and it stems from the closed-form solutions to the Navier-Stokes equation (4) applied to the cardiovascular system. As shown in Fig. 5, the cardiovascular network model is composed of the following elements:

- The **Cardiac Input** $Q_{in}(\omega_k)$, which is the flow $Q_{in}(\omega_k)$ exerted by the heart as functions of the heartbeat frequency component ω_k. The blood pressure is defined as the force induced by the blood on the walls of a blood vessel, while the blood flow is defined as the quantity of blood traversing the cross section of a blood vessel per unit time. The computation of $Q_{in}(\omega_k)$ is detailed in Sec. 3.4.1.

- The **Small Arteries Model**. Small arteries are defined as the systemic circulation vessel with a radius comprised between $0.05mm$ and $2mm$. They have muscular walls and deliver blood to capillaries. This model is developed in Sec. 3.4.2 and gives the *transfer matrix* and *load impedance* for a small artery l.

- The **Large Arteries Model**. Large arteries are defined as the systemic circulation vessels with a radius larger than $2mm$. They have elastic walls and branch ultimately into small arteries. Their model is developed in Sec. 3.4.3 and also yields the *transfer matrix* and *load impedance* for a large artery l.

- The **General Transfer Matrix and Load Impedance** $\mathbf{T}(\omega_k)$. It characterizes the cardiovascular network between the heart and any small or large artery l and it is computed from the aforementioned elements by applying the transmission line theory [30]. We express $\mathbf{T}(\omega_k)$ as a 2×2 matrix with elements $A(\omega_k)$, $B(\omega_k)$, $C(\omega_k)$, and $D(\omega_k)$ in Sec. 3.4.4.

- The **Blood Velocity**. The output of the cardiovascular network is the blood velocity $u_l(r,t)$ in a large or a small artery l. We suppose that it is homogeneous along the longitude of the artery and that it only depends on time variable t and the radial coordinate r in the artery. We find in Sec. 3.4.5 a final relationship that gives the blood velocity $u_l(r,t)$ of any artery l of the cardiovascular system CV from the cardiac input $Q_{in}(\omega_k)$ through the following formula:

$$u_l(r,t) = \frac{1-\frac{r^2}{r_l^2}}{\pi r_l^2} \sum_{k=-\infty}^{+\infty} \frac{Q_{in}(\omega_k)}{Z_l(\omega_k)C(\omega_k)+D(\omega_k)} e^{j\omega_k t}. \tag{8}$$

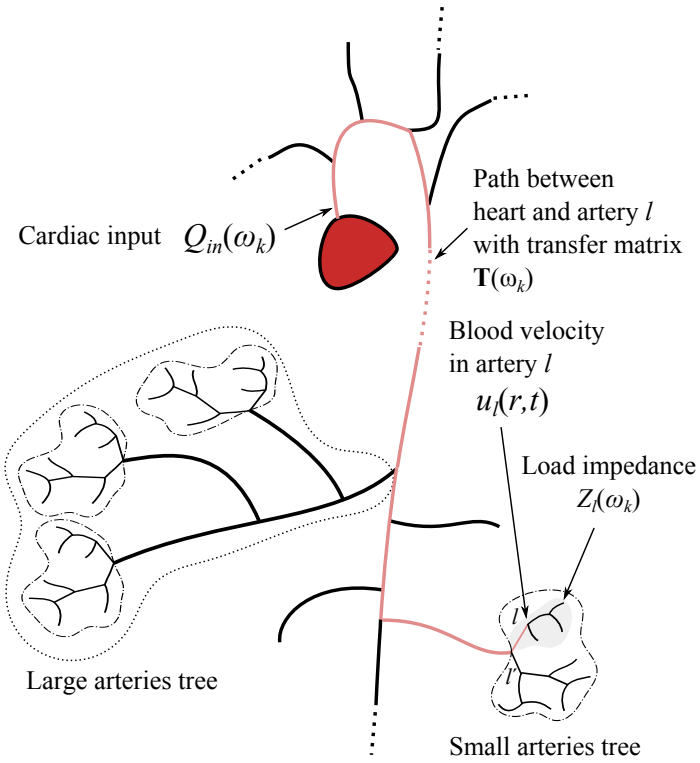

Figure 5. Path between the cardiac input and the small artery l.

where $Q_{in}(\omega_k)$ is the cardiac input, $Z_l(\omega_k)$ is the load impedance of the artery l, and $C(\omega_k)$ and $D(\omega_k)$ are the first and second elements of the second row of the transfer matrix $\mathbf{T}(\omega_k)$ representing the cardiovascular network between the heart and the artery l sampled at angular frequency ω_k respectively.

3.4.1 Cardiac Input

The cardiac input $Q_{in}(\omega_k)$ is the blood flow ejected by the heart in the cardiovascular system as functions of the heartbeat frequency component ω_k. $Q_{in}(\omega_k)$ is considered to be the Fourier coefficients of the blood flow $q_{in}(t)$ taken from clinical measurements provided in [37] and performed by using Magnetic Resonance (MR) on a set of human individuals. By exploiting the periodicity of the cardiac input, we compute the Fourier coefficients [39] and obtain the cardiac input $Q_{in}(\omega_k)$ as function of the Fourier series index k:

$$Q_{in}(\omega_k) = \frac{1}{T}\int_{-\frac{T}{2}}^{\frac{T}{2}} q_{in}(t)e^{-j\omega_k}\,dt\,. \tag{9}$$

3.4.2 Small Arteries Model

3.4.2.1 Load Impedance of a Small Artery

The modeling of a small artery l as an electrical component with a load impedance $Z_l(\omega_k)$ is explained in the following. The load impedance $Z_l(\omega_k)$ is calculated recursively according to the algorithm described in Algorithm 1. The harmonic impedance $Z'_l(\omega_k)$ of the sister branch is calculated similarly.

Small arteries possess the following properties:

- The *scaling parameters* α and β, which are scaling parameters that relate the radii of the two bifurcating arteries r_l at the left and r'_l at the right to the radius r_{l-1} of their parent artery $l-1$ ($r_l = \alpha r_{l-1}$ and $r'_l = \beta r_{l-1}$)

  The tree is terminated when the radius is no larger than a minimal radius r_{min}. The tree representation for the renal artery is given in Fig. 18.

- The length ℓ_l, which is proportional to the radius r_l of the small artery. Since, the tapering is no longer significant in small arteries, it is possible to consider small arteries as cylinders. It has been observed from measurements that the length-radius ratio l_{rr} is constant for small arteries. In fact the length of a small artery l can be expressed approximately in function of its radius r_l as follows:

$$\ell_l = l_{rr} r_l = (50 \pm 10)\, r_l\,. \tag{10}$$

- The *volume compliance* c_l, which is supposed to be similar to the volume compliance for large arteries (20).

Due to the different mechanical and geometric properties between large and small arteries, we use a different transmission line model for small arteries.

According to [40], the harmonic pressure $P_l(\omega_k)$ and the harmonic flow $Q_l(\omega_k)$ in a small artery l can be related by a load impedance $Z_l(\omega_k)$ as follows:

$$P_l(\omega_k) = Z_l(\omega_k) Q_l(\omega_k)\,. \tag{11}$$

Eq. (11) is similar to Ohm's law [41] if pressure is seen as voltage and flow as current. More importantly, the harmonic impedance at the inlet of the small artery $Z_l(\omega_k)$ and the harmonic impedance at the outlet of the small artery $Z_l^{out}(\omega_k)$ are related by the following relationship [40]:

$$Z_l(\omega_k) = \frac{j\tau_l(\omega_k)\sin\left(\tau_l(\omega_k)\right)/\ell_l + Z_l^{out}(\omega_k)\cos\left(\tau_l(\omega_k)\right)}{\cos\left(\tau_l(\omega_k)\right) + j\ell_l Z_l^{out}(\omega_k)\sin\left(\tau_l(\omega_k)\right)/\tau_l(\omega_k)}\,, \tag{12}$$

with [40]:

$$\tau_l(\omega_k) = \frac{l_{rr}}{\sqrt{\pi}}\sqrt{\frac{\rho c_l}{1 - \frac{2J_1(jr_l^2\omega/\nu)}{jr_l^2\omega/\nu J_0(jr_l^2\omega/\nu)}}}\,, \tag{13}$$

where r_l is the small artery radius, ℓ_l is the small artery length, l_{rr} is the length-to-radius ratio, ρ is the blood density, μ is the blood viscosity, $\upsilon = \mu/\rho$ is the blood kinematic viscosity, c_l is the small artery volume compliance, j is the imaginary unit, J_0 and J_1 are the Bessel function of the first kind and, respectively, zero and first order [42].

For $\omega_k = 0$, we calculate the limit of the function $Z_l(\omega_k)$ in (12) as $\omega_k \to 0$ to get:

$$Z_l(\omega_k) = \frac{8\mu\ell_l}{\pi r_l^4} + Z_l^{out}(\omega_k)\,. \tag{14}$$

The conservation of flow at the bifurcation, and continuity of pressure justify the modeling of bifurcations as the branching of perfectly conducting wires in the electric analogue of blood flow and pressure, and allow the application of Kirchhoff's current and voltage laws [43]. The harmonic impedance at the output $Z_l^{out}(\omega_k)$ can be related to the harmonic impedance at the daughter small artery $l+1$ $Z_{l+1}(\omega_k)$ and the harmonic impedance of its sister $Z_{l'+1}$, by the following relationship:

$$Z_l^{out}(\omega_k) = \left(\frac{1}{Z_{l+1}(\omega_k)} + \frac{1}{Z_{l'+1}(\omega_k)}\right)^{-1}\,. \tag{15}$$

The tree of small arteries is truncated when the radius r_l is no larger than r_{min}. The harmonic impedance of a small artery l such as $r_l < r_{min}$ is taken to be zero. With this condition, we can compute the load impedance $Z_l(\omega_k)$ of a small artery l according to the recursive function in Algorithm 1, where $f(ZOut, r)$, implementing the expression defined in (12), returns the impedance ZIn given the output impedance $ZOut$ and the radius r.

Algorithm 1 Recursive computation of the load impedance of a small artery.

```
1: Global alpha, beta, rMin                                   ▷ Parameters
2: function ImpedanceSmall(r)
3:     if r ≤ rMin then
4:         ZR ← ImpedanceSmall(beta ∗ r)                      ▷ ZR: Impedance of the right daughter artery
5:         ZL ← ImpedanceSmall(alpha ∗ r)                     ▷ ZL: Impedance of the left daughter artery
6:         ZOut ← 1/(1/ZR + 1/ZL)
7:         ZIn ← f(ZOut, r)
8:     else
9:         ZIn ← 0
10:    end if
11:    return ZIn
12: end function
```

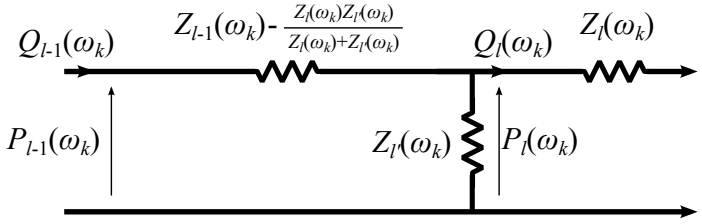

Figure 6. Transmission line model for a tree of small arteries.

3.4.2.2 Small Artery Transfer Matrix

Here, we find a transfer matrix $\mathbf{T}_l(\omega_k)$ that relates the harmonic flow and pressure $[P_l(\omega_k)\, Q_l(\omega_k)]'$ in a small artery l located in a tree of small arteries to the flow and pressure at the root i_l of the tree of small arteries $[P_{i_l}(\omega_k)\, Q_{i_l}(\omega_k)]'$ (cf. Fig. 7).

By calculating the harmonic impedance at the root artery $Z_{i_l}(\omega_k)$ the harmonic impedance at the small artery l $Z_l(\omega_k)$ and at its sister small artery $Z_{l'}(\omega_k)$, we can represent the tree of small arteries by the two-port network in Fig. 6. Using Kirchhoff's circuit laws, we find a linear system involving the input pressure $P_{i_l}(\omega_k)$, the input flow $Q_{i_l}(\omega_k)$, the output pressure $P_l(\omega_k)$, and the output flow $Q_l(\omega_k)$. Hence, the flow and pressure in a small artery l and the root of the tree of small arteries i are related by the following matrix relationship using the transmission line theory:

$$\begin{bmatrix} P_{i_l}(\omega_k) \\ Q_{i_l}(\omega_k) \end{bmatrix} = \mathbf{T}_l(\omega_k) \begin{bmatrix} P_l(\omega_k) \\ Q_l(\omega_k) \end{bmatrix}, \tag{16}$$

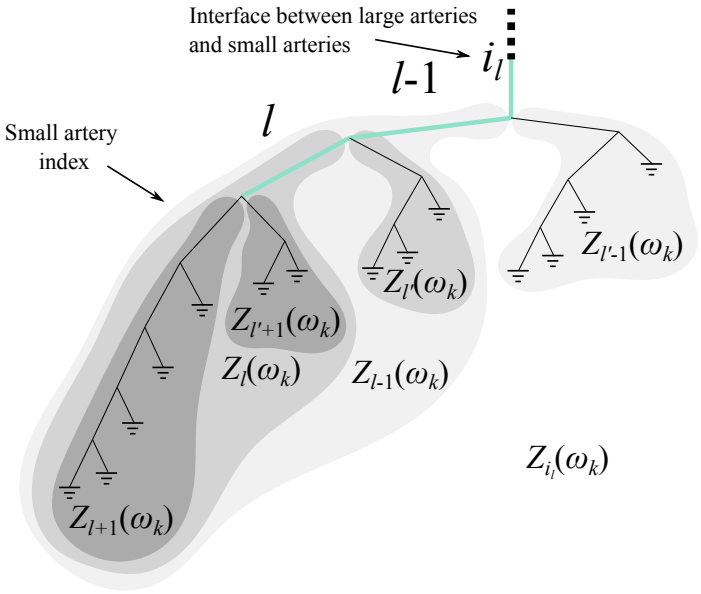

Figure 7. A small arterial tree as a network of impedances.

with:

$$\mathbf{T}_l(\omega_k) = \prod_{m \in \mathrm{S}_l} \begin{bmatrix} 1 + \frac{\Delta Z_{m-1}(\omega_k)}{Z'_m(\omega_k)} & \Delta Z_{m-1}(\omega_k) \\ \frac{1}{Z_{m'}(\omega_k)} & 1 \end{bmatrix}, \tag{17}$$

where $\mathrm{S}_l = (..., m, ..., l-1, l)$ is the sequence of all small arteries carrying blood from the interface to the small artery l, $[P_l(\omega_k)\, Q_l(\omega_k)]'$ is the harmonic flow and pressure in a small artery l, and $[P_{i_l}(\omega_k)\, Q_{i_l}(\omega_k)]'$ is the harmonic flow and pressure at the root of the tree of small arteries i_l, and $\Delta Z_{m-1}(\omega_k)$ is the impedance between the inlets the small arteries m and $m-1$ which is computed as in the following,

$$\Delta Z_{m-1}(\omega_k) = Z_{m-1}(\omega_k) - \frac{Z_m(\omega_k) Z_{m'}(\omega_k)}{Z_m(\omega_k) + Z_{m'}(\omega_k)}\,. \tag{18}$$

$Z_m(\omega_k)$, $Z_{m'}(\omega_k)$, and $Z_{m-1}(\omega_k)$ are, respectively the harmonic impedance of the small artery m, its sister small artery m', and its parent small artery $m-1$. At the interface, we take that $\Delta Z_{i_l}(\omega_k) = 0$.

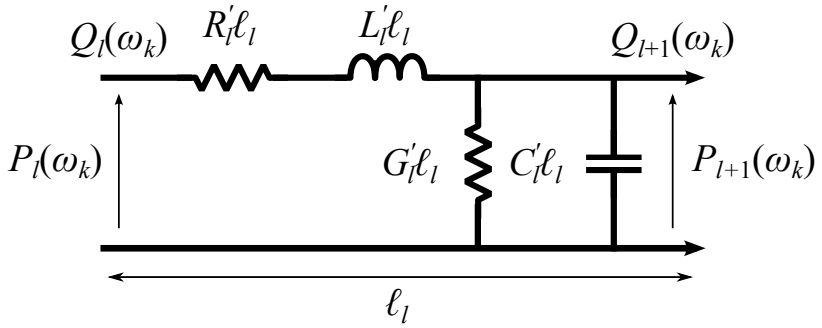

Figure 8. Electrical scheme of the transmission line representation of a large artery segment.

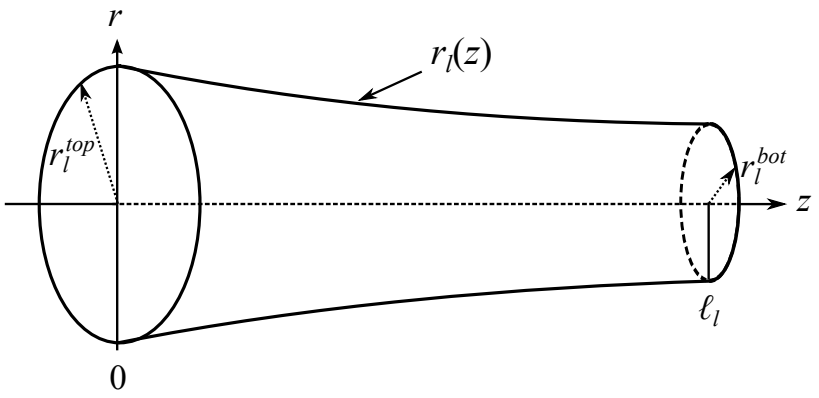

Figure 9. A large artery m as an axisymmetric tube with tapering radius in the (r,z) plan.

3.4.3 Large Arteries Model

The objective of this section is to present an expression of the transfer matrix $\mathbf{T}_l(\omega_k)$ for a large artery l and an algorithm to calculate the load impedance $Z_l(\omega_k)$ for a large artery located in the cardiovascular system.

3.4.3.1 Large Artery Transfer Matrix

The transfer matrix $\mathbf{T}_l(\omega_k)$ for a large artery l depends on its geometric dimensions and physiological parameters of the artery, which are as follows:

- *Radius tapering*. A large artery l is considered as an axisymmetric tube with decreasing radius as illustrated in Fig. 9 and length ℓ_l. The inlet of the large artery l has a top radius r_l^{top} and its outlet has a bottom radius r_l^{bot} where $r_l^{bot} \leq r_l^{top}$. The numerical values for r_l^{top},r_l^{bot}, and ℓ_l are found from anatomical measurements (cf. Table 1).We consider z as the longitude coordinate along the axis of the large artery, and $r_m(z)$

as the radial distance of the tube surface to the axis at z, the radius $r_l(z)$ decreases exponentially from r_l^{top} at $z = 0$ to r_m^{bot} at $z = \ell_l$, as follows:

$$r_l(z) = r_l^{top} \exp(-k_l z)\,, \tag{19}$$

where k_l, the tapering factor for a large artery l, is defined as $k_l = \frac{log\left(r_l^{top}/r_l^{bot}\right)}{\ell_l}$.

- The *volume compliance*, which quantifies the tendency of the artery walls to yield to pressure and other external forces. Using statistical studies of physiological measurements [37], the volume compliance c_l can be estimated by the following equation:

$$c_l(z) = \frac{\pi {r_l}^2(z)}{k_1 \exp(-k_2 r_l(z)) + k_3}\,, \tag{20}$$

where $k_1 = 1.34 \times 10^7 g/(s^2.cm)$, $k_2 = 22.53 cm^{-1}$, and $k_3 = 5.77 \times 10^5 g/(s^2.cm)$.

The blood flow in a large artery is assumed to be laminar, viscous, and incompressible, and that pressure is constant over the cross-section of the large artery. Starting from the Navier-Stokes equation (4), equating the variance of the flow in a large artery with the volume absorbed by the large artery due to its compliance, we get a system of coupled differential equations [44] for one-dimensional blood flow $\hat{q}_l(z,t)$ and one-dimensional blood pressure $\hat{p}_l(z,t)$:

$$-\frac{\partial \hat{p}_l(z,t)}{\partial z} = \frac{\rho}{\pi r_m^2}\frac{\partial \hat{q}_l(z,t)}{\partial t} + \frac{8\mu}{\pi {r_l}^4}\hat{q}_l(z,t) \tag{21}$$

$$-\frac{\partial \hat{q}_l(z,t)}{\partial z} = c_l \frac{\partial \hat{p}_l(z,t)}{\partial t}\,. \tag{22}$$

This system is governed by differential equations which resemble the Telegrapher's equations. A Telegrapher's equation have an electrical circuit analogue as illustrated in Fig. 8. The components of this circuit are the resistance per unit length $R_l^{'} = \frac{8\mu}{\pi {r_l}^4}$, inductance per unit length $L_l^{'} = \frac{\rho}{\pi {r_l}^2}$, the capacitance per unit length $C_l^{'} = \frac{\pi {r_l}^2}{k_1 \exp(-k_2 r_l) + k_3}$, and

the admittance per unit length $G_l^{'} = 0$, and are expressed as function of the physiological parameters previously defined, with $r_l = r_l(z = \ell_l)$. Stemming from these electrical components, two important parameters are hence defined for a large artery segment l:

- The *propagation coefficient* $\gamma_l(\omega_k)$, which is expressed by:

$$\gamma_l(\omega_k) = \sqrt{\left(R_l^{'} + j\omega_k L_l^{'}\right)\left(G_l^{'} + j\omega_k C_l^{'}\right)}. \tag{23}$$

- The *characteristic impedance* $Z_l^{\circ}(\omega_k)$, defined as the impedance that the transmission line segment would have if it was a part of an infinitely long transmission line with homogeneous parameters [45]:

$$Z_l^{\circ}(\omega_k) = \sqrt{\frac{R_l^{'} + j\omega_k L_l^{'}}{G_l^{'} + j\omega_k C_l^{'}}}. \tag{24}$$

By applying the two-port network circuit analysis [41], the Fourier coefficients of the pressure $P_l(\omega_k)$ and flow $Q_l(\omega_k)$ in the large artery segment l can be related to the Fourier coefficients of the pressure $P_{l+1}(\omega_k)$ and flow $Q_{l+1}(\omega_k)$ of the next large artery segment $l+1$ as follows:

$$\begin{bmatrix} P_{l+1}(\omega_k) \\ Q_{l+1}(\omega_k) \end{bmatrix} = \mathbf{T}_l(\omega_k) \begin{bmatrix} P_l(\omega_k) \\ Q_l(\omega_k) \end{bmatrix}, \tag{25}$$

with:

$$\mathbf{T}_l(\omega_k) = \begin{bmatrix} A_l(\omega_k) & B_l(\omega_k) \\ C_l(\omega_k) & D_l(\omega_k) \end{bmatrix}, \tag{26}$$

where $A_l(\omega_k)$, $B_l(\omega_k)$, $C_l(\omega_k)$, and $D_l(\omega_k)$ are the elements of the transfer matrix $\mathbf{T}_l(\omega_k)$ of the large artery l, defined as [46]:

$$\begin{aligned} A_l(\omega_k) &= \cosh\left(\gamma_l(\omega_k)\ell_l\right) \\ B_l(\omega_k) &= Z_l^{\circ}(\omega_k)\sinh\left(\gamma_l(\omega_k)\ell_l\right) \\ C_l(\omega_k) &= \frac{1}{Z_l^{\circ}(\omega_k)}\sinh\left(\gamma_l(\omega_k)\ell_l\right) \\ D_l(\omega_k) &= \cosh\left(\gamma_l(\omega_k)\ell_l\right) . \end{aligned} \tag{27}$$

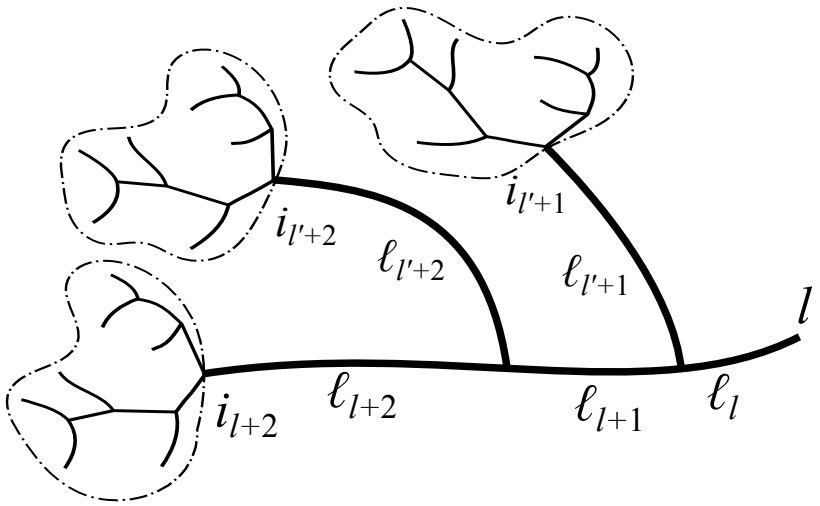

Figure 10. A branching large artery terminated by trees of small arteries and their lengths.

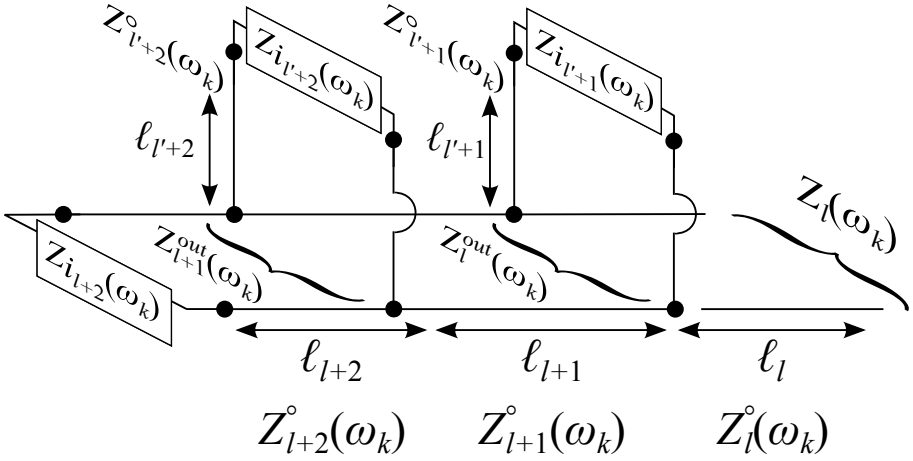

Figure 11. A tree of large arteries as branching transmission lines.

where $\gamma_l(\omega_k)$ is the propagation coefficient of large artery segment l, $Z^{\circ}_l(\omega_k)$ is the characteristic impedance of large artery segment l, and ℓ_l is its length.

3.4.3.2 Load Impedance of a Large Artery

The load impedance of a large artery $Z_l(\omega_k)$ is a measure of the opposition experienced by the blood flow at the inlet of a large artery l. It depends on the topology of all large arteries that branch out from large artery l and their geometric dimensions. Large arteries are arranged in a tree-like structure. The arteries grow out from the aorta, the systemic artery originating at the heart, and branch out to reach the peripheral body tissues and organs. Measurements of the position of arteries and the points of bifurcations are available from

anatomy books [47], and are presented in Table 1. The large arteries are ended by a tree of small arteries which are presented in 3.4.2.

Fig. 10 illustrates the topology of the tree of large arteries branching out from a large artery l. As shown in Fig. 11, the tree of large arteries is terminated by trees of small arteries with load impedance $Z_{i_{l'+1}}(\omega_k)$, $Z_{i_{l'+2}}(\omega_k)$, $Z_{i_{l+1}}(\omega_k)$, etc. which are calculated according to the algorithm presented in Sec. 3.4.2.1.

Using transmission line theory [45], it is possible to express the load impedance of the large artery l in function of the load impedance at its outlet, which is denoted $Z_l^{out}(\omega_k)$.

$$Z_l(\omega_k) = Z_l^{\circ}(\omega_k)\frac{Z_l^{out}(\omega_k) + Z_l^{\circ}(\omega_k)\tanh\left(\gamma_l(\omega_k)\ell_l\right)}{Z_l^{\circ}(\omega_k) + Z_l^{out}(\omega_k)\tanh\left(\gamma_l(\omega_k)\ell_l\right)}, \tag{28}$$

where $Z_l^{\circ}(\omega_k)$ and $\gamma_l(\omega_k)$ are respectively the propagation coefficient and characteristic impedance for the large artery l as found in (23) and (24). If the large artery l branches out into two large arteries $l+1$ and $l'+1$, the load impedance at the outlet of large artery l is given by:

$$Z_l^{out}(\omega_k) = \left(\frac{1}{Z_{l+1}(\omega_k)} + \frac{1}{Z_{l'+1}(\omega_k)}\right)^{-1}. \tag{29}$$

Otherwise, if the large artery l is terminated by a tree of small arteries, the load impedance at the outlet of large artery l is exactly the load impedance of interface with small arteries $Z_{i_l}(\omega_k)$.

$$Z_l^{out}(\omega_k) = Z_{i_l}(\omega_k) = \left(\frac{1}{Z_{l+1}(\omega_k)} + \frac{1}{Z_{l'+1}(\omega_k)}\right)^{-1}. \tag{30}$$

where $l+1$ and $l'+1$ are the indexes of the small arteries braching out if the large artery l.

We can describe the procedure required to get the load impedance $Z_l(\omega_k)$ of the large artery l by the recursive algorithm in Algorithm 2 by defining:

- $f : (ZOut, L, R) \rightarrow ZIn$ as the function that returns the load impedance ZIn of a large artery with radius R and length L, and the load impedance at its outlet $ZOut$.
- $r(l)$, $rBot(l)$ and $l(i)$ as the functions that return the radius at the top, the radius at the bottom, and the length of the large artery i, respectively.

Algorithm 2 Recursive computation of the load impedance for a large artery.

```
1: Global alpha, beta                                              ▷ Parameters
2: function ImpedanceLarge(i)
3:     if r ≤ 2e − 3 then                                          ▷ Large artery branches
4:         iR ← IdR(i)
5:         iL ← IdL(i)
6:         ZR ← f(ImpedanceLarge(iR), l(iR), r(iR))
7:         ZL ← f(ImpedanceLarge(iL), l(iL), r(iL))
8:         ZOut ← 1/(1/ZR + 1/ZL)
9:     else                                                        ▷ Small artery interface
10:        ZR ← ImpedanceSmall(alpha ∗ r(i))
11:        ZL ← ImpedanceSmall(beta ∗ r(i))
12:        ZOut ← 1/(1/ZR + 1/ZL)
13:    end if
14:    return ZOut
15: end function
```

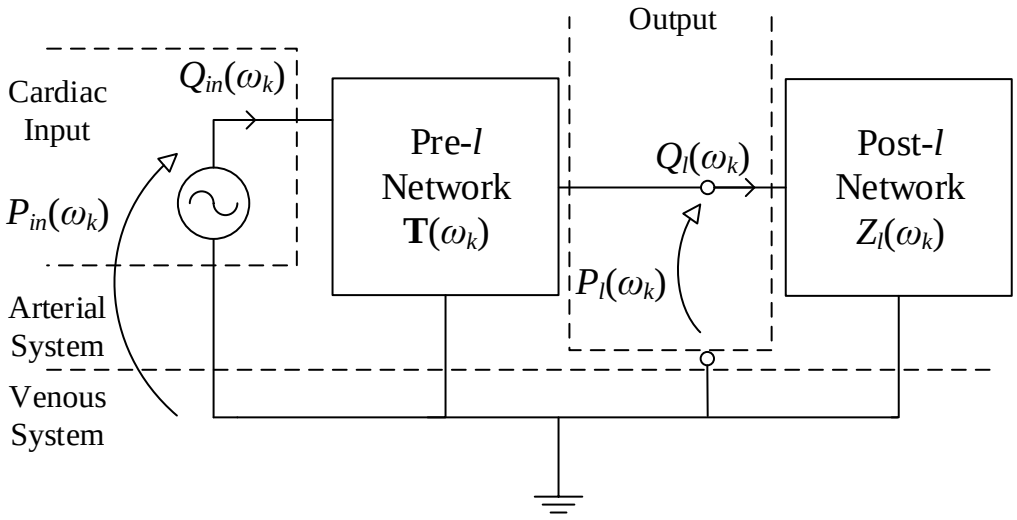

Figure 12. Overview of the transmission line network of the cardiovascular system.

- $IdR(i)$ and $IdL(i)$ as the functions that return the index of the large artery branching out of the artery i to the right and to the left, respectively.

These functions are based on the data provided in Table 1 and the topology of the large arteries in Fig. 21.

We present in this section the expression of the transfer matrix $\mathbf{T}(\omega_k)$. This transfer matrix represents the propagation effect of the cardiovascular network between the heart where the cardiac input $Q_{in}(\omega_k)$ is pumped and an artery l experiencing a blood flow $Q_l(\omega_k)$ and a pressure $P_l(\omega_k)$.

3.4.4 General Transfer Matrix and Load Impedance

The part of the cardiovascular vascular system between the heart and the artery l in the direction of the flow is called here the *pre-l network*, and the part between the artery l and the venous system in the direction of the flow is called the *post-l network* as illustrated in Fig. 12.

- The *pre-l network* is characterized by a a transfer matrix $\mathbf{T}(\omega_k)$ that imposes a linear relationship between the cardiac input $Q_{in}(\omega_k)$, the pressure exerted by the heart $P_{in}(\omega_k)$, the blood flow $Q_l(\omega_k)$, and the pressure $P_l(\omega_k)$ in the artery l as follows:

$$\begin{bmatrix} P_{in}(\omega_k) \\ Q_{in}(\omega_k) \end{bmatrix} = \mathbf{T}(\omega_k) \begin{bmatrix} P_l(\omega_k) \\ Q_l(\omega_k) \end{bmatrix}, \tag{31}$$

  where $A(\omega_k)$, $B(\omega_k)$, $C(\omega_k)$, and $D(\omega_k)$ are the matrix elements of $\mathbf{T}_l(\omega_k)$:

$$\mathbf{T}(\omega_k) = \begin{bmatrix} A(\omega_k) & B(\omega_k) \\ C(\omega_k) & D(\omega_k) \end{bmatrix}. \tag{32}$$

- The *post-l network* is characterized by a load impedance $Z_l(\omega_k)$ that imposes a relationship between the blood flow $Q_l(\omega_k)$ and the pressure $P_l(\omega_k)$ in artery l as follows:

$$P_l(\omega_k) = Z_l(\omega_k) Q_l(\omega_k). \tag{33}$$

We have previously presentend the algorithms that return the load impedance $Z_l(\omega_k)$ for a small artery l in Sec. 3.4.2.1 and for a large artery l in Sec. 3.4.3.2.

By cascading the transfer matrices [45] of all large arteries m carrying blood from the heart to the large artery l and the transfer matrices of large artery branches along this path (cf. Fig. 13), the transfer matrix $\mathbf{T}(\omega_k)$ for a large artery is calculated as follows:

$$\mathbf{T}(\omega_k) = T_1(\omega_k) \prod_{m \in \mathrm{L}_l} \begin{bmatrix} A_m(\omega_k) + \frac{B_m(\omega_k)}{Z_{m'}(\omega_k)} & B_m(\omega_k) \\ C_m(\omega_k) + \frac{D_m(\omega_k)}{Z_{m'}(\omega_k)} & D_m(\omega_k) \end{bmatrix}, \tag{34}$$

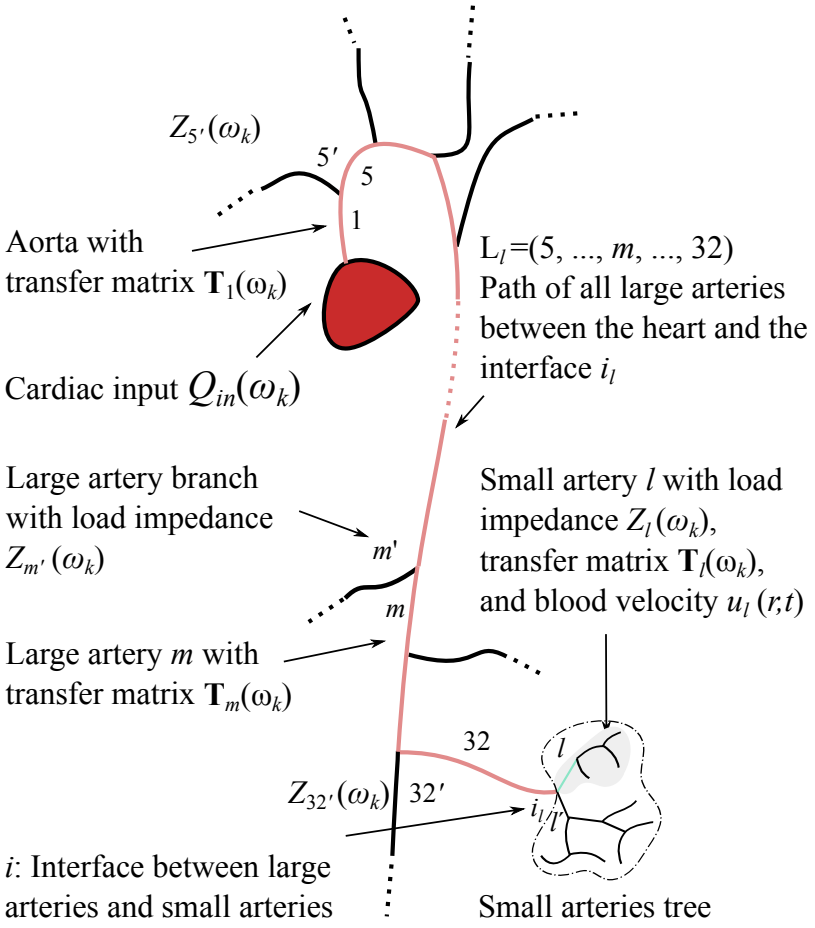

Figure 13. Path between the cardiac input and a small artery *l*.

where $\mathrm{L}_l = (..., m, ..., l-1, l)$ is the sequence of all large arteries carrying blood from the heart to the artery l, $A(\omega_k)$, $B(\omega_k)$, $C(\omega_k)$, and $D(\omega_k)$ are the matrix elements of the transfer matrix $\mathbf{T}_m(\omega_k)$ of an artery m (27), $T_1(\omega_k)$ is the transfer matrix of the aorta (the large artery directly connected to the heart), $T_l(\omega_k)$ is the transfer matrix of the artery l, whether it is a small artery (17) or a large artery (27), and $Z_{m'}(\omega_k)$ is the load impedance of the artery m' parallel to m (See Fig. 13).

For a small artery, we further multiply by the small artery transfer matrix as follows:

$$\mathbf{T}(\omega_k) = T_1(\omega_k) \prod_{m \in \mathrm{L}_l} \begin{bmatrix} A_m(\omega_k) + \frac{B_m(\omega_k)}{Z_{m'}(\omega_k)} & B_m(\omega_k) \\ C_m(\omega_k) + \frac{D_m(\omega_k)}{Z_{m'}(\omega_k)} & D_m(\omega_k) \end{bmatrix} T_l(\omega_k)\,, \tag{35}$$

where $\mathrm{S}_{i_l} = (..., m, ..., i_l)$ is the sequence of all large arteries carrying blood from the heart to the interface i_l of the tree of small arteries to which l belongs.

3.4.5 Blood Velocity

The objective of this section is to present the expression of the blood velocity $u_l(r,t)$ given the cardiac input $Q_{in}(\omega_k)$, the transfer matrix $\mathbf{T}(\omega_k)$, and the load impedance $Z_l(\omega_k)$ which were expressed in the preceding section.By connecting a pre-l network with load impedance $Z_l(\omega_k)$ to the post-l network with transfer matrix $\mathbf{T}(\omega_k)$, we enforce the equations (31) and (33), and we collapse the two-port network into a one-port network. Therefore, we eliminate the pressures $P_{in}(\omega_k)$ and $P_l(\omega_k)$, and the harmonic flow $Q(\omega_k)_l$ in the artery l can be computed directly from the cardiac input $Q_{in}(\omega_k)$ by:

$$Q_l(\omega_k) = \frac{Q_{in}(\omega_k)}{Z_l(\omega_k)C(\omega_k) + D(\omega_k)}\,, \tag{36}$$

where $C(\omega_k)$ and $D(\omega_k)$ are the first and second elements of the second row of the transfer matrix representing the cardiovascular network between the heart and the artery l sampled at angular frequency ω_k respectively, and $Z_l(\omega_k)$ is the harmonic impedance of the artery l.

We can get the blood velocity $u_l(r,t)$ as function of r, the distance from the axis of the

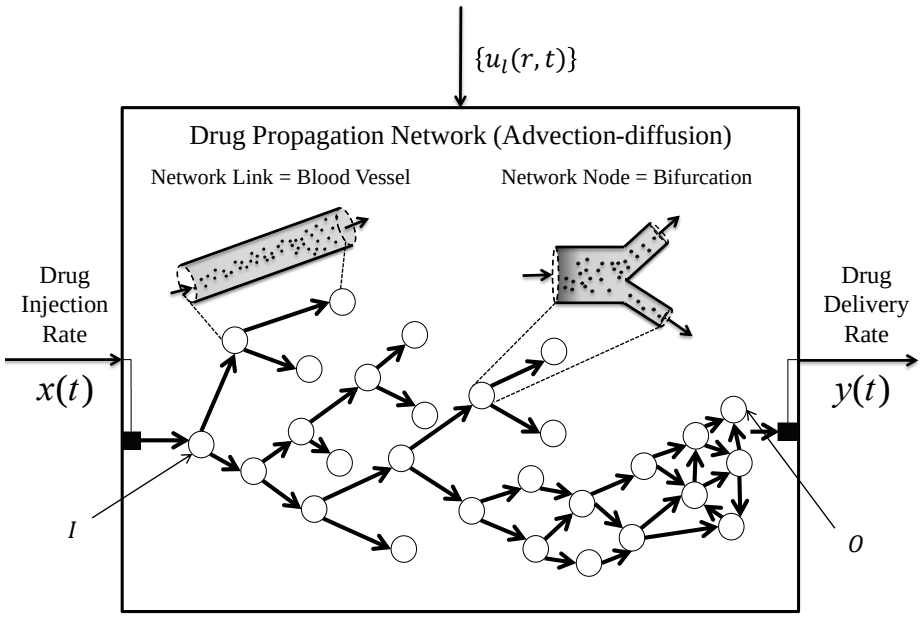

Figure 14. Drug propagation network model.

vessel, and the time t from the periodic blood flow in the time-domain $q_l(t)$ by assuming a parabolic profile for the blood velocity, which gives:

$$u_l(r,t) = \frac{1 - \frac{r^2}{r_l^2}}{\pi r_l^2} \sum_{k=-\infty}^{+\infty} Q_l(\omega_k) e^{j\omega_k t} \,. \tag{37}$$

3.5 Drug Propagation Network Model

The drug propagation network model allows to compute the drug delivery rate $y(t)$ at the targeted site as function of the time t from the knowledge of the blood velocity $u_l(r,t)$ in every artery l of the cardiovascular system, function of the distance r from the artery axis and the time t, computed through the cardiovascular network model detailed in Sec. 3.4. The drug propagation network model stems from the solutions to the advection-diffusion equation expressed in (6), and it is composed of the following elements:

- **Artery Link Models**. An artery link is defined as the arterial blood vessel segment which connects two adjacent bifurcations. The artery link models are derived from the *solution to the General Taylor Dispersion equation* [48], which is a simplification

of the advection-diffusion equation (6) in case of advection in a cylindrical pipe. Each artery link l model is expressed by a Linear Periodically Time-Varying (LPTV) impulse response $h_l^{link}(t, t')$ as function as function of the time variables t and t', as detailed in Sec. 3.5.1.

- **Junction Node Models**. A junction node is defined as the arterial location where an incoming blood flow is split into two outgoing diverging flows. The junction node models are derived from the *principle of mass conservation* [49] in fluid mechanics, and each junction node n model is expressed by an LPTV impulse response $h_n(t, t')$, as detailed in Sec. 3.5.2.

- **Bifurcation Node Models**. A bifurcation node is defined as the venal location where two incoming blood flows are joined into one single flow. Similarly, the bifurcation node n is characterized by an LPTV impulse response $h_n(t, t')$, as detailed in Sec. 3.5.3.

From the knowledge of the location of injection I and the targeted site O, the **Drug Propagation Network Model** is expressed by a LPTV impulse response $h_{I,O}(t, t')$ as function of the time variables t and t', through which we compute the drug delivery rate $y(t)$ given the drug injection rate $x(t)$, functions of the time t, as follows:

$$y(t) = \int_{-\infty}^{+\infty} h_{I,O}(t, t')x(t')\,dt' \,. \tag{38}$$

In Sec. 3.5.4 we detail the procedure to compute the expression of the LPTV impulse response $h_{I,O}(t, t')$, function of the time t and the periodic time variable t', by applying the Harmonic Transfer Matrix (HTM) theory [35] to the artery link and bifurcation node models.

3.5.1 Artery Link Models

The model of the artery link l, as illustrated in Fig. 15, corresponds to the relation between the drug delivery rate $y_l(t)$ at the output of the artery link and a drug injection rate $x_l(t)$ at

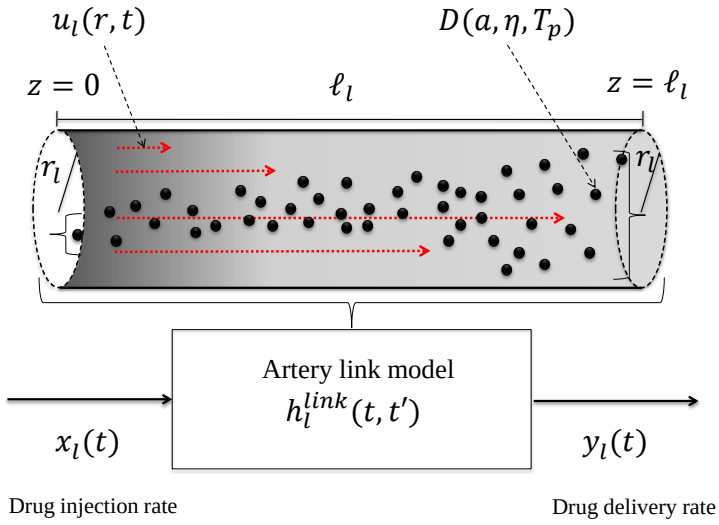

Figure 15. A segment of a blood vessel modeled as an artery link.

the input of the artery link l, functions of the time t. This model is expressed through the LPTV impulse response $h_l^{link}(t,t')$, function of the time variables t and t', as follows:

$$y_l(t) = \int_{-\infty}^{+\infty} h_l^{link}(t,t')x_l(t')dt' \,. \tag{39}$$

The LPTV impulse response $h_l^{link}(t,t')$, function of the time variables t and t', corresponds to the the drug particle concentration $c_l(z,t)$ at the artery link longitudinal coordinate $z=\ell_l$ when the drug injection rate $x_l(t)$ at the input of the artery link l is equal to a Dirac delta $\delta(t-t')$ centered at time t'. This is expressed as follows:

$$h_l^{link}(t,t') = c_l(\ell_l,t)|_{x_l(t)=\delta(z)\delta(t-t')} \,, \tag{40}$$

where ℓ_l is the length of the artery link l.

The drug particle concentration $c_l(\ell_l,t)$ is computed through the inhomogeneous advection-diffusion equation [38], simplified into the inhomogeneous General Taylor Dispersion equation [48], since in the artery link the drug particles are subject to advection in a cylindrical pipe.

The inhomogeneous General Taylor Dispersion equation when the input drug injection

rate is equal to a Dirac delta $\delta(t-t')$ centered at time t' is expressed as follows:

$$\frac{\partial c_l(z,t)}{\partial t} + \bar{u}_l(t)\frac{\partial c_l(z,t)}{\partial z} = \delta(z)\delta(t-t') + D_l^{eff}(t)\frac{\partial^2 c_l(z,t)}{\partial z^2}\,, \tag{41}$$

where $c_l(z,t)$ is the drug particle concentration at longitudinal coordinate z in the artery link l, $\bar{u}_l(t)$ is the average cross-sectional velocity in the artery link l, defined as

$$\bar{u}_l(t) = \frac{2}{{r_l}^2}\int_0^{r_l} r u_l(r,t)dr\,, \tag{42}$$

where $u_l(r,t)$ is the blood velocity at the output of the artery l as function of the distance r from the artery axis and the time t. $D_l^{eff}(t)$ is the effective diffusivity [48] in the artery link l, expressed as follows:

$$\begin{aligned} D_l^{eff}(t) = D &- \frac{{r_l}^3\bar{u}_l^2(t)}{8D} \\ &+ \frac{2}{Dr_l}\int_0^R r\bar{u}_l(t)\int_0^r \frac{1}{r'}\int_0^{r'} r''u_l(r'',t)dr''dr' \\ &- \frac{2}{Dr_l}\int_0^R r u_l(r,t)\int_0^r \frac{1}{r'}\int_0^{r'} r''u_l(r'',t)dr''dr' \\ &+ \frac{2}{Dr_l}\int_0^R \frac{r^3}{4}\bar{u}_l(t)u_l(r,t)dr\,, \end{aligned} \tag{43}$$

where r_l is the radius of the artery link, and D is the diffusion coefficient [50] of the drug particles in the blood, whose expression is

$$D = \frac{K_B T_p}{6\pi\eta a}\,, \tag{44}$$

where K_B is the Boltzmann's constant, T_p is the blood absolute temperature, η is the intrinsic viscosity of the particle, which depends on the geometry of the drug particles, and a is the radius of the drug particles.

To obtain the expression of the drug particle concentration $c_l(\ell_l,t)$, we apply the Fourier transform [51] $\mathcal{F}\{\cdot\}$ with respect to the variable z, which is the longitudinal coordinate in

the artery, to both terms of the advection-diffusion equation (41), which results in

$$\frac{\partial}{\partial t}\mathcal{F}\left\{c_l(z,t)\right\} + 2i\pi\xi\bar{u}_l(t)\mathcal{F}\left\{c_l(z,t)\right\} = \delta(t-t')\,, \qquad (45)$$
$$+4\pi^2\xi^2 D_l^{eff}(t)\mathcal{F}\left\{c_l(z,t)\right\}$$

where ξ is the frequency variable along the artery link longitudinal coordinate z. Using Green's method for solving inhomogeneous differential equations [52], we obtain

$$\mathcal{F}\left\{c_l(z,t)\right\} = \exp -\left(\pi^2\frac{\sigma_l^2(t,t')}{2}\xi^2 + 2i\pi\xi\mu_l(t,t')\right)U(t-t')\,, \qquad (46)$$

where $U(\cdot)$ is the Heaviside step function [53], and where $\mu_l(t,t')$ corresponds to the particle displacement as function of the time variables t and t'. It depends on the average cross-sectional velocity $\bar{u}_l(t)$ in the artery link l as follows:

$$\mu_l(t,t') = \int_{t'}^{t}\bar{u}_l(\tau)d\tau\,, \qquad (47)$$

and $\sigma_l(t,t')$ corresponds to the particles spread as function of the time variables t and t'. It depends on the effective diffusivity $D_l^{eff}(t)$ of the particles (43), and the radius of the link r_l:

$$\sigma_l^2(t,t') = \left|2\int_{t'}^{t}D_l^{eff}(\tau)d\tau\right|. \qquad (48)$$

Finally, the expression of the LPTV impulse response $h_l^{link}(t,t')$ is obtained through the inverse Fourier transform [51] of (46) computed at the artery link longitudinal coordinate $z = \ell_l$, which has the following expression:

$$h_l^{link}(t,t') = \frac{1}{\sqrt{2\pi\sigma_l^2(t,t')}}\exp\left(-\frac{(\ell_l-\mu_l(t,t'))^2}{2\sigma_l^2(t,t')}\right), \qquad (49)$$

where $\mu_l(t,t')$ is given by (47), $\sigma_l^2(t,t')$ is given by (48), and ℓ_l is the length of the artery link l.

3.5.2 Junction Node Model

The model of a junction node n, as illustrated in Fig. 16, corresponds to the relation between the drug delivery rates $y_n(t)$ at the output branch of the junction node n and a drug injection

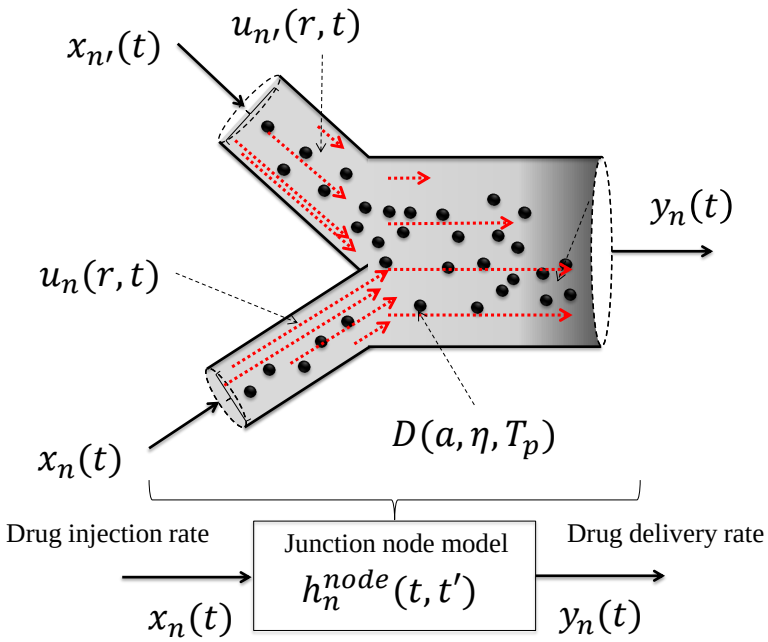

Figure 16. A blood vessel junction modeled as a cardiovascular network node.

rate $x_n(t)$ at the input of the bifurcation node n, functions of the time t. This model is expressed through the LPTV impulse response $h_n^{node}(t,t')$, function of the time variables t and t', as follows:

$$y_n(t) = \int_{-\infty}^{+\infty} h_n^{node}(t,t')x_n(t')dt'. \tag{50}$$

To compute the LPTV impulse response $h_n^{node}(t,t')$, function of the time variables t and t', we assume that in a junction node the propagation of the drug particles is given mainly by their advection in the blood flows, while the contribution of their diffusion is negligible. Under this assumption, the relation between drug delivery rate $y_n(t)$ of the junction node n and a drug injection rate $x_n(t)$ at the input of the bifurcation node n, functions of the time t is computed through the the *principle of mass conservation* [49] in fluid mechanics, which is expressed as follows:

$$y_n(t) = \frac{\bar{u}_n(t) + \bar{u}_{n'}(t)}{\bar{u}_n(t)} x_n(t)\,, \tag{51}$$

where n' is the index of the sister of the input branch n, $\bar{u}_n(t)$ and $\bar{u}_{n'}(t)$ are the average cross-sectional blood velocities at the input branches indexed by n and n', respectively. As a consequence, by comparing the expressions in (50) and (51), we obtain the following

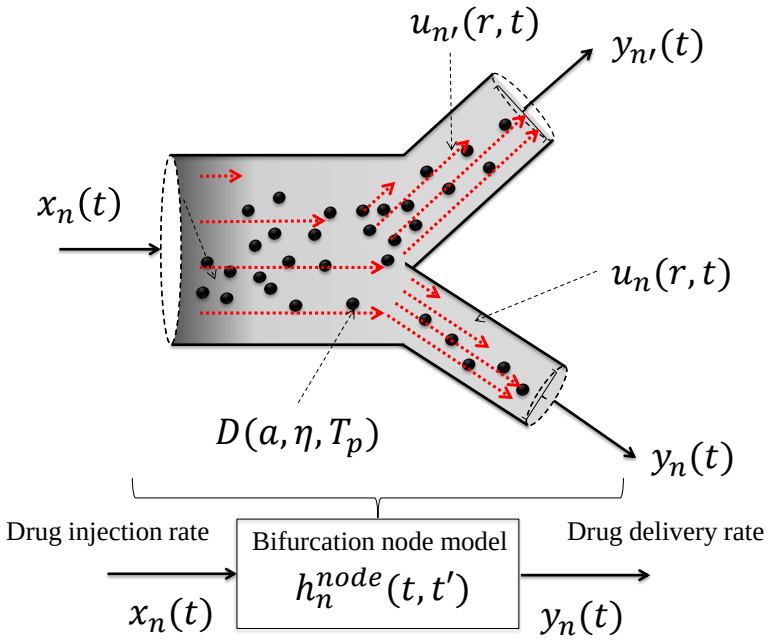

Figure 17. A blood vessel bifurcation modeled as a cardiovascular network node.

expression for the LPTV impulse response $h_n^{node}(t,t')$ as function of the time variables t and t':

$$h_n^{node}(t,t') = \frac{\bar{u}_n(t) + \bar{u}_{n'}(t)}{\bar{u}_n(t)}\delta(t)\,, \tag{52}$$

where $\delta(t)$ is the Dirac delta time function, n is the index of the junction node input branch, and n' is the index of the sister of the input branch n.

3.5.3 Bifurcation Node Model

The model of a bifurcation node n, as illustrated in Fig. 17, corresponds to the relation between the drug delivery rates $y_n(t)$ at the output branch of the junction node n and a drug injection rate $x_n(t)$ at the input of the bifurcation node n, functions of the time t. Similarly, this model is characterized by an LPTV impulse response $h_n^{node}(t,t')$, function of the time variables t and t', as follows:

$$h_n^{node}(t,t') = \delta(t)\,, \tag{53}$$

This relationship stems from the fact that the concentration is continuous in a bifurcation node.

3.5.4 LPTV Impulse Response of the Drug Propagation Network Model

The LPTV impulse response $h_{I,O}(t,t')$ of the drug propagation network model having location of injection I and the targeted site O, as function of the time variables t and t', is computed from the Fourier coefficient $h_k(\tau)$ as follows:

$$h_{I,O}(t,t') = \sum_{k=0}^{\infty} h_k(t-t') e^{jk\omega_0(t-t')}\,, \tag{54}$$

where ω_0 is the angular heartbeat frequency, and each Fourier coefficient $h_k(\tau)$ is computed from the equivalent HTM $\mathbf{H}_{I,O}(s)$ of the drug propagation network model through the following expression:

$$h_k(\tau) = \sum_{n=-(m-|k|)}^{m-|k|} \{\mathbf{H}_{I,O}(s)\}_{k+n,n}\Big|_{s=0} e^{jn\omega_0\tau}\,, \tag{55}$$

where m is the matrix truncation index, $|.|$ is the absolute value operator, and $\{\mathbf{H}_{I,O}(s)\}_{k+n,n}$ denotes the element of the equivalent HTM $\mathbf{H}_{I,O}(s)$ of the drug propagation network model having $k+n$-th row and n-th column indexes. The equivalent HTM $\mathbf{H}_{I,O}(s)$ of the drug propagation network model is computed by applying the HTM theory to the LPTV impulse response $h_l^{link}(t,t')$ and $h_n^{node}(t,t')$ of the artery link and the bifurcation node models, respectively. This is achieved by considering that both $h_l^{link}(t,t')$ and $h_n^{node}(t,t')$ are periodic with period T, which is the heartbeat period, with respect to both time variables t and t', expressed as

$$\begin{aligned} h_l^{link}(t+T,t'+T) &= h_l^{link}(t,t') \\ h_n^{node}(t+T,t'+T) &= h_n^{node}(t,t')\ \forall t,t' \in R\,. \end{aligned} \tag{56}$$

This periodicity allows to compute Fourier series [51] coefficients for both $h_l^{link}(t,t')$ and $h_n^{node}(t,t')$.

$$h_k^{model,m}(\tau) = \frac{1}{T}\int_0^T h_k^{model}(t,t-\tau) e^{-jk\omega_0 t} dt\,, \tag{57}$$

where *model* and m correspond either to *link* and l, or to *node* and n, respectively, ω_0 is the angular heartbeat frequency, and τ is an auxiliary time variable. According to the Fourier series theory [51], we can express the relation between the drug delivery rate $y_m(t)$ at the output and a drug injection rate $x_m(t)$ at the input of an artery link or a bifurcation model as

$$y_m(t) = \sum_{k=-\infty}^{k=+\infty} e^{jk\omega_0 t} \int_{-\infty}^{+\infty} h_k^{model,m}(\tau) x_m(t-\tau) d\tau. \tag{58}$$

If we define $Y_m(s)$, $H_k^{model,m}(s)$, and $X_m(s)$ as the respective Laplace transforms of $y_m(t)$, $h_k^{model,m}(\tau)$, and $x_m(t)$, Equation (58) becomes

$$Y_m(s) = \sum_{k=-\infty}^{k=+\infty} H_k^{model,m}(s - jk\omega_0) X_m(s - jk\omega_0). \tag{59}$$

The expression in (59) can be transformed into a matrix multiplication by defining the infinite-dimensional vectors $\underline{Y}_m(s)$, $\underline{X}_m(s)$, and the doubly infinite matrix $\mathbf{H}_m^{model}(s)$ as:

$$\underline{X}_m(s) = \left[X_m(s + jk\omega_0)\right]'_{k\in\mathbb{Z}} \tag{60}$$

$$\underline{Y}_m(s) = \left[Y_m(s + jk\omega_0)\right]'_{k\in\mathbb{Z}} \tag{61}$$

$$\mathbf{H}_m^{model}(s) = \left[H_k^{model,p-q}(s + jq\omega_0)\right]_{p,q\in\mathbb{Z}}, \tag{62}$$

where $[\cdot]'$ denotes the matrix transpose operation. As a consequence, the expression (59) is transformed into a linear matrix relationship:

$$\underline{Y}_m(s) = \mathbf{H}_m^{model}(s)\underline{X}_m(s)\,. \tag{63}$$

$\mathbf{H}_m^{model}(s)$ is the Harmonic Transfer Matrix (HTM) of the arterial link l, in case $model = link$ and $m = l$, or the bifurcation node n, in the case where $model = node$ and $m = n$. In practice, the infinite matrices $\mathbf{H}_m^{model}(s)$ and the vectors $\underline{Y}_m(s)$ and $\underline{X}_m(s)$, are truncated to contain only the significant harmonics [54].

Using the HTM for every link and node, it becomes possible to obtain the HTM $\mathbf{H}_{I,O}(s)$ of the drug propagation network model between the location of injection I and the targeted site O, which allows to compute the LPTV impulse response $h_{I,O}(t,t')$ through the expressions in (55) and (54). This is accomplished using the two following rules:

- The *cascade rule*, which states that the harmonic transfer matrix $\mathbf{H}^{\circ}_{m,m'}(s)$ of the cascade of two network models m and m', which can be links, nodes, or combination thereof, is obtained by multiplying their respective harmonic transfer matrices $\mathbf{H}^{model}_{m}(s)$ and $\mathbf{H}^{model'}_{m'}(s)$ as follows:

$$\mathbf{H}^{\circ}_{m,m'}(s) = \mathbf{H}^{model}_{m}(s)\mathbf{H}^{model'}_{m'}(s)\,. \tag{64}$$

- The *parallel rule*, which states that the harmonic transfer matrix $\mathbf{H}^{\|}_{m,m'}(s)$ of the parallel of two network models m and m', which can be links, nodes, or combination thereof, is obtained by summing their respective harmonic transfer matrices $\mathbf{H}^{model}_{m}(s)$ and $\mathbf{H}^{model'}_{m'}(s)$ as follows:

$$\mathbf{H}^{\|}_{m,m'}(s) = \mathbf{H}^{model}_{m}(s) + \mathbf{H}^{model'}_{m'}(s)\,. \tag{65}$$

By using the cascade rule (64) and the parallel rule (65), the HTM $\mathbf{H}_{I,O}(s)$ of the drug propagation network model between the location of injection I and the targeted site O is:

$$\mathbf{H}_{I,O}(s) = \sum_{p\in P(I,O)} \prod_{(l,n)\in p} \mathbf{H}^{link}_{l}(s)\mathbf{H}^{node}_{n}(s)\,, \tag{66}$$

where $P(I,O)$ is the set of parallel paths p linking the location of injection I to the targeted site O. Every path $p \in P(I,O)$ is a sequence of link l and node n couples (l,n) ($p = \{...,(l,n),...\}$). Finally, the LPTV impulse response $h_{I,O}(t,t')$ is computed by applying (66) to the expressions in (55) and (54).

3.6 Numerical results

3.6.1 Topology

As a numerical application of our model, we choose to study drug propagation between one location of injection I and four different targeted sites O_2, O_4, O_8, and O_{17}. These locations are different points in the small artery tree taking root at the renal artery as represented in Fig. 18. The blood velocity calculation takes into account the numerical values for large

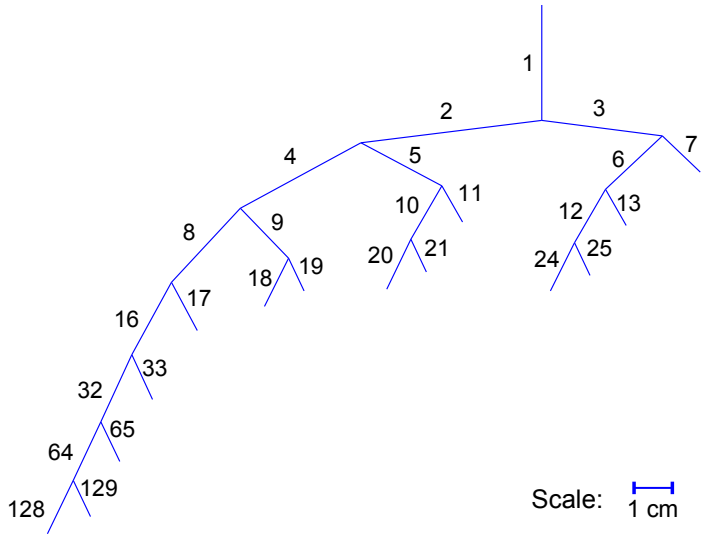

Figure 18. Tree of small arteries at the end of the renal artery with their corresponding link numbers.

arteries dimensions presented in Table 1 and their topology represented in Fig. 21 collected from anatomical data [37].

In Fig. 18, the geometry of the renal arterial tree is illustrated. The topology reflecting the asymmetry of small arteries geometry and their reducing lengths are explained in 3.4.2. The numbers in the figures correspond to the link indexes l. The arteries with radius r_l inferior to $r_{min} = 0.8mm$ are not included, in fact, when the artery radius is smaller than $r_{min} = 0.8mm$, the subtree is truncated, and replaced with a leaf with null hydraulic impedance as explained in Sec. 3.4.2.1. where γ is called the asymmetry ratio and ξ is a parameter that characterizes the turbulence of the flow. Physiological studies yield values $\gamma = 0.41$ of the asymmetry ratio and $\xi = 2.76$, which characterizes the turbulence of the flow. Using these values, we get asymmetry factors $\alpha = 0.9$ and $\beta = 0.6$.

3.6.2 Cardiovascular Network Model

The blood velocity network model was validated against the magnetic resonance measurements made available by [55], which was used to validate a model implemented numerically by finite difference methods. Fig. 19 compares the flow rate measurements in three locations of the cardiovascular system, namely, the descending aorta, the iliac, and the femoral arteries, with the flow rates obtained using the transmission line model developed

in Sec. 3.4. We see a very good agreement between the experimental measurements and the results of the developed model. We used the same topology as in [55], and we used the flow measured in the aortic arc as an input to the cardiovascular network model.

3.6.3 Drug Propagation Network

The LPTV impulse response $h(t, t')$ is calculated for a fixed location of injection I set at the inlet of the arterial tree, and different targeted sites O_2, O_4, O_8, and O_{17}, located respectively at the outlet of links 2, 4, 8, and 17. A change of variables is performed on $h(t, t')$ for a better representation, such that $h'(t, \tau) = h(t, t - \tau)$. t is the periodic time variable, in which the LPTV impulse response is T-periodic:$h'(t, \tau) = h'(t + T, \tau)$. τ is the propagation time variable: $h(t, \tau) \to 0$ as $\tau \to +\infty$. A 3D representation of the functions $h'(t, \tau)$ is rendered in Fig. 20. In Fig. 20a, we can observe the LPTV impulse response goes to zero after a propagation period of $1200ms$. It can be seen that the time-variance is significant. In fact, we obtain two main peaks in the impulse response for the link 2 in Fig. 20 b), separated by an important fading, due to the considerable blood velocity fluctuations in that artery. In Fig. 20e, the drug propagates through link 2 with LPTV impulse response $h_2^{link}(t, \tau)$, with radius $r_2 = 2.5mm$, and a link 2 with LPTV impulse response $h_4^{link}(t, \tau)$, with radius $r_4 = 2.2mm$, passing by a node 2 with LPTV impulse response $h_2^{node}(t, \tau)$. Due to the bifurcation, the cascading of these two links and node causes a spread of the delay and slower convergences to zero of the equivalent LPTV impulse response between I and O_4. In Fig. 20g, the drug propagates through an additional node 4 with LPTV impulse response $h_2^{node}(t, \tau)$, and an additional link 8 with LPTV impulse response $h_8^{link}(t, \tau)$. The bifurcation effect is slightly more pronounced here, with a considerable portion of the drug rate that is lost at the node. The drug delivery rate experiences a drop after the the peak and then converges slowly to zero which would cause a dispersion of the drug between I and O_8. In the preceding examples, we chose a path through the left links which, by geometrical asymmetry, experience a higher blood velocity compared with the right links. In Fig. 20e,

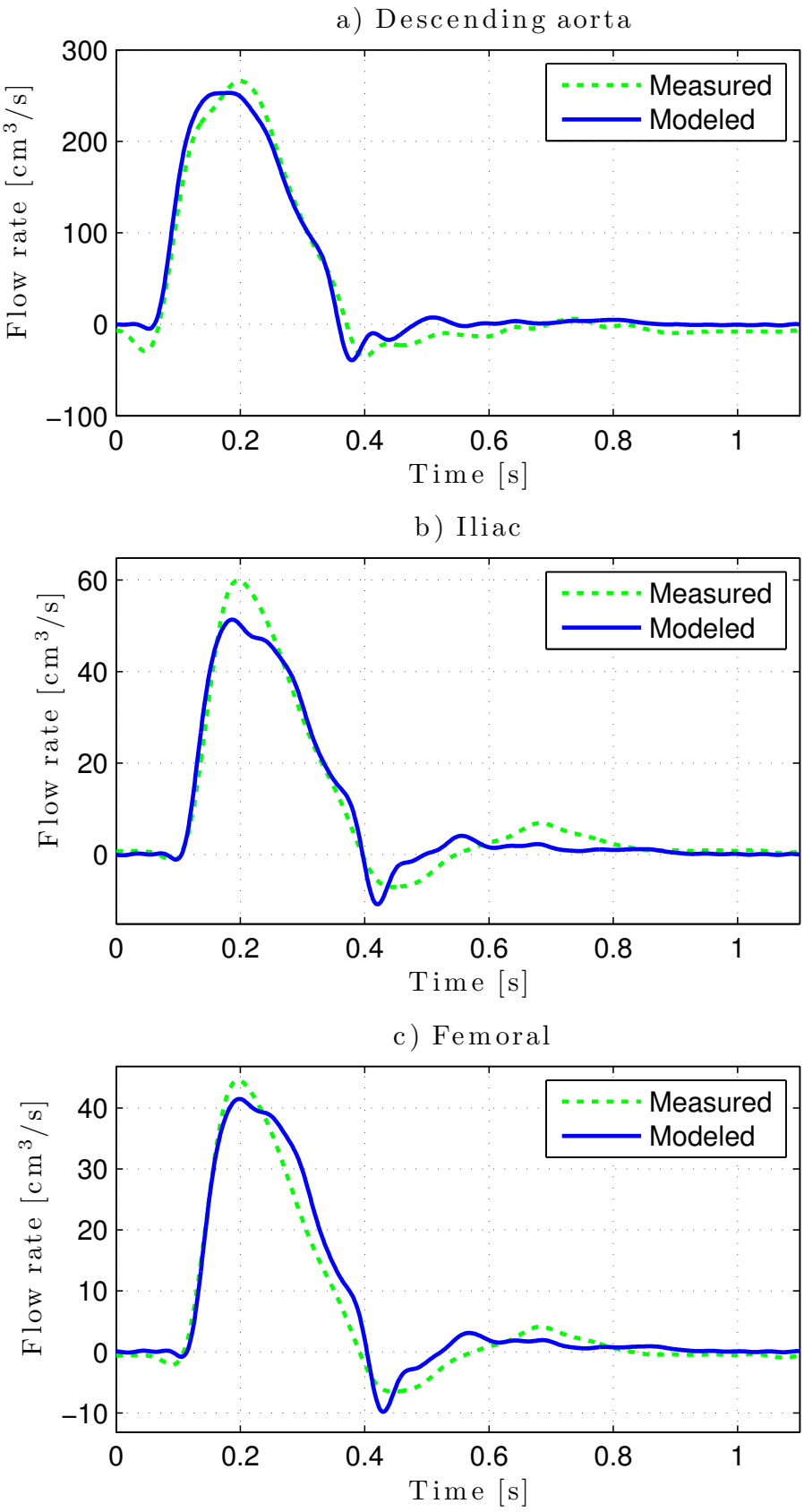

Figure 19. Comparison of the flow rates calculated using the transmission line model with physiological measurements in various locations of the cardiovascular system.

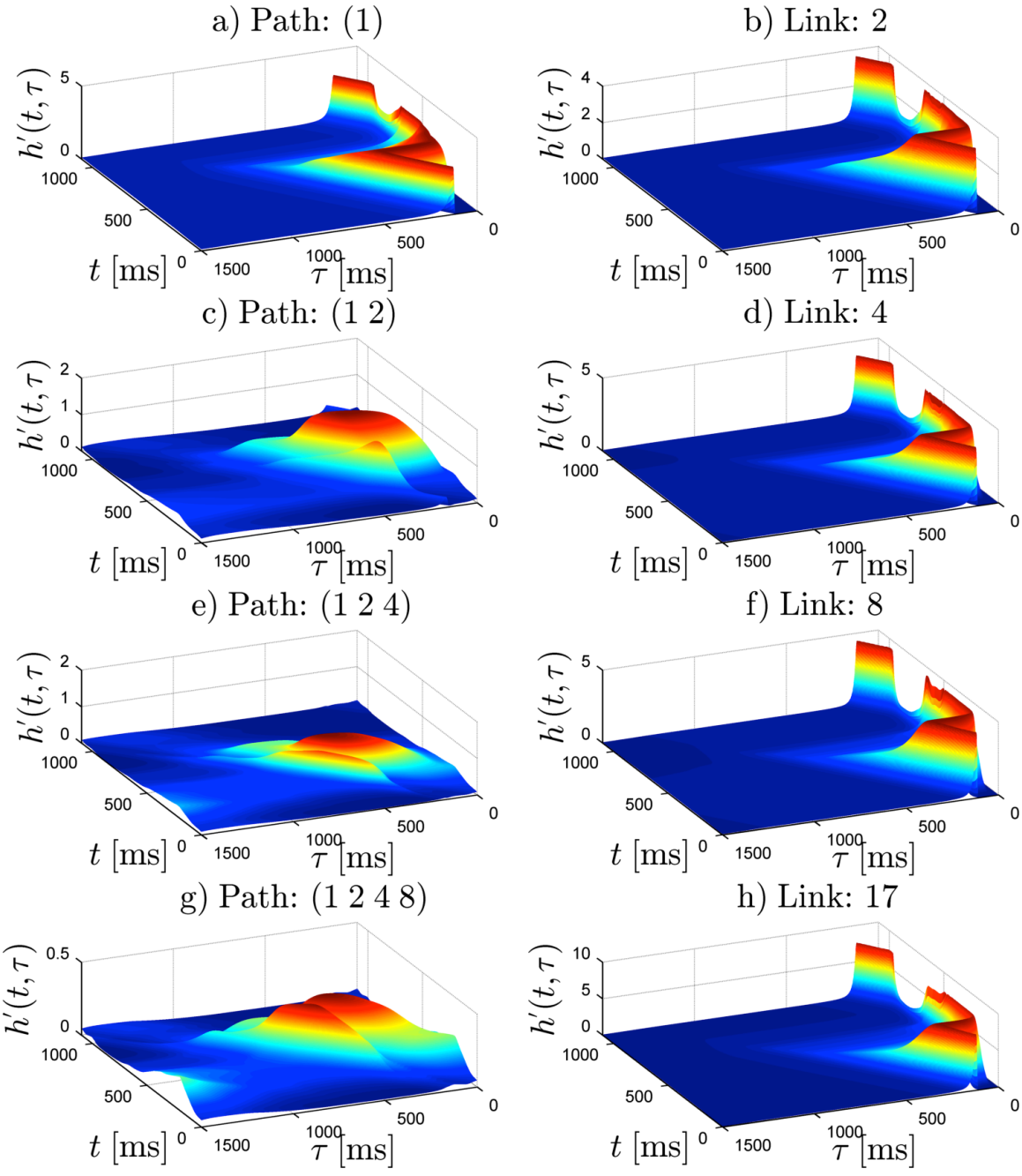

Figure 20. Time-varying impulse response for different vessel topologies.

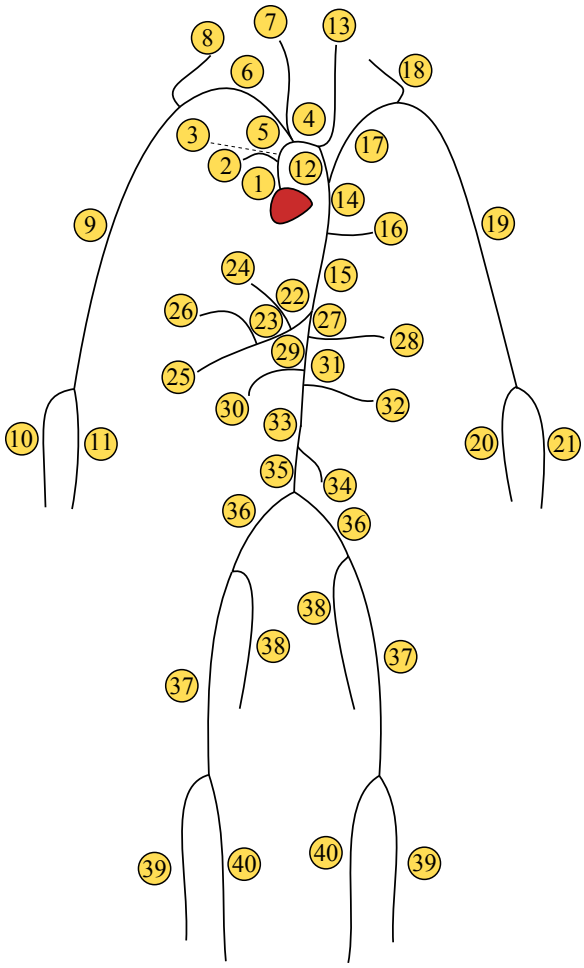

Figure 21. Topology of large arteries.

we consider that the drug network includes an additional node 8 with LPTV impulse response $h_8^{node}(t,\tau)$, and an additional link 17 with LPTV impulse response $h_{17}^{link}(t,\tau)$ which is positioned to the right. Since the node 8 relays most of the drug rate to the left link which has much higher effective diffusivity, a more significant portion is lost to the left link. The asymmetry of the small arteries tree causes most of the drug to be propagated in the left-most blood links in the tree of small arteries. Here, the dispersion is more pronounced, and the reflections from the preceding nodes is apparent.

Table 1. List of large arteries and their dimensions

Index l	Name	$\ell_l[cm]$	$r_l^{top}[cm]$	$r_l^{bot}[cm]$
1	Ascending aorta	1	1.525	1.502
3	Ascending aorta	3	1.502	1.42
4	Aortic arch	3	1.42	1.342
12	Aortic arch	4	1.342	1.246
14	Thoracic aorta	5.5	1.246	1.124
15	Thoracic aorta	10.5	1.124	0.924
27	Abdominal aorta	5.25	0.924	0.838
29	Abdominal aorta	1.5	0.838	0.814
31	Abdominal aorta	1.5	0.814	0.792
33	Abdominal aorta	12.5	0.792	0.627
35	Abdominal aorta	8	0.627	0.55
36	External iliac	5.75	0.4	0.37
37	Femoral	14.5	0.37	0.314
40	Femoral	44.25	0.314	0.2
38	Internal iliac	4.5	0.2	0.2
39	Deep femoral	11.25	0.2	0.2
2	Coronaries	10	0.35	0.3
5	Brachiocephalic	3.5	0.95	0.7
6,17	Subclavians	3.5	0.425	0.407
9,19	Brachials	39.75	0.407	0.25
10,21	Radials	22	0.175	0.175
11,20	Ulnars	22.25	0.175	0.175
8,18	Vertebrals	13.5	0.2	0.2
7	R. carotid	16.75	0.525	0.4
13	L. carotid	19.25	0.525	0.4
16	Intercostals	7.25	0.63	0.5
28	Sup. mesenteric	5	0.4	0.35
22	Celiac	2	0.35	0.3
23	Hepatic	2	0.3	0.25
24	Hepatic	6.5	0.275	0.25
25	Gastric	5.75	0.175	0.15
26	Splenic	5.5	0.2	0.2
30,32	Renals	3	0.275	0.275
34	Mesenteric	3.75	0.2	0.175

3.7 Conclusions

The goal of a Drug Delivery System (DDS) is to provide a localized drug presence where the medication is needed, while, at the same time, preventing the drug from affecting other healthy parts of the body. Amongst others, the most advanced solutions use drugs composed of micro or nano-sized particles (particulate DDS) that are able to cross barriers to the transit of particles out of the bloodstream. The Molecular Communication (MC) paradigm abstracts the propagation of information between a sender and a receiver realized through mass transport phenomena, since information-bearing molecules have to physically cover the distance from one location to the other. In this chapter, we advocate for the Molecular Communication (MC) paradigm as a straightforward and efficient abstraction of a particulate DDS, thus enabling the control and prediction of particulate drug delivery by using tools from communication engineering.

In this chapter, we realized the molecular communication abstraction of a particulate DDS by developing a MC channel model of the drug particle propagation through the cardiovascular system. For this, we identified two separate contributions within the model, namely, the cardiovascular network model and the drug propagation network model. The cardiovascular network model allows to analytically compute the blood velocity profile in every location of the cardiovascular system from the knowledge of the blood pressure profile and flow input from the heart. The drug propagation network model allows the analytical expression of the drug delivery rate at the targeted site from the knowledge of the drug location of injection and injection rate profile. The derived model takes into account also the individual specificities in the physiological parameters of the cardiovascular system, such as the compliance of the blood vessels, heartbeat rate profile and the heartbeat stroke volume. An example application of the developed model is also presented through numerical results to assess the flexibility and accuracy of the analytical results of this work.

We propose as future work to investigate the safety issues of MC for the human being. First, care should be taken to ensure that the drug concentration does not reach toxic levels

in the body. Second, the interaction with naturally-occurring MC phenomena in the body such as the cell signaling through the endocrine system should be considered. Third, the MC system should be resilient against possible 'malicious' attacks. Such attacks may be undertaken by benign bacterial and viral organisms, which develop defenses against the therapy, or by the immune system which considers the foreign therapeutic agent as an intruder to the body. Safety issues of MC could be studied in analogy with security issues in classical communication systems.

The results detailed in this chapter open up the possibility to study optimization techniques for particulate DDSs which could allow a careful selection of the location of injection and drug injection profile with the goal of obtaining a desired drug delivery profile at a targeted site while minimizing the drug presence in the rest of the cardiovascular system. In addition, the models developed in this research could potentially serve to investigate novel communication techniques for Intra-Body Communication (IBC) networks.

CHAPTER 4

MOLECULAR COMMUNICATION NOISE AND CAPACITY ANALYSIS FOR PARTICULATE DRUG DELIVERY SYSTEMS

4.1 Motivation and Related Work

Particulate Drug Delivery Systems (PDDS) are therapeutic methods that use drug nanoparticles to specifically target the cause of the disease while avoiding to affect other healthy parts of the body. Drug nanoparticles are able to penetrate inside the body cells to deliver therapy, and therefore can bypass all physiological barriers that are in place inside the human body to protect it from foreign elements. The PDDS aims to engineer drug nanoparticles not only in terms of their chemical properties, size, and shape, but also in terms of the injection pattern, location, and other mechanisms that enable the optimal reception of drug nanoparticles by the diseased cells. By analyzing the PDDS, it is possible to know exactly where the drug accumulates in the body, measure the efficiency of the PDDS solution, and optimize the drug injection pattern.

The modeling of complex spatiotemporal dynamics of drug nanoparticles has been identified as one of the major challenges to develop a new generation of efficient therapies [56]. From the drug injection site, to the absorption by diseased cells, the nanoparticles undergo several biophysical processes that are noisy in nature. In this chapter, an analytical noise model of the PDDS in the human body is derived, reflecting all the possible noise effects for the PDDS. First, the drug injection may suffer from imprecision due to the injection device limitations, the pressure difference between the syringe and the blood flow, and the creation of turbulences around the needle. Second, the nanoparticles are randomly dispersed by the possibly turbulent blood flow in an intricate network of irregularly shaped blood vessels, and exhibiting Brownian motion. Third, the penetration of drug nanoparticles to the tissues surrounding the blood vessels is complicated by the stochastic nature of the chemical reactions, and the time-varying mechanical forces interfering with these

chemical reactions.

Our previous work in [57] uses transmission line theory to obtain the blood velocity everywhere in the cardiovascular system, and uses the theory of Taylor dispersion to obtain the deterministic drug propagation in the body from the injection to the delivery point. In this chapter, the Fokker-Planck equation and the theory of inhomogeneous Poisson processes are used to mathematically derive a new stochastic and information-theoretical framework to model the random transport and binding of nanoparticles in the cardiovascular system and to quantify the effect of noise through the use of the concept of the information-theoretical capacity. This analysis uses the expressions obtained in [57] to estimate several parameters, namely the blood velocities and the PDDS drug propagation probability. The noise and capacity analysis fills an important limitation in [57] in regards to the random behavior of drug nanoparticles. An end-to-end Molecular Communication (MC) framework is proposed to analyze the noise effects in the PDDS. The novel MC paradigm [2], where the information is conveyed through molecules, instead of the conventional electromagnetic signals, is employed to enable the communication in biological environments that are governed by molecular signals, such as bacterial communication [58] [16], with the long-term aim of establishing communication networks between nanomachines inspired by intracellular signaling.

In the literature, the noise effects in the intercellular communication are shown to have both beneficial and detrimental effects in intracellular MC [59]. The noise in MC by diffusion is analyzed in relation to the underlying physical processes [11]. Also, the stochastic effects in the ligand-receptor binding kinetics and interference are modeled through the MC framework [12] [60]. The maximum achievable information rates in diffusion-based MC under the constraints of Brownian motion noise are derived in [13] by using a novel thermodynamic information theoretical framework. These existing models rigorously reflect the unique noise effects in MC, but they cannot be directly applied for the PDDS in the complex cardiovascular network [57], because they assume linear time-invariant channel

models for the propagation medium, which is not realistic to assume in the cardiovascular system where the blood flow is highly time-varying, and they suppose diffusion in the free and isotropic space (i.e. the molecules propagate in all the Cartesian directions in the same manner and without any obstacles), while the MC in the cardiovascular system is confined to the complex topology of blood vessels. The MC reception of nanoparticles is also heavily affected by the blood flow that interferes with the chemical interactions between ligands and receptors [17].

In addition to the analysis of the noise effects in the PDDS, the use of information theory is proposed to evaluate the performance of the PDDS through the MC paradigm. The main objective of the PDDS is to engineer a system that can induce a therapeutic effect in the location where it is needed. The desired drug delivery at the location of the disease may vary from one individual to another, depending on the nature and the stage of the illness, the genomics that greatly affect the binding of drug nanoparticles to the receptors in the diseased cells [61], and the desired intensity of the treatment. Therefore, it is highly desirable that, for a given clinical setting, the PDDS can be employed effectively and reliably for the treatment of a diversity of individuals. In this chapter, the PDDS is considered to be similar to a communication system, where the drug injection which corresponds to a signal transmission, induces the drug reception which corresponds to a signal reception, after being distorted by the human body which corresponds to the communication channel. Through this paradigm, the set of desired responses may be viewed as an alphabet of different responses $\mathbf{y}_A$, $\mathbf{y}_B$, ..., $\mathbf{y}_Z$, etc. If the PDDS can reliably deliver different kinds of responses unambiguously at the same time, this PDDS can be qualified to be very performant. The size of this alphabet can be measured in bits (1 bit for two possible different therapeutic responses, 2 bits for four possible different therapeutic responses, etc.). The existing PDDS models are mostly based on deterministic approaches, while stochastic approaches are mainly developed for the purpose of statistically estimating the required parameters of the system from experimental results. In this chapter, based on the comprehensive model

of the noise effects in PDDS, the capacity of the PDDS under the constraints of the noise effects is mathematically derived, and this concept is used to evaluate the performance of the PDDS. The expression of the capacity can be used as an objective function encompassing all the PDDS parameters in order to optimize its design and the drug injection rate. In classical communication theory, this optimization is solved through the water-filling algorithm which assists in designing the transmitted signal in such a way that most of the power is used in clear channel conditions, and the power is minimized in noisy channel conditions. Similarly, in the PDDS, this analysis will enable to construct a drug injection rate that transmits most of the valuable drug nanoparticles when the chances of having them absorbed are high, and a minimal amount of drug nanoparticles when the chances of their non-targeted dispersion is inevitable.

The paper is organized as follows: First, in Section 4.2, all the noise effects that exist in the PDDS are presented, which are going to be modeled by using the MC paradigm. Second, in Section 4.3, the elements of the MC abstraction of the PDDS noise effects are presented, and the notion of capacity in the PDDS is defined and justified. Third, the MC end-to-end drug reception noise is derived in Section 4.4. Fourth, in Section 4.5, the MC capacity of the PDDS is derived within an information theoretical framework, and is expressed as a function of all parameters of the noise effects from the drug injection to the drug reception by diseased cells. Fifth, a kinetic Monte-Carlo scheme of the PDDS in the cardiovascular system is described in Section 4.6, and the numerical results from this scheme are compared with the analytical MC noise. Finally, Section 6.8 concludes the paper by discussing the key outcomes of the MC noise modeling for the PDDS, the PDDS capacity, and its application to the design and optimization of the PDDS.

4.2 PDDS Noise Scheme

The **PDDS noise scheme** consists of all the noise effects that affect the injection, propagation, and reception of drug nanoparticles. As illustrated in Fig. 22, the following noise

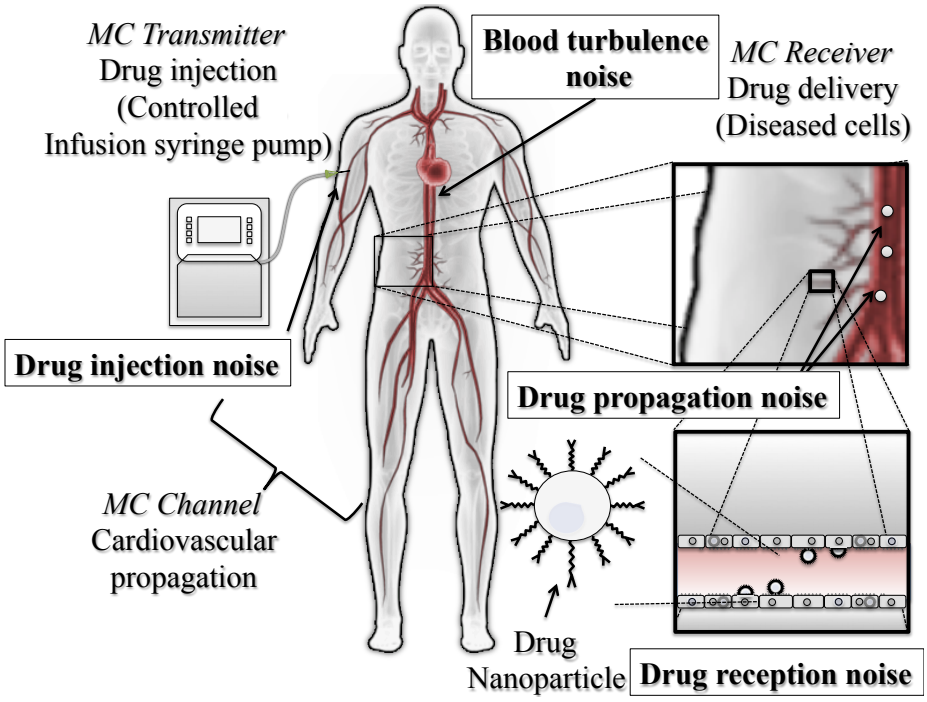

Figure 22. MC noise effects in particulate drug delivery systems.

effects are identified in the PDDS:

- The **drug injection noise** is caused by the mechanical limitations of the drug injection device. The drug injection device is a computer-controlled infusion syringe pump that allows the control of the drug injection rate in the drug injection site. This device is likely to suffer from imperfections that cause an inaccurate drug injection rate. Also, the drug injection device cannot be controlled arbitrarily fast, because of the mechanical friction and compression phenomena occurring in the pump. In addition, the drug injection rate is limited by the toxicity level. All these effects will be considered for the MC noise and capacity modeling of the PDDS.

- The **drug propagation noise** is due to the stochastic nature of the motion of drug nanoparticles in a possibly turbulent blood flow. After being injected, drug nanoparticles are lost randomly at the level of blood vessel bifurcations, towards organs and tissues where their effect is not desired. Especially at high concentration levels, drug nanoparticles become more agitated, causing a noticeable Brownian noise

effect, since drug nanoparticles try to move from the regions with high concentration to the regions with low concentration.

- The **drug reception noise** affects the reception of drug nanoparticles by the diseased cells. In fact, the ligand-binding interactions by which drug nanoparticles bind to the surface of diseased cells is very stochastic. The diseased cells surface is a site where different kinds of energies interact, such as the kinetic energy due to the blood flow, the chemical energy of reaction between the ligands and the receptor, characterized by a chemical potential, and the thermal energy related to the Brownian motion in the blood medium. The small surface of interaction, irregularities in the cells, the weakness of the chemical affinity between ligands and receptor, and the negative effect of blood flow, which impede the drug delivery to the diseased cells.

These noise effects are numerous, complex, and inter-dependent, making their modeling tedious and challenging. However, the MC paradigm is well suited to address these issues. In fact, it provides a comprehensive PDDS noise from the drug injection to the drug reception, and enables the performance evaluation of the PDDS through the concept of the capacity.

4.3 MC Noise And Capacity Abstraction for the PDDS

The **MC Noise And Capacity Abstraction for the PDDS** provides the model of the noise effects in the PDDS, how the aggregate consequences of the noise effects are evaluated by using the concept of the capacity, and how the noise is validated by using kinetic Monte-Carlo simulations. As illustrated in Fig. 23, the PDDS is modeled as an MC channel with the following components:

- The **MC Transmitter** represents the drug injection device, which applies a *drug injection rate* $x(t)$ at the *drug injection site*, where the drug injection device syringe is inserted.

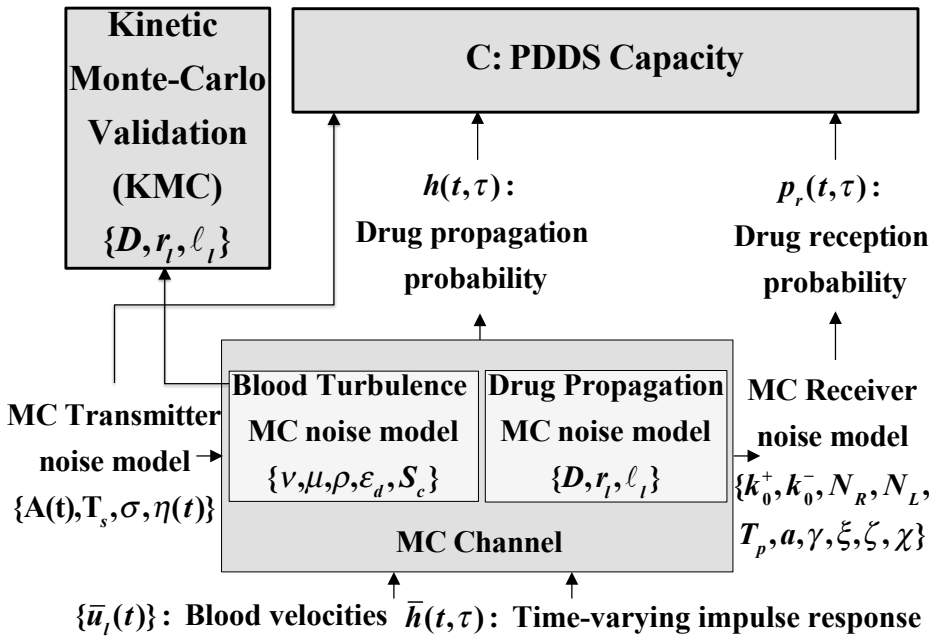

Figure 23. Elements of the MC abstraction of the noise effects in the PDDS, and their relationship with the PDDS capacity.

- The **MC Channel** reflects the effect of the blood flow on the propagation of drug nanoparticles in a complex network of interconnected blood vessels. As presented in our previous work [57], the PDDS channel is characterized by a *time-varying drug propagation probability* $h(t, \tau)$, and by cross-sectional blood velocities in every blood vessel l, denoted by $\{u_l(t); l \in CV\}$.

- The **MC Receiver** is the set of the diseased cells that require the PDDS therapeutic effect. The MC receiver, located in the *drug reception rate* $y(t)$, receives drug nanoparticles through the ligand-binding mechanism. This mechanism allows ligand-coated drug nanoparticles to have a high affinity to receptors located in the surface of the diseased cells. The MC reception is complicated due to the fact that the influence of the blood flow on the affinity between ligand and receptors varies periodically with time.

MC noises for all the components of the PDDS system are provided. These noises are

derived individually and then combined to obtain the aggregate effect of the end-to-end drug reception noise in the PDDS, as follows:

- The **drug injection noise** describes the noise limitations of the drug injection device. This model depends on the maximum injection rate $A(t)$, the sampling period T_s, the average drug injection constraint, and the drug leakage rate $\eta(t)$. In Section 4.4.1, these noise limitations are formulated depending on the pump injection syringe.

- The **drug propagation noise** depends on the drug diffusivity D and the topology of the cardiovascular system. In Section 4.4.2, a detailed probabilistic derivation of the drug propagation noise is provided, which gives the *drug propagation probability* $h(t, \tau)$, where t and τ are time variables.

- The **drug reception noise** gives the probability that drug nanoparticles located in the drug reception site are received by the diseased cells through the ligand-binding mechanism. This model depends on the number of ligands in a drug nanoparticle N_L, the number of receptors in the diseased cells N_R, the temperature T_p, the drug nanoparticle spheroid dimensions, with a radius a and an aspect-ratio γ, the maximum attraction distance ξ, the bond equilibrium length ζ, the characteristic length χ, and the cross-sectional average blood velocity at the drug reception site $u_l(t)$. In Section 4.4.3, these parameters are explained in detail, and are related to the *drug reception probability* $p_r(t)$.

These noise effects are aggregated to obtain an end-to-end model of the MC noise effects for the PDDS. In this chapter, it is found that the drug reception rate $y(t)$ is an inhomogeneous Poisson process related to the drug injection rate $x(t)$ through the following relationship:

$$y(t) \sim Pois\left(p_r(t)\eta(t) + \int_{-\infty}^{+\infty} h(t,\tau) p_r(t) x(\tau) d\tau \right), \tag{67}$$

where $Pois\,(.)$ denotes the Poisson distribution.

Based on the result in (67), the MC capacity of the system is presented which is a measure derived from information theory quantifying how much the drug injection rate $x(t)$ can reliably affect the drug reception rate $y(t)$ under the constraints of the various aforementioned noise effects. The capacity is found to be expressed as:

$$C_N = T_s \sum_{m=1}^{M} \psi_m \left(\sum_{n=1}^{N} \alpha_{n,m} A_n p_m \right), \tag{68}$$

where $\alpha_{n,m}$ is an expression of the drug propagation probability and the drug reception probability at the drug injection time sample n and the drug reception time sample m, A_n is the maximum non-toxic number of drug nanoparticles at the time nT_s, p_m is a coefficient depending on the maximum drug reception rate and the drug reception noise, m is the drug injection time sample, n is the drug reception time sample, M is the length of the discretized MC channel memory, N is the length of the drug injection rate $x(t)$, $\psi_m(\cdot)$ is a function depending on the drug injection noise parameters, the drug leakage rate, and the drug injection time sample m. The MC channel for the PDDS is unique in many senses. First, it is not Gaussian, as it is often assumed to derive the capacity in molecular and electromagnetic communications. Second, all its parameters are time-varying. Third, the PDDS channel has important memory effects due to the spread by diffusion.

Regarding inter-individual variations, one of the main advantages of the MC approach is that all system parameters are directly related to the physiology of the patient and the chemical properties and shape of drug nanoparticles (cf. Fig. 23). This allows the design of personalized medicine that is specific to each individual. The existing pharmacokinetic models use statistical methods to estimate the parameters of the system, which are valid only for one individual. The MC model allows the incorporation of individual variabilities mathematically.

Finally, the PDDS end-to-end noise is validated by comparing the results with simulation obtained by a kinetic Monte-Carlo scheme presented in Section 4.6.

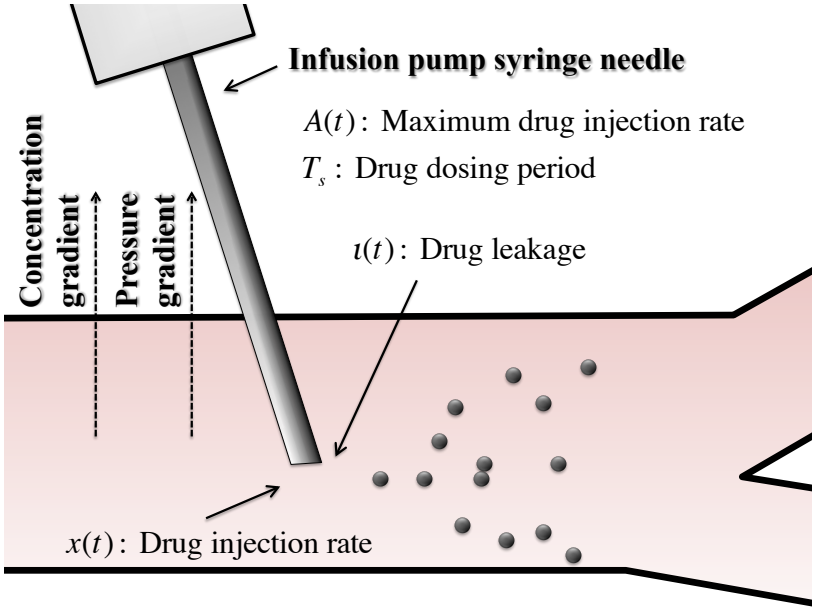

Figure 24. Elements of the drug injection noise.

4.4 Drug Delivery Noise

The **drug reception noise** allows to probabilistically describe the noise effects from the drug injection to the drug reception. Here it is shown that the drug reception rate $y(t)$ is an inhomogeneous Poisson process related to the drug injection rate $x(t)$ as expressed in (67).

4.4.1 Drug Injection Noise

The **drug injection noise** is composed of all limitations and noise effects that are caused by the imperfections of the drug injection device, as illustrated in Fig. 24. Our PDDS scheme requires that the drug injection rate is controllable. Here the drug injection rate is assumed to be modulated by an infusion pump syringe, which is connected to a computer system. The computer system is programmed to induce a desired drug injection rate by changing the pressure of the infusion pump. The drug injection device creates the following limiting factors:

- The **injection leakage**, which is the uncontrolled leaking of drug nanoparticles from the tip of the needle. The pump infusion syringe can leak drug nanoparticles because of the concentration gradient between the drug solution, and the pressure difference

between the needle and the blood flow. The leakage is independent of the drug injection rate $x(t)$. Since the blood flow is periodic, the drug leakage ratevaries periodically, and creates additional drug nanoparticles in the drug reception site. The the drug reception rate is expressed as follows:

$$y(t) = g(x(t)) + \eta(t)\,, \tag{69}$$

where $g(x(t))$ represents the part of the drug reception rate that is dependent on the drug injection rate $x(t)$. Since the drug propagation is linear, the drug delivery rate $\eta(t)$ depends on the *drug syringe spill rate* $\iota(t)$ as follows:

$$\eta(t) = g(\iota(t))\,. \tag{70}$$

The leakage is supposed to be slower than the drug injection. Therefore, the drug leakage rate $\eta(t)$ is also sampling rate limited by the sampling period T_s.

- The **maximum injection rate** is limited, because the drug injection rate should not create a drug concentration of drug nanoparticles that is toxic to the location where the drug is injected. This constraint is expressed as follows:

$$x(t) \leq A(t)\,, \tag{71}$$

where $A(t)$ is a periodic function ($A(t) = A(t + T)$), which specifies the maximum drug injection rate during a heartbeat period, and T is the blood velocity period. The maximum drug injection rate will vary with time due to the periodic blood flow.

- The **sampling rate** is the maximum rate at which the drug injection can be changed in time. This rate is limited by the mechanical deficiencies of the pump infusion syringe, such as the friction of the syringe rubber piston, or the presence of small compressible gas bubbles in the solution. Therefore, the drug injection cannot be arbitrarily fast. The maximum sampling rate limitations is expressed as follows:

$$|f| \geq \frac{1}{T_s} \implies X(f) = 0\,, \tag{72}$$

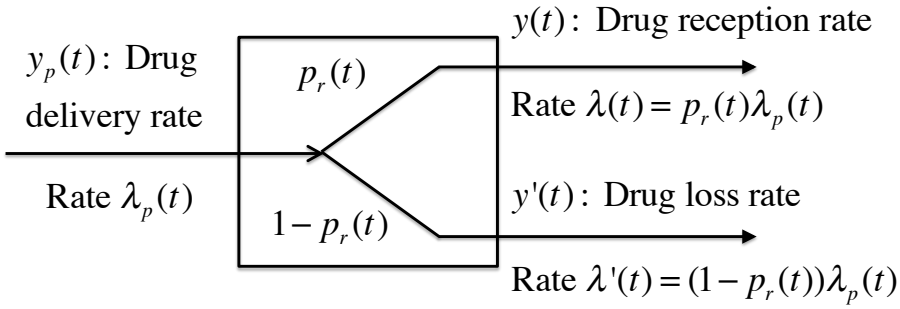

Figure 25. Drug nanoparticle reception as the time-varying splitting of an inhomogeneous Poisson process.

where f is the frequency and $X(f)$ is the frequency transform of the drug injection rate $x(t)$.

4.4.2 Drug Propagation Noise

The **drug propagation noise** gives a probabilistic description of the presence of drug particles in the delivery site. The drug propagation along the cardiovascular system is noisy because of the Brownian motion of drug nanoparticles, which are randomly dispersed in the blood vessels, and lost at vessel bifurcations to regions of the body where the drug is not needed. Here it is shown that drug nanoparticles that propagate to reach the drug reception site, given a drug injection rate, is expressed as follows:

$$y_p(t) \sim Pois\left(\eta(t) + \int_{-\infty}^{+\infty} h(t,\tau)x(\tau)d\tau\right), \tag{73}$$

where $y_p(t)$ is the drug propagation rate which denotes the number of drug nanoparticles that reach the drug reception site at the time t as shown in Fig. 25.

4.4.2.1 Drug Propagation Poisson Binomial Noise

This gives the drug propagation rate $y_p(t)$ at the drug reception site, given a drug injection rate $x(t)$, as a function of the probability that one single drug nanoparticle injected at the time τ in the drug injection site is located at the drug reception site at the time t, which is denoted by $p_s(t,\tau)$, which is the *single drug nanoparticle propagation probability* developed in Section 4.4.2.2. The drug propagation Poisson binomial model expresses the drug

propagation rate $y_p(t)$ as a function of the drug injection rate $x(t)$ as follows [62]:

$$P\left[y_p(t) = k\right] = \frac{1}{K}\sum_{n=0}^{K-1} e^{\frac{-2ink\pi}{K}} \prod_{m=1}^{K-1}\left(1 + (e^{\frac{2ik\pi}{K}} - 1)p_s(t, mT_s)\right), \tag{74}$$

where k is the number of nanoparticles that reach the drug reception site after propagation in the cardiovascular system, $p_s(t, mT_s)$ is the probability that one single drug nanoparticle injected at a time τ at the drug injection site is delivered at the time mT_s at the drug reception site, the number of trials K is the total of injected nanoparticles expressed as:

$$K = \sum_{n=0}^{N-1} x(nT_s)\,, \tag{75}$$

with N the number of time samples drug injection rate $x(t)$, such as the drug injection rate $x(t)$ is written as a sequence of Dirac impulses with different weights, as follows:

$$x(t) = \sum_{n=0}^{N-1} x(nT_s)\delta(t - nT_s)\,. \tag{76}$$

The aforementioned relationship is proved by considering the probability that k nanoparticles among a batch of $x(nT_s)$ nanoparticles, all injected at the time nT_s, reach the drug reception site at the time t. The probability that exactly k nanoparticles among the ones enveloped in the drug injection rate $x(t)$ be delivered at the time t is the probability that the total number of nanoparticles among the N different batches that are successfully delivered is equal to k. In other words, the number of successful nanoparticle receptions is a sum of independent Binomial trials each with different probabilities of success. Therefore, $y_p(t)$ follows a *Poisson binomial distribution* [63], where the number of trials is the total number of nanoparticles enveloped by the drug injection rate $x(t)$, and the success rates are the probabilities of the drug delivery for each nanoparticle m, with $m = 0, \ldots, N-1$, as expressed by (74).

4.4.2.2 Single Drug Nanoparticle Propagation Noise

This provides a description of the random movement of one nanoparticle injected in the cardiovascular system. The probability that one single drug nanoparticle is delivered at

the drug reception site at the time t if it is injected at the time τ is denoted as $p_s(t, \tau)$. A single drug nanoparticle delivery is found to follow a Bernoulli distribution with probability $p_s(t, \tau)$ that is equal to $h(t, \tau)$. This is proved based on the analogy between the advection-diffusion equation and the Fokker-Planck equation, which is the basis of the random motion of drug nanoparticles. A deterministic model of the movement of drug nanoparticles in the cardiovascular system is proposed in [57]. The deterministic model was based on the generalized Taylor dispersion equation that governs the cross-sectional concentration of drug nanoparticles $c(z, t)$ under the effect of advection by a fluid with cross-average velocity $u(z, t)$ and effective diffusivity $D_{eff}(t)$, as follows:

$$\frac{\partial c(z,t)}{\partial t} = -u(t)\frac{\partial u(z,t)}{\partial z} + D_{eff}(t)\frac{\partial^2 c(z,t)}{\partial z^2}\,, \tag{77}$$

where ∂ is the symbol for the partial derivative. Since the advection-diffusion equation does not capture the micro-scale variations in the propagation of nanoparticles, the deterministic model that solves it is only adequate for describing the average space and time evolution of the movement of drug nanoparticles. Therefore, a stochastic model is needed to reflect both the macro-scale and micro-scale variations in the movement of drug nanoparticles.

The stochastic nature of drug nanoparticles is described by the Fokker-Planck equation [64]. The Fokker-Planck equation is the basis of dynamic techniques for obtaining the random path of a drug nanoparticle subject to Brownian motion [65]. The one-dimensional form of the Fokker-Planck equation states that the position $z(t)$ of the drug nanoparticles at the time t has a probability density function $p(z, t)$ governed by the following equation:

$$\frac{\partial p(z,t)}{\partial t} = -\frac{\partial \mu(z,t)p(z,t)}{\partial z} + \frac{\partial^2 D(z,t)p(z,t)}{\partial z^2}\,, \tag{78}$$

where $\mu(z, t)$ is the nanoparticle drift related to the advection process and $D(z, t)$ is a function related to the diffusion process, such as, in the micro-scale, the position $z(t)$ of the nanoparticle is incremented by the random process $dz(t)$ obeying the following stochastic differential equation:

$$dz(t) = \mu\left(z(t), t\right) dt + \sqrt{2D\left(z(t), t\right)}dw(t)\,, \tag{79}$$

where $dw(t)$ is called a Wiener process, with the following probability density function:

$$f_{w(t)}(z) = \frac{1}{\sqrt{2\pi t}} e^{-\frac{z^2}{2t}} . \tag{80}$$

The generalized Taylor dispersion equation (77) and the Fokker-Planck equation (78) have the same form, and therefore, by assuming spatially uniform drift and diffusivity, and by taking the drift term $\mu(z,t)$ to be equal to the cross-sectional average velocity $u(t)$, the equations become identical. Given that these equations are linear, it is possible to conclude that the deterministic solution of the advection-diffusion equation $c(z,t)$ and the probability density function of the movement of a drug nanoparticle $p(z,t)$ are equal to each other up to a multiplicative constant, i.e.:

$$p(z,t) = \frac{1}{c_0} c(z,t) , \tag{81}$$

where c_0 is the multiplicative constant, which is obtained from the fact that the integral of the probability density function over the entire space and time is equal to one, i.e.:

$$c_0 = \int_{z \in CV} \int_{-\infty}^{+\infty} c(z,t) dz dt , \tag{82}$$

where CV denotes the spatial domain in the cardiovascular system, z is the space coordinate, and t is the time coordinate. From the results above, the probability density function that describes the drug propagation rate $y_p(t)$ close to a drug reception site by interpreting the time-varying impulse response $h(t,\tau)$ at a drug reception site for an input at drug injection site can be expressed as a probability density function. The time-varying drug propagation probability of the PDDS $h(t,\tau)$ is equal to the drug propagation rate $c(z,t)$ at the longitudinal coordinate $z = \ell_l$ with a drug injection rate $x(t)$ equal to an impulse $\delta(t-\tau)$ centered around the time τ, as expressed in the following:

$$c(z,t)|_{x(t)=\delta(t-\tau), z=\ell_l} = p(z,t)|_{z=\ell_l} . \tag{83}$$

It follows by definition that:

$$h(t,\tau) = p_s(t,\tau) . \tag{84}$$

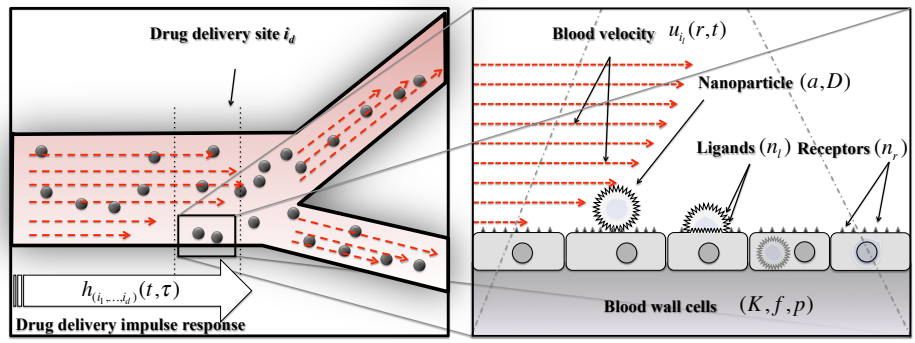

Figure 26. Ligand-binding reception scheme.

Therefore, the probability that k nanoparticles ($k \in \{0, 1\}$), injected at the time $t - \tau$ at the drug injection site, are delivered at the time t at the drug reception site is expressed by the following:

$$P\left[y_s(t) = k\right] = h^k(t,\tau)(1 - h(t,\tau))^{1-k}\,, \tag{85}$$

where $y_s(t)$ denotes the number of drug nanoparticle located at the drug reception site.

4.4.2.3 Drug Propagation Poisson Noise

This provides an approximation of the drug propagation Poisson binomial noise described in Section 4.4.2.1. By using Le Cam's theorem [66], a Poisson binomial distribution can be approximated by a Poisson process with a rate equal to the sum of the probabilities of the Poisson binomial distribution. Therefore:

$$y(t) \sim Pois\left(\lambda(t)\right)\,, \tag{86}$$

where $Pois(\lambda(t))$ denotes an inhomogeneous Poisson process with rate $\lambda(t)$. The rate $\lambda(t)$ is equal to the following:

$$\lambda(t) = \int_{-\infty}^{+\infty} x(\tau)h(t,\tau)d\tau\,. \tag{87}$$

4.4.3 Drug Reception Noise

The **drug reception noise** provides the probability that particles that reach the drug reception site after propagating in the cardiovascular system will be received by the diseased

cells, which are here modeled as an MC receiver, through the adhesion to the cells and absorption into the interior of the cell. This reception process is characterized by a **drug reception probability** $p_r(t)$. The time-variance is due to the periodic blood flow, which affects the ligand-binding mechanism by which drug nanoparticles are received by the diseased cells.

The study of MC stochastic receiver models is proposed in [12] in a diffusion-based environment, which allows simulating the random behavior of the chemical reactions of an MC receiver. Such diffusion-only MC models would not accurately describe the ligand-binding reception in a flow-dominated environment. In fact, several qualitative and experimental studies [67] [17] have shown that flow creates a shear stress along the blood vessel walls, which significantly affects the deposition and the reception of the drug nanoparticles.

The MC receiver proposed here is based on the mathematical modeling of receptor-mediated endocytosis of nanoparticles under shear stress, which means the absorption of drug nanoparticles inside blood vessel wall cells under the effect of the blood velocity [68]. As shown in Fig. 26, this model is extended by taking into account the blood velocity $u_l(r,t)$ in the drug reception site, the size of the diseased region, and the parameters of the drug nanoparticle coating. The MC receiver model scheme is pictured in Fig. 27. The MC receiver is affected by the following elements and parameters:

- The **nanoparticle characteristic size** a, which is equal to the radius for a sphere.
- The **nanoparticle aspect ratio** γ, which is equal to the ratio between the polar diameter and the equatorial diameter of a spheroid-shaped nanoparticle. It is equal to one for a sphere.
- The **number of ligands** N_L is the total number of ligands that cover the nanoparticle surface. The ligands are supposed to be uniformly distributed on the surface of the nanoparticle. The density of the ligands is assumed to be the same for all nanoparticles.

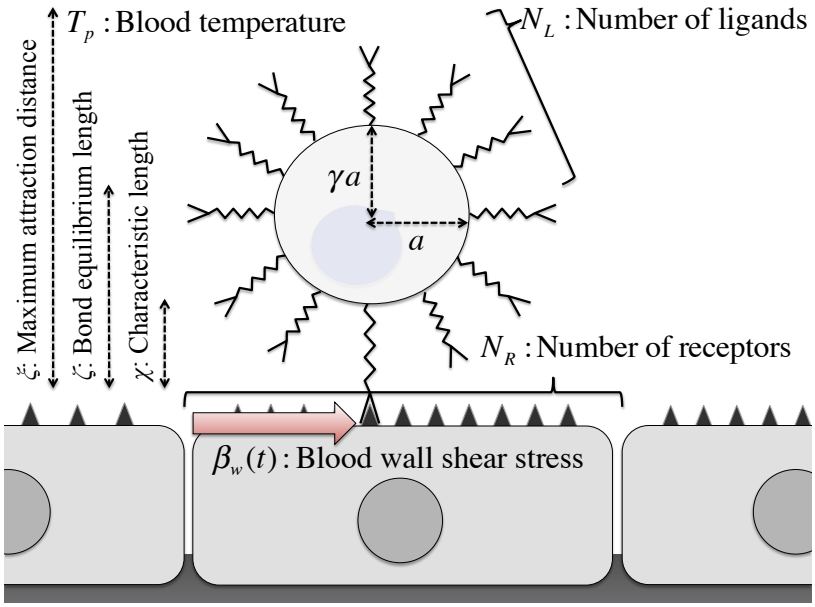

Figure 27. Elements of the Drug Reception Noise.

- The **number of receptors** N_R is the total number of receptors that are available in the drug reception site. It is supposed that there are more receptors than ligands (i.e. $N_R >> N_L$).

- The **ligand-receptor bond characteristic length** χ, which is the distance between the ligand and the receptor when they are bound together without any external force affecting the bond, and which is approximately equal to 0.1 *nm*.

- The **ligand-receptor bond equilibrium** ζ, which is the distance between the ligand and the receptor when they are bound together in equilibrium under the effect of shear stress.

- The **ligand-receptor maximum attraction length** ξ, which is the maximum distance between the ligand and the receptor at which the bonding is possible.

It is supposed that a drug nanoparticle is delivered when at least one stable bond is established between the nanoparticle and the drug reception site. This work is based on classical results from [69] and [70]. In this chapter, the relationship between the drug

reception probability and the time-varying blood velocity is derived. The resulting drug reception probability $p_r(t)$ can be expressed as:

$$p_r(t) = \pi r_0^2 m_R m_L e^{-\frac{\chi a \beta_w(t)}{k_B T_p r_0 m_R}\left(\left(\frac{a}{\gamma}+\zeta\right)F_s + \frac{a^2}{r_0}R_s\right)}, \tag{88}$$

where:

- r_0 is the radius of the section of the nanoparticle located at a ligand-receptor maximum attraction length ξ from the blood vessel wall cells, and is expressed as follows:

$$r_0 = a\sqrt{1-\left(1-\frac{\xi-\zeta}{a}\gamma\right)^2}. \tag{89}$$

- m_R is the receptor surface density, defined as follows:

$$m_R = \frac{\gamma N_R}{\frac{4}{3}\pi a^3}. \tag{90}$$

- m_L is the ligand surface density, defined as follows:

$$m_L = \frac{\gamma N_L}{\frac{4}{3}\pi a^3}. \tag{91}$$

- k_B is the Boltzmann constant, which is approximately equal to the following:

$$k_B = 1.4806488 \times 10^{-23} \mathrm{m^2 kg\ s^{-2}\ K^{-1}}. \tag{92}$$

- T_p is the blood temperature, which is approximately equal to 310 K.

- F_s is a coefficient that is proportional to the drag force due to the blood flow, and is equal to $F_s = 6 + \left(10.416 - 0.8280\gamma + 0.768\gamma^2 + 0.54\gamma^3\right)e^{-\gamma}$, with γ the nanoparticle aspect ratio.

- R_s is a coefficient that is proportional to the rotational moment of force due to the blood flow, and is equal to $R_s = 8 + \left(-164 - 372\gamma - 280\gamma^2 + 71.6\gamma^3\right)e^{-\gamma}$ with γ the nanoparticle aspect ratio.

- $\beta_w(t)$ is the wall shear stress, which is derived below. Supposing the approximation of blood flow as a Newtonian fluid, by definition, the shear stress $\beta_w(t)$ at the wall is expressed as $\tau = \mu\beta_w(t)$, where μ is the blood dynamic viscosity, which is approximately equal to $\mu = 4.88 \times 10^{-3}$Pa.s, and $\beta_w(t)$ is the wall shear rate, defined as:

$$\beta_w(t) = \left.\frac{\partial u(r,t)}{\partial r}\right|_{r=r_l}, \tag{93}$$

where r_l is the radius of the blood vessel located in the drug reception site. Based on a result from [71], the shear rate is time-varying, and can be expressed as follows:

$$\beta_w(t) = \frac{1}{2i\pi r_l}\int_{-\infty}^{+\infty}\frac{\alpha^2(\omega)W(\omega)}{1-W(\omega)}U_l(\omega)e^{i\omega t}d\omega\,, \tag{94}$$

where i is the imaginary unit number, ω is the radial frequency, and $\alpha(\omega)$ is the Womersley number, defined as $\alpha(\omega) = r_l\sqrt{\frac{\omega}{\nu}}$. $W(\omega)$ is the Womersley function, defined as:

$$W(\omega) = \frac{2J_1\left(\alpha(\omega)\,i^{\frac{3}{2}}\right)}{\alpha(\omega)\,i^{\frac{3}{2}}J_0\left(\alpha(\omega)\,i^{\frac{3}{2}}\right)}, \tag{95}$$

which is expressed as a function of the Bessel function of the first kind, and, respectively, of the zero and first order, $J_0(\cdot)$ and $J_1(\cdot)$ [42]. $U_l(\omega)$ is the Fourier transform of the cross-sectional average blood velocity $u_l(t)$ in the drug reception site, which is expressed as follows:

$$U_l(\omega) = \int_{-\infty}^{+\infty}u_l(t)e^{-i\omega t}dt\,. \tag{96}$$

Biologically plausible numerical values are used for the parameters for the PDDS. For the numerical evaluation, it is considered that the nanoparticle size to be $a = 20$ μm, the maximum attraction length $\xi = 10^{-8}$ m, the bond characteristic length $\zeta = 5 \cdot 10^{-9}$ m, the receptor density $m_R = 5 \cdot 10^{13}$ m^{-2}, the ligand density $m_L = 3 \cdot 10^{-3}$ m^{-2}, the blood density $\rho = 1.06 \cdot 10^3$ kg $\cdot$ m^{-3}, the blood kinematic viscosity $\nu = 4.603 \cdot 10^{-6}$ m$^2 \cdot$ s^{-1}, and a spherical nanoparticle shape with $\gamma = 1$. The dimensions and topology of the considered portion of the arterial network are presented in Fig. 30. The blood velocity network is calculated by using the same numerical values as in [57]. These numerical values can be used

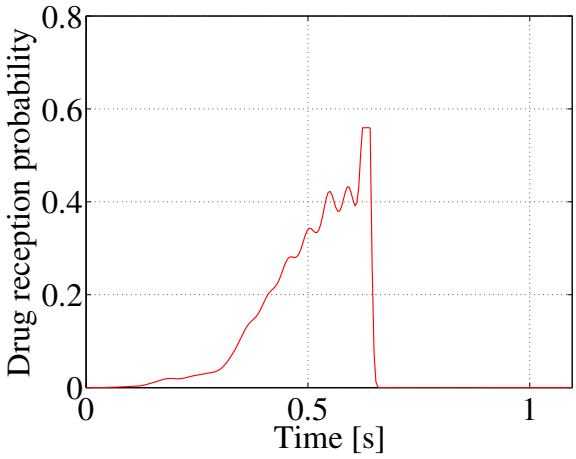

Figure 28. Drug reception probability in the drug reception site as a function of time.

to extrapolate for individuals of different ages by using empirical laws such as the Preece-Baines model, which conforms to the human growth curve [72]. Fig. 28 shows how the drug reception probability changes with respect to time during one heartbeat period. The numerical evaluations show that properly designing the time pattern of the drug reception rate $y(t)$ can highly affect the efficiency of the PDDS.

4.4.4 End-to-End Drug Reception Noise

The **end-to-end drug reception noise** provides a model of the noise effects from the injection to the reception of drug nanoparticles by the diseased cells. This model is based on the drug injection noise (Section 4.4.1), the drug propagation noise (Section 4.4.2), and the drug reception noise (Section 4.4.3). The following relationship between the drug reception $y(t)$, and the drug injection rate $x(t)$, is obtained through this model as expressed in (67). To prove the expression in (67), the property of splitting inhomogeneous Poisson processes [73] is used. In fact, based on the Poisson approximation of the drug propagation model presented in Section 4.4.2.3, the drug propagation rate $y_p(t)$ is an inhomogeneous Poisson process with rate $\lambda_p(t)$ expressed as follows:

$$\lambda_p(t) = \eta(t) + \int_{-\infty}^{+\infty} h(t,\tau)x(\tau)d\tau\,. \tag{97}$$

The delivered drug nanoparticles are received by the diseased cells according to the drug reception probability $p_r(t)$ presented in Section 4.4.3. By using a property of the splitting inhomogeneous Poisson processes [73] illustrated in Fig. 25, the drug reception rate is also an inhomogeneous Poisson process with rate $\lambda(t)$ expressed as follows:

$$\lambda(t) = p_r(t)\lambda_p(t)\,. \tag{98}$$

4.5 Capacity Analysis of the PDDS

Here the capacity of the PDDS expressed in (68) is derived based on the drug delivery noise developed in Section 4.4. The **average mutual information** I of the PDDS is defined as:

$$I = \lim_{N\to\infty} \frac{1}{N} I(\mathbf{x}_N; \mathbf{y}_N)\,, \tag{99}$$

where lim is the limit symbol, the **drug injection sequence** $\mathbf{x}_N$ represents the drug injection rate, and is defined by $\mathbf{x}_N = [x_1, \ldots, x_n, \ldots, x_{N-1}]$, where **the n-th drug injection sample** x_n is the number of drug nanoparticles injected at the time nT_s and N is the length of the drug injection sequence $\mathbf{x}_N$, the **drug reception sequence** $\mathbf{y}_N$ represents the drug reception rate, and is defined by $\mathbf{y}_N = [y_1, \ldots, y_m, \ldots, y_{N+L-2}]$ where **the m-th drug reception sample** y_m is the number of drug nanoparticles delivered during the time interval $[mT_s, (m+1)\,T_s[$, and L is the channel memory. $M = N + L - 1$ is the length of the drug reception sequence. The channel memory is defined as the number of time samples for which any drug injected at the time τ is no longer observed at any time t larger than $\tau + LT_s$. The memory is here considered finite, such as $\forall\ t, \tau \in \mathbb{R}\ \ t \leq \tau + LT_s \implies h(t,\tau) = 0$, and $I(\mathbf{x}_N; \mathbf{y}_N)$ is the **mutual information** between the random drug injection sequence $\mathbf{x}_N$ and the random drug reception sequence $\mathbf{y}_N$.

4.5.1 Drug Injection Sequence

The drug injection sequence consists of N time samples of the drug injection rate, such as it is possible to write the drug injection sequence as $\mathbf{x}_N = [x(nT_s)\,|\,n = 0, \ldots, N-1]$. By using the Dirac function, the drug injection rate $x(t)$ can be expressed as a function of the

drug injection sequence $\mathbf{x}_N$ as follows:

$$x(t) = \sum_{n=0}^{N-1} x_n \delta(t - nT_s)\,, \tag{100}$$

where N is the length of the drug injection sequence $\mathbf{x}_N$. The drug injection rate is composed of N Dirac functions, each delayed by n time samples, and weighted by the number of injected nanoparticles at the time nT_s. The drug injection sequence $\mathbf{x}_N$ is subjected to the two following constraints:

- the **toxicity constraint**, which limits the number of injected nanoparticle to a maximum allowed toxicity level. Beyond the toxicity level, the drug injection has an adverse effect on the body. This constraint is written as follows:

$$\forall n \in \{0, \ldots, N-1\} \quad x_n \leq A_n\,. \tag{101}$$

- the **average number of injected nanoparticles** σ, which can be written as follows:

$$\frac{1}{N} \sum_{n=0}^{N-1} x_n = \sigma\,. \tag{102}$$

4.5.2 Drug Reception Sequence

The drug reception sequence is a sequence of M random variables $[y_m \,|\, m = 0, \ldots, M-1]$, which represent the number of delivered nanoparticles during each the T_s-long m-th time duration. It is shown here that the number of nanoparticles delivered during the time interval $[mT_s, (m+1)\,T_s[$ y_m, which is called the m-th drug reception sample, follows a Poisson distribution with rate λ_m expressed as $y_m \sim Pois(\lambda_m)$, where the rate λ_m is expressed as:

$$\lambda_m = \eta_m T_s + \sum_{n=0}^{N-1} x_n \alpha_{n,m}\,, \tag{103}$$

with η_m the discrete drug leakage rate in the drug reception site at the m-th time sample (i.e. $\eta_m = \eta(mT_s)$), and:

$$\alpha_{n,m} = \int_{mT_s}^{(m+1)T_s} h(t, t - nT_s) p_r(t) dt\,. \tag{104}$$

where $h(t, t - nT_s)$ denotes the time-varying drug propagation probability with injection time $t - nT_s$ and observation time t. In the following part of this section, the derivation of the result in (103) is presented. The result is obtained in (103) by moving from the continuous domain of Poisson processes to the discrete domain of Poisson distribution. This is performed by building the Poisson distribution y_m from the Poisson process $y(t)$ as the expected number of drug nanoparticle deliveries in the interval $[mT_s, (m+1)\,T_s[$. The rate of y_m is the integrated continuous rate of the inhomogeneous Poisson process $y(t)$ in the interval $[mT_s, (m+1)\,T_s[$ [74]. According to the expressions (87) and (105), this is expressed as follows:

$$\begin{aligned}\lambda_m &= \int_{mT_s}^{(m+1)T_s} \lambda(t)dt \\ &= \int_{mT_s}^{(m+1)T_s} \left(\eta_m + \int_{-\infty}^{+\infty} x(t-\tau)p_r(t)h(t,\tau)d\tau\right)dt\,,\end{aligned} \tag{105}$$

which can be simplified as follows with a discrete drug injection rate.

$$\lambda_m = \sum_{n=0}^{N-1} x_n \left(\eta_m T_s + \int_{mT_s}^{(m+1)T_s} p_r(t)h(t, t-nT_s)dt\right). \tag{106}$$

Finally, by using the definition of the coefficients $\alpha_{n,m}$ in (104), the following expression of the rate λ_m is obtained:

$$\lambda_m = \eta_m T_s + \sum_{n=0}^{N-1} x_n \alpha_{n,m}\,. \tag{107}$$

4.5.2.1 Capacity expression

The mutual information between the drug injection sequence $\mathbf{x}_N$ and the drug reception sequence $\mathbf{y}_N$ used in (99) is as follows [75]:

$$I(\mathbf{x}_N; \mathbf{y}_N) = H(\mathbf{y}_N) - H(\mathbf{y}_N \mid \mathbf{x}_N)\,, \tag{108}$$

where $H(\mathbf{y}_N \mid \mathbf{x}_N)$ is the conditional entropy of the drug reception sequence defined as:

$$H(\mathbf{y}_N \mid \mathbf{x}_N) = -E\left[\log\left(p_{\mathbf{y}_N|\mathbf{x}_N}\right)\right], \tag{109}$$

where $p_{\mathbf{y}_N|\mathbf{x}_N}$ is the conditional probability mass function of the discrete random variables $y_1, y_2, \ldots, y_{M-1}$ of the drug reception sequence given the occurence of the discrete random variables $x_1, x_2, \ldots, x_{M-1}$, and $H(\mathbf{y}_N)$ is the marginal entropy of the drug reception sequence:

$$H(\mathbf{y}_N) = -E\left[\log\left(p_{\mathbf{y}_N}\right)\right], \tag{110}$$

where $p_{\mathbf{y}_N}$ is the joint conditional probability mass function of the discrete random variables $y_1, y_2, \ldots, y_{M-1}$ of the drug reception sequence. In the following, the derivation of the conditional and marginal entropies of the drug reception sequence is presented.

4.5.2.2 Conditional Entropy

The conditional entropy is expressed in (109). Conditioned on the drug injection sequence, the drug reception samples $\{y_m; m = 0, \ldots, M-1\}$ are independent and have the probability mass function $p_{y_m|\mathbf{x}_N}$. It is then possible to write:

$$H(\mathbf{y}_N \mid \mathbf{x}_N) = \sum_{m=0}^{M-1} H(y_m \mid \mathbf{x}_N), \tag{111}$$

where $H(y_m \mid \mathbf{x}_N)$ is the conditional entropy of the m-th drug reception sample given the occurrence of the drug injection sequence $\mathbf{x}_N$. $H(y_m \mid \mathbf{x}_N)$ is by definition equal to the following [75]:

$$H(y_m \mid \mathbf{x}_N) = -\log\left(E\left[p_{y_m|\mathbf{x}_N}\right]\right), \tag{112}$$

where $E[\cdot]$ is the expectation operator, $p_{y_m|\mathbf{x}_N}$ denotes the conditional probability mass function of the m-th drug reception sample given the occurrence of the drug injection sequence $\mathbf{x}_N$. By identification with the Lemma 1 obtained in [76],the conditional entropy $H(\mathbf{y}_N \mid \mathbf{x}_N)$ can be expressed as follows:

$$H(\mathbf{y}_N \mid \mathbf{x}_N) = -\sum_{m=0}^{M-1} E\left[\lambda_m T_s \log\left(\lambda_m\right)\right] + \sum_{m=0}^{M-1} E\left[\lambda_m T_s\right]. \tag{113}$$

4.5.2.3 Marginal Entropy

The marginal entropy in (110) of the drug reception sequence is derived. The drug reception samples $\{y_m; m = 0, \ldots, M-1\}$ are independent and have the probability mass function $p_{y_m|\mathbf{x}_N}$. Therefore, the marginal entropy is $H(\mathbf{y}_N) = \sum_{m=0}^{M-1} H(y_m)$, where $H(y_m)$ is the marginal entropy of the m-th drug reception sample. $H(y_m \mid \mathbf{x}_N)$ is by definition equal to $H(y_m) = -\log\left(E\left[p_{y_m}\right]\right)$ where p_{y_m} is the probability mass function of the m-th drug reception sequence.

By identification with the expression of the least-square estimator of Poisson-distributed random variables performed in [76] by using semimartingale methods, and supposing that the channel does not vary in time during T_s, the marginal entropy of the drug reception sequence $H(\mathbf{y}_N \mid \mathbf{x}_N)$ can be expressed as follows:

$$H(\mathbf{y}_N) = -\sum_{m=0}^{M-1} E\left[\hat{\lambda}_m T_s \log\left(\hat{\lambda}_m\right)\right] + \sum_{m=0}^{M-1} E\left[\lambda_m T_s\right] , \tag{114}$$

where $\hat{\lambda}_m$ is the least-squares estimator of λ_m given the occurrence of the drug reception sequence $\mathbf{y}_N$, i.e. $\hat{\lambda}_m = E\left[\lambda_m \mid \mathbf{y}_N\right]$. The least-squares estimator $\hat{\lambda}_m$ of the rates λ_m can be expressed as a function of the least-squares estimator $\hat{x}_n$ of the drug injection samples x_n, as follows:

$$\hat{\lambda}_m = \sum_{n=0}^{N-1} \hat{x}_n \alpha_{n,m} + \eta_m T_s , \tag{115}$$

where the least-squares estimator $\hat{x}_n$ of the drug injection samples x_n is equal to the following:

$$\hat{x}_n = E\left[x_n \mid \mathbf{y}_N\right] , \tag{116}$$

The expression of the mutual information $I(\mathbf{x}_N; \mathbf{y}_N)$ is obtained by substituting in (108) the drug injection sequence conditional and marginal entropies by their expressions (113) and (114), respectively, as follows:

$$I(\mathbf{x}_N; \mathbf{y}_N) = T_s \sum_{m=0}^{M-1} E\left[\lambda_m \log\left(\lambda_m\right)\right] - E\left[\hat{\lambda}_m \log\left(\hat{\lambda}_m\right)\right] , \tag{117}$$

where $\hat{\lambda}_m$ is the least-squares estimator of the rate λ_m given the drug reception sequence $\mathbf{y}_N$.

By using the notation proposed in [77] for the treatment of the single-input single-output Poisson channel, the mutual information in (117) can be rewritten as the difference between two quantities, where the first is larger than the second, as follows:

$$\begin{aligned} I(\mathbf{x}_N;\mathbf{y}_N) = & \\ T_s \sum_{m=0}^{M-1} \psi_m \left(\sum_{n=0}^{N-1} x_n \alpha_{n,m} \right) - E\left[\psi_m \left(\sum_{n=0}^{N-1} x_n \alpha_{n,m} \right) \right] & \\ -T_s \sum_{m=0}^{M-1} \psi_m \left(\sum_{n=0}^{N-1} x_n \alpha_{n,m} \right) - E\left[\psi_m \left(\sum_{n=0}^{N-1} \hat{x}_n \alpha_{n,m} \right) \right], & \end{aligned} \tag{118}$$

where the functions $\psi_m(\cdot)$ $(m = 0, \ldots, M-1)$ are defined as follows:

$$\begin{aligned} \psi_m(x) = & \frac{x}{B_m} \left[(\eta_m + B_m) \log (\eta_m + B_m) - \eta_m \log \eta_m \right] \\ & - (\eta_m + x) \log (\eta_m + x) - \eta_m \log \eta_m \,, \end{aligned} \tag{119}$$

where x is a variable of η_m, and $B_m = \sum_{n=0}^{N-1} A_n \alpha_{n,m}$ is the m-th drug reception sample given the occurrence of a drug injection sequence at the maximum levels A_n (101) that constrain it, and $\alpha_{n,m}$ are the channel coefficients defined in (104). By identification with the derivation in [77], the capacity is found to be closely bounded by the expression in (68) where the coefficients p_m are equal to $p_m = \min\left(\frac{(1+s_m)^{(1+s_m)}}{e s_m^{s_m}} - s_m, \sigma \right)$, where s_m is the ratio between the reception noise and the average received number of drugs in the m-th sample, which can be written as $s_m = \frac{\eta_m}{B_m}$. Finally, the capacity of the delivery system is obtained as:ave

$$C_\infty = \lim_{N \to +\infty} \frac{1}{T_s} C_N \,. \tag{120}$$

4.5.3 Spatial Capacity Numerical results

4.5.3.1 Effect of Blood Vessel Dimensions

Fig. 29(a)shows how the length of the blood vessel affects the performance of the PDDS capacity. The longer the vessel is, the more dispersive the channel becomes, and therefore the capacity of the channel is negatively affected. Fig. 29(c), shows how the radius of the

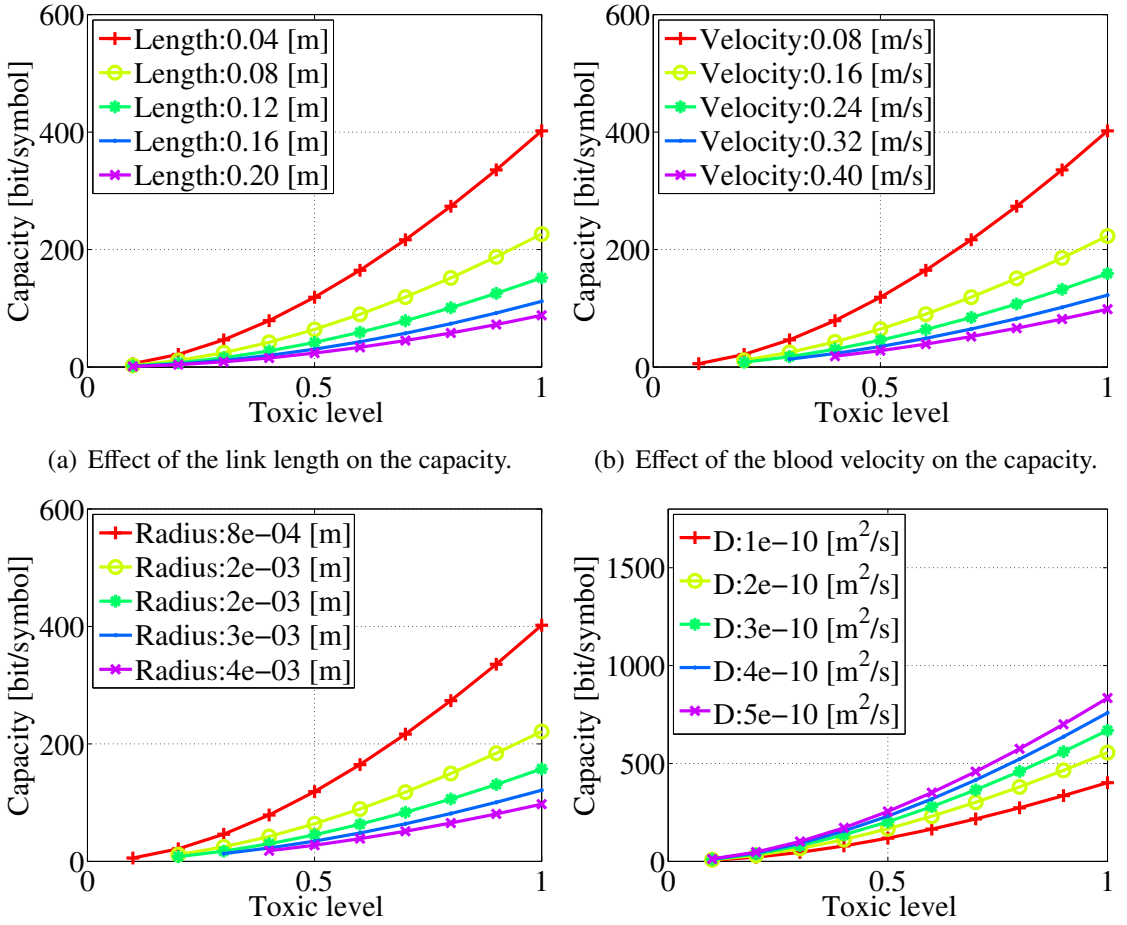

(a) Effect of the link length on the capacity.

(b) Effect of the blood velocity on the capacity.

(c) Effect of the link radius on the capacity.

(d) Effect of the diffusion coefficient on the capacity.

Figure 29. The effect of the drug parameters, the vessel dimensions, and the toxic level on the capacity of the PDDS channel.

blood vessel affects the performance of the system capacity. When the length of the vessels is long, the variance of the drug propagation probability increases, which creates a more severe memory effect, and reduces the capacity of the channel. Similarly, when the radius of the vessels increase, the mixing along the radial coordinate is reduced, which makes the drug propagation probability more dispersive.

4.5.3.2 Effect of Blood Velocity

Fig. 29(b) shows how the length of the blood vessel affects the performance of the system capacity. At this regime, when the blood velocity becomes high, the channel becomes more dispersive, and therefore the capacity of the channel is affected. However, due to the Taylor dispersion effect, the blood velocity can actually reduce the dispersion in the channel, and produce the opposite observationin some conditions.

4.5.3.3 Effect of Diffusion Coefficient

Fig. 29(a), shows how the diffusion coefficient affects the performance of the system capacity. The higher the diffusion coefficient is, the more dispersive the channel becomes, and therefore the capacity of the channel is affected. When the diffusion coefficient is high, the drug disperses faster in the blood, causing a longer delay and higher memory effect.

4.6 Monte-Carlo Simulation of the PDDS

In this section, a simulation method to study the propagation of a drug nanoparticle in the cardiovascular system with unsteady flow by introducing a Monte-Carlo simulation method of the PDDS is presented. The deterministic impulse response model developed in [57] has been validated by using finite-element simulation on COMSOL in [78]. For the noise analysis of the PDDS, the kinetic Monte-Carlo technique [49] is used to observe the random path of nanoparticles caused by random Brownian motion and validate it against the developed stochastic model. The random Brownian motion is generated by the model described in Section 4.4. In the kinetic Monte-Carlo technique, the path of nanoparticles is simulated by assuming that every nanoparticle is a random walker affected by Brownian

motion (diffusion) and by a randomly fluctuating velocity field (convection).A model is proposed where parameters of the Brownian are directly related to the diffusion coefficient of the nanoparticles, and the random velocity field is generated by assuming that the radial and transversal components of the blood velocity field are correlated Gaussian random variables. The objective of the simulation is to study the effect of the blood turbulence on the movement of drug nanoparticles, and to compare these results with the analytical model of drug propagation.

4.6.1 Monte-Carlo Nanoparticle Random Walk

The stochastic differential equation governing the displacements of the nanoparticles according to the Langevin equations [79] describing the movement of a drug nanoparticle in a fluid are $dz(t) = Re\{u_z(z,r,t)\}\,dt + G_z\sqrt{2Ddt}$ and $dr(t) = Im\{u_r(z,r,t)\}\,dt + G_r\sqrt{2Ddt}$, where D is the nanoparticle diffusion coefficient defined, $u_z(z,r,t)$ and $u_r(z,r,t)$ are the axial and the radial components of the random blood velocity process at time t in the point with coordinates (z,r) respectively, $Re\{\cdot\}$ is the operator giving the real part, $Im\{\cdot\}$ is the operator giving the imaginary part, G_z and G_r are independent standard normal random variables.

4.6.2 Monte-Carlo Simulation Results

Fig. 30(a)- 30(c) compare the drug propagation probability obtained by using the analytical for the PDDS and the drug propagation probability obtained by kinetic Monte-Carlo simulation. The results are obtained by placing nanoparticles in the injection point of the blood vessel network, and the nanoparticles that arrive to the drug delivery site of the blood vessel network are counted as the simulation time advances. Fig. 30(a)-Fig. 30(c) show the topologies of the corresponding networks. A good agreement between the analytical model and the kinetic Monte-Carlo results is observed. The drug propagation probability obtained by kinetic Monte-Carlo simulation is noisy because of the discrete number of nanoparticles and their Brownian motion.

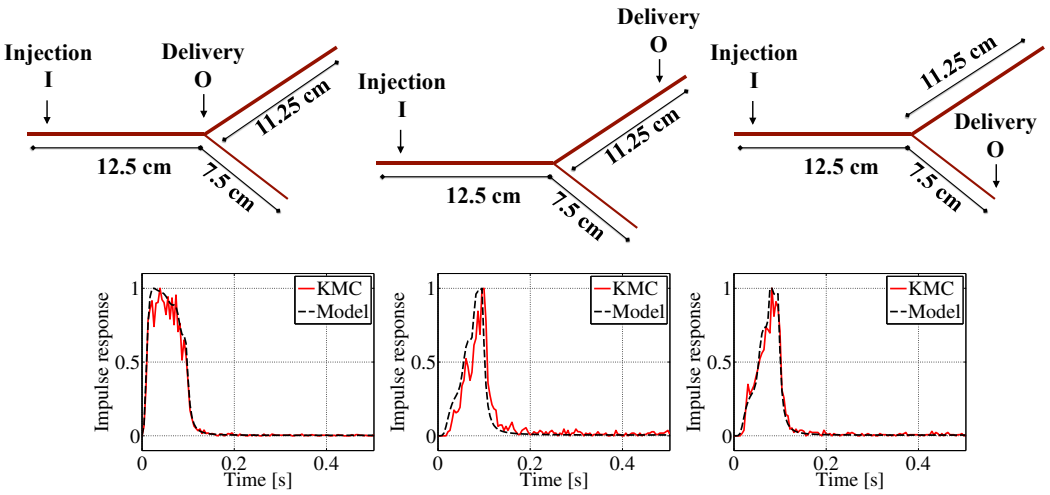

Figure 30. Comparison between the drug propagation probabilities obtained by the MC model and the drug propagation probabilities obtained by the Monte-Carlo simulation for different delivery locations.

4.7 Conclusions

Particulate drug delivery systems (PDDS) aim to delivery a drug load to the parts of the body where it is needed, at the right time and the right concentration levels, through the use of drug nanoparticles that are able to penetrate inside the cells and unleash their drug load. The analysis of the PDDS is crucial for the development of optimal drug delivery formulations and techniques. The modeling of PDDSs allows the prediction of the locations where drug nanoparticles propagate, their number, and the noisiness in their movement. It has been shown in this chapter that the MC communication paradigm where the information is conveyed through molecules enables a thorough analysis of the PDDS in the human body. In fact, an MC model of the PDDS is developed, taking into account all the possible physiological parameters of the system, such as the drug injection device, the propagation in the intricate network of blood vessels, the time-variance and turbulence of the blood flow, as well as the absorption of drug nanoparticles by the diseases cells through the ligand-binding mechanisms.

Drug nanoparticles undergo many noise effects such as the injection noise, the blood velocity turbulence, the ligand-binding noise, and the Brownian motion of nanoparticles. In this chapter, these noise effects have been modeled through the MC paradigm where

information is conveyed through the propagation of nanoparticles. These noise effects have been modeled as interference in an MC system. The use of information theory was advocated for the design of the PDDS. The analogy between the number of possible therapeutic responses deliverable by the PDDS and the size of the alphabet in a communication system was used. The PDDS was assessed as an efficient system if it is able to reliably deliver a diverse set of therapeutic responses, depending on the stage and nature of the disease and the individual specificities.

To our knowledge, this is the first work to propose the use of information theory in the PDDS design. Other works were mainly based on deterministic and probabilistic analysis of the long-term drug distribution throughout the body. Our information-theoretical approach can be applied to put into use high precision nanomedicine delivery, in contrast with traditional medicine where the drug injection is not optimized with respect to the body variabilities such as the blood flow, the ligand-binding kinetics, and their interaction.

The noise effects in the propagation of drug nanoparticles in the cardiovascular system have been simulated by using kinetic Monte-Carlo simulations. The simulations show a good agreement between the analytical model and the kinetic Monte-Carlo simulation results. This study confirms that the MC paradigm can be conveniently used for the analysis and optimization of the PDDS.

We suggest as future work to experimentally measure the distribution of drug nanoparticles in the cardiovascular system at an accurate time and space scale. These experimental results would be beneficial to validate the MC model. The existing experimental work on the distribution of nanoparticles is constrained to study their space and time evolution on a very large scale, in the order of hours and on the level of organs as a whole. We believe that the advent of nanomedicine allows to control the drug injection at a much more accurate resolution, and that therefore the distribution of nanoparticles should be studied in the order of millimeters and seconds to develop a highly targeted PDDS.

The PDDS model makes it possible to engineer therapeutic solutions that are inspired

by the naturally-occurring defense mechanisms that the body deploys to combat diseases and anomalies in its functioning. The noise modeling is particularly important to the field of cancer therapy, where the choice of low concentration of drug nanoparticles is made to avoid toxic effect of the drugs, at the expense of the accuracy of the drug delivery. The PDDS model provides quantitative models to find trade-offs between toxicity and drug efficiency to facilitate cancer therapy. Ultimately, the MC paradigm can be used to create bio-inspired molecular nanonetworks for the advanced nano-scale monitoring and healing of the human body.

CHAPTER 5

PHARMACOKINETIC MODELING USING MOLECULAR COMMUNICATION

5.1 Motivation and Related Work

Targeted Drug Delivery Systems (TDDSs) [80] are cutting-edge therapeutic methods, which aim at delivering the drug exactly where it is needed while minimizing the adverse effects of the drug on the other healthy parts of the body, by using micro- or nano-sized drug-loaded particles. The estimation of how the drug-loaded particles distribute within the body, named biodistribution, is essential for TDDS engineering, and it is directly related to the processes involved in the particle propagation, such as their advection and diffusion in the blood stream, their absorption from surrounding tissues, and their chemical and physical interactions with other biomolecules present in the body. Although drug biodistribution can be estimated empirically through clinical experiments, these are rarely performed because of the ethical and financial constraints they pose [81] and their specificity to each individual subject.

Recent advances in biomaterials allow the engineering of drug particles with very specific chemical and geometric properties in order to provide a targeted drug delivery. To benefit from these technological advances and study the properties of drug particles to guarantee an optimal biodistribution, the aforementioned particle propagation processes have to be modeled through the study of the so-called drug pharmacokinetics. The most successful existing TDDS pharmacokinetic models are based on the multi-compartmental approach [82], where large portions of the human body are considered as single compartments, with homogeneous chemical and physical properties. The pharmacokinetics in one compartment is commonly described through first-order differential equations, and the evolution of the pharmacokinetics is obtained for a time scale in the order of hours. These models include: i) TMDD (Target-Mediated Drug Disposition) [20], where the equations

are based on a very limited number of parameters that are empirically derived; ii) PK/PD (Pharmacokinetics and Pharmacodynamics) [83], where the equation parameters are statistically derived from experimental work, and the pharmacokinetics is modeled only locally within a spatial scale of a cell; iii) PBPK (physiologically-based pharmacokinetics) [84], where pharmacokinetics is modeled globally for the whole body but by considering each organ as a single compartment where the drug is homogeneously distributed.

Especially, nanomedicine-enabled TDDSs require new pharmacokinetic models where the particle propagation processes within the body are described in greater precision at a much smaller time and space resolution, and in a tractable manner, whereas the aforementioned models account for particle propagation only at the spatial resolution of organs and the time scale of days. Moreover, the existing models are not sufficiently scalable and are not customizable to the patients and their specific diseases [82].

To tackle the aforementioned problems, we propose a TDDS pharmacokinetic model based on the abstraction of Molecular Communication (MC), a recently developed paradigm in communication theory that defines information exchange through the emission, propagation, and reception of molecules. In [57], we developed an MC model to calculate the time-varying blood velocity in any location of the cardiovascular system, and to predict the propagation of the drug-loaded particles due to advection and diffusion in the blood flow. In this chapter, by stemming from our previous work, we develop a TDDS pharmacokinetic model able to predict the propagation of the particles by taking into account other specific physicochemical processes, as well as abnormal health conditions. Through the MC paradigm, we consider the following physicochemical processes:

- The *advection process*, which represents the transport of particles due to the blood velocity.
- The *diffusion process*, which corresponds to the Brownian motion of particles
- The *absorption process*, which quantifies the particles absorption through tissues

surrounding the blood vessels [85].

- The *reaction process*, which is a consequence of the degradation of particles in the blood [86].

- The *adhesion process*, which accounts for other biomolecules binding to the drug-loaded particles. The adhesion process is one of the main adverse effects to the performance of the TDDSs [87].

In the proposed pharmacokinetic model, we also account for the effects on the drug pharmacokinetics of cardiovascular diseases, which include blood vessel leakage, e.g., due to tumors, and rigidity, e.g., due to arteriosclerosis. These effects are analytically considered in the proposed pharmacokinetic model, and are shown to greatly affect the drug particle distribution through numerical evaluations of the pharmacokinetic model and the biodistribution estimation.

In the proposed pharmacokinetic model, we also account for the effects on the drug pharmacokinetics of cardiovascular diseases, which include blood vessel leakage, e.g., due to tumors, and rigidity, e.g., due to arteriosclerosis. These effects are analytically considered in the proposed pharmacokinetic model, and are shown to greatly affect the drug particle distribution through numerical evaluations of the pharmacokinetic model and the biodistribution estimation.

By stemming from the proposed MC-based pharmacokinetic model, we propose a method to estimate the drug biodistribution. We propose to characterize the presence of the drug at the delivery location through communication engineering metrics, namely, channel delay and path loss, analytically derived from the proposed pharmacokinetic model. The **channel delay** corresponds to the time needed by the drug particles to reach their peak concentration at the delivery location after they are injected, while the **channel path loss** is the ratio of the drug particles that effectively reach the delivery location over the drug particles that were initially injected. In addition, we also demonstrate that the proposed

pharmacokinetic model allows to analytically estimate the drug accumulation in the rest of the body.

The proposed MC-based pharmacokinetic model is validated through finite-element simulations on COMSOL, which consider 3D Navier-Stokes and advection-diffusion-reaction equations to simulate the drug propagation in a time-varying blood flow through a 3D model of a blood arterial network. The proposed MC-based pharmacokinetic model proves to be in good agreement with the results of the simulation, therefore reproducing similar results with analytical expressions, which do not require the computational complexity of the finite-element simulations. Additionally, numerical results are provided for the biodistribution estimation in different health scenarios, namely, in the presence of arteriosclerosis and tumor-induced blood blood vessel leakage. Through these results, we show that the transport and kinetic properties are important factors influencing the pharmacokinetics of the drug-loaded particles.

Finally, by stemming from the proposed model, we detail a procedure to analytically express the optimal drug injection rate given a target drug delivery rate. For this, we suppose that the healing of the disease requires an objective drug delivery rate, and that the drug injection and delivery locations are known. The proposed pharmacokinetic model is then applied to analytically obtain the optimal drug injection rate.

The rest of the paper is organized as follows. In Section 5.2, we mathematically describe the **pharmacokinetic model** based on the MC abstraction of the physicochemical processes in the drug-loaded particle propagation, namely, advection, diffusion, reaction, absorption, and adhesion. Moreover, we incorporate in the pharmacokinetic model possible cardiovascular diseases affecting the blood flow. In Section 5.3, we obtain the **biodistribution estimation** of the particles through the communication engineering metrics of channel path loss and delay, and the expressions to compute the drug accumulation in the rest of the body. Numerical results are provided for the biodistribution in different scenarios. In Section 5.4, the **validation of the MC-based pharmacokinetic model with multiphysics**

finite element simulation is presented. In Section 5.5, we apply the MC-based pharmacokinetic model to find the **optimal drug injection rate** that would achieve an objective drug delivery rate at the delivery location. Finally, Section 6.8 concludes the paper with comments about the validity of the model and the various factors influencing the performance of TDDSs.

5.2 MC-based Pharmacokinetic Model

In this section, we mathematically describe the pharmacokinetic model of a TDDS based on the analytical MC channel abstraction, which considers additional physicochemical processes in the particle propagation from the injection location to the delivery location, in addition to the advection and diffusion processes already considered in [57].

The network of blood vessels is abstracted here as an MC network. Fig. 31 illustrates the physicochemical processes in a blood network consisting of several blood vessels. $u_n(t)$ denotes the blood velocity in a blood vessel n, and t is the time variable. The drug propagates in this blood network subject to an absorption with rate ρ_n, reaction with rate μ_n, adhesion with an adsorption rate k^+ and a desorption rate k^-, diffusion with a diffusion coefficient D, and advection driven by the blood velocity. The drug propagation is abstracted as an MC channel, and completely characterizes the relationship between the drug injection rate and the drug delivery rate. The drug injection rate is the MC signal transmitted at the inlet of the blood vessel and the drug delivery rate is the MC signal received at the outlet of the blood vessel. This is achieved by a time-varying impulse response $h_{(n)}^{(\rho_n,\mu_n)}(t,\tau)$, where τ is a time variable, for every blood vessel n ($n = 1, 2, \ldots, 7$). The MC link channels are cascaded to obtain an MC path, which provides the relationship between the drug injection rate $x(t)$ and the drug delivery rate $y(t)$, through the time-varying impulse response for the path channel, denoted, e.g., by $h_{(1,2,4)}^{(\rho_1,\mu_1,\rho_2,\mu_2,\rho_4,\mu_4)}(t,\tau)$ for the cascade of MC links 1, 2, and 4 as shown in Fig. 31.

In Section 5.2.1, we present how a blood vessel is abstracted as an MC link. In Section 5.2.2, we describe how the physicochemical processes between the drug particles and the body can be modeled by combining MC links. Finally, in Section 5.2.3, the modeling of cardiovascular diseases using equivalent circuits is proposed.

5.2.1 Molecular Communication Link Model

We found in [57] that the drug injection rate $x(t)$ and the drug delivery rate $y(t)$ in the blood vessel n are related mathematically by the following expression:

$$y(t) = \int_{-\infty}^{+\infty} x(\tau) h_{(n)}^{(\rho_n, \mu_n)}(t, \tau) d\tau \,. \tag{121}$$

Due to the fluctuations in the blood flow, the impulse response of the system depends on the state of the blood flow at the time of the injection, therefore the system is not linear time-invariant (LTI). The response of non-LTI systems cannot be expressed in the form of a convolution operation. For the aforementioned reasons, the expression in (121) is different from a convolution. We derive the analytical expression of the time-varying impulse response of the MC link n, as follows:

$$h_{(n)}^{(\rho_n, \mu_n)}(t, \tau) = \frac{\exp\left(-\frac{(l_n - m_n(t,\tau))^2}{2\sigma_n^2(t,\tau)} - \mu_n(t-\tau)\right)}{\sqrt{2\pi\sigma_n^2(t,\tau)}} \,, \tag{122}$$

where:

- $m_n(t, \tau)$ is a function of *apparent velocity* $v_n(t)$ as follows:

$$m_n(t, \tau) = \int_{\tau}^{t} v_n(t') dt' \,, \tag{123}$$

  where t' is the time integration variable.

- $\sigma_n^2(t, \tau)$ is a function of the *effective diffusivity* $D_n(t)$ as follows:

$$\sigma_n^2(t, \tau) = 2 \int_{\tau}^{t} D_n(t') dt' \,. \tag{124}$$

- μ_n is a characteristic of the *reaction process*, and represents the rate of reaction between the particles and the blood.

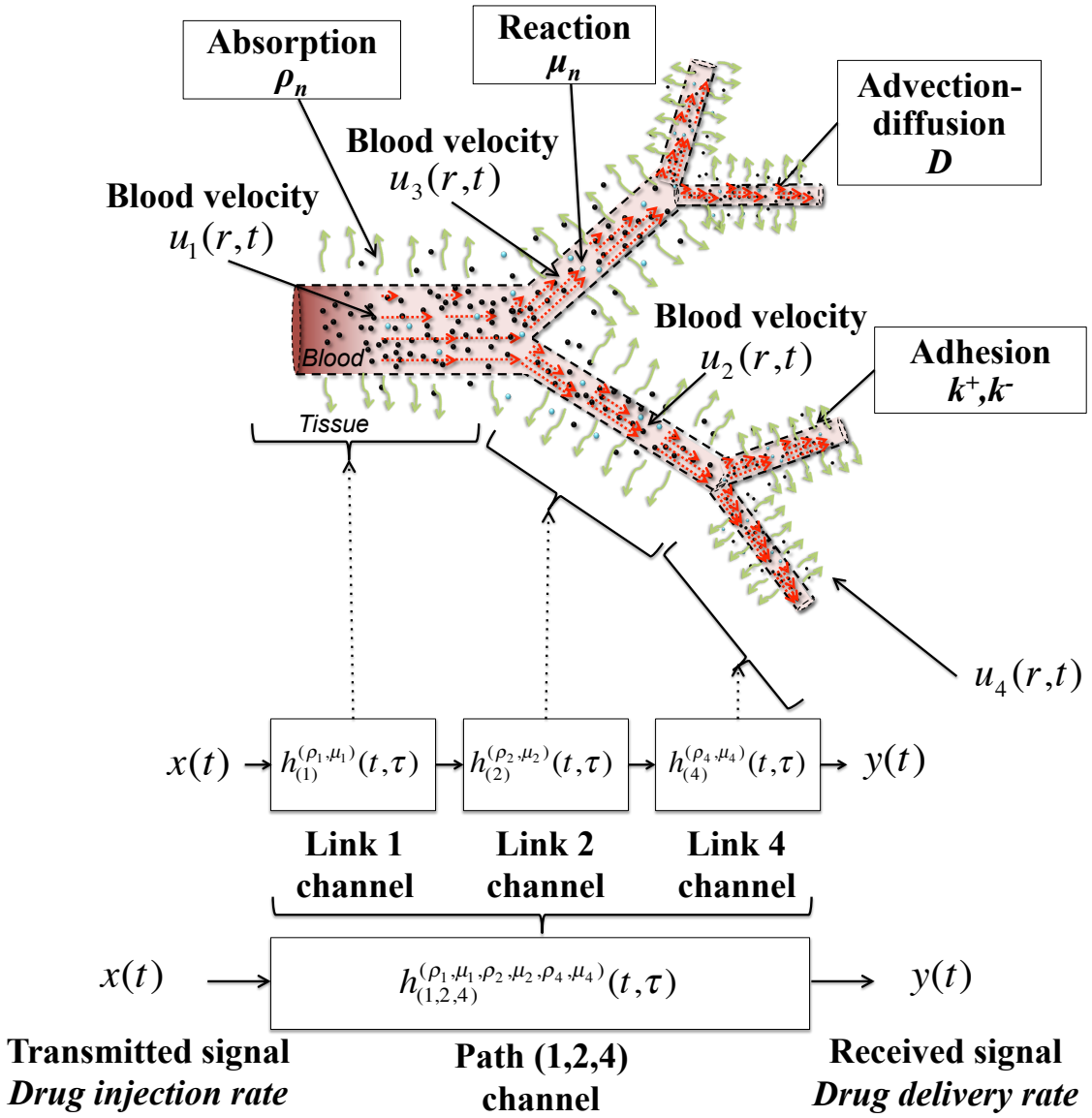

Figure 31. Scheme of the MC modeling of TDDSs pharmacokinetics.

In the following, we provide the expression of the apparent velocity $v_n(t)$ and the effective diffusivity $D_n(t)$ for advection-diffusion (Section 5.2.1.1), absorption (Section 5.2.1.2), and adhesion (Section 5.2.1.3).

5.2.1.1 Advection-diffusion Case (No Reaction)

When the reaction process is absent, and only the advection-diffusion is occurring, the *apparent velocity in the case of no reaction* $v_n^{none}(t)$ and the *effective diffusivity in the case of no reaction* $D_n^{none}(t)$ are:

$$\begin{cases} v_n^{none}(t) = u_n(t) \\ D_n^{none}(t) = D + \frac{u_n^2(t) r_n^2}{192D}, \end{cases} \tag{125}$$

which is a result we derived in [57].

5.2.1.2 Absorption Case

When there is absorption due to the tissues that surround the blood network, the *apparent velocity in the case of absorption* $v_n^{absorption}(t)$ and the *effective diffusivity in the case of absorption* $D_n^{absorption}(t)$ are [88]:

$$\begin{cases} v_n^{absorption}(t) = \left(1 + \frac{2}{15}\rho_n\right) u_n(t) \\ D_n^{absorption}(t) = D + \frac{{u_n}^2(t) r_n^2}{192D} \left(1 - \frac{4}{15}\rho_n\right). \end{cases} \tag{126}$$

5.2.1.3 Adhesion Case

When adhesion to the proteins in the blood plasma or to the blood vessel walls is occurring, the *apparent velocity in the case of adhesion* $v_n^{adhesion}(t)$ and the *effective diffusivity in the case of adhesion* $D_n^{adhesion}(t)$ are [89]

$$\begin{cases} v_n^{adhesion}(t) = \frac{1}{1+\frac{k^+}{k^-}} u_n(t) \\ D_n^{adhesion}(t) = \frac{r_n^2 u_n^2(t)}{48D} \frac{44 r_n^2 \left(\frac{k^+}{k^-}\right)^2 + 12 r_n^2 \frac{k^+}{k^-} + r_n^3}{\left(r_n + 2\frac{k^+}{k^-}\right)^3} \\ \quad + \frac{2 u_n^2(t) r_n^2 \frac{k^+}{k^-}}{k^- \left(r_n + 2\frac{k^+}{k^-}\right)^3} \end{cases}. \tag{127}$$

Section 5.4.2 provides numerical values for the cross-sectional average blood velocities of three blood vessels, obtained using the transmission line method described in [57].

5.2.2 Molecular Communication Path Model

The MC channel model of a path $(n; n = 1 \dots N)$ where n is the index of a link n, is obtained by using the *Harmonic Transfer Matrix* function $HTM\{\cdot\}$ and its inverse $HTM^{-1}\{\cdot\}$ [57]

$$y(t) = \int_{-\infty}^{+\infty} x(\tau) h_{(n;n=1\dots N)}^{(\rho_n,\mu_n;n=1\dots N)}(t,\tau) d\tau \,, \tag{128}$$

where the time-varying impulse response of the path $h_{(n;n=1\dots N)}^{(\rho_n,\mu_n;n=1\dots N)}$ is expressed as follows:

$$h_{(n;n=1\dots N)}^{(\rho_n,\mu_n;n=1\dots N)} = \tag{129}$$

$$HTM^{-1}\left\{\prod_{n=N}^{n=1} HTM\left\{h_{(n)}^{(\rho_n,\mu_n)}(t,\tau)\right\}\right\} , \tag{130}$$

Through the HTM method [35], we can find analytical solutions of the end-to-end impulse response of TDDSs, as opposed to numerical solutions by finite-element models.

5.2.3 Disease Models with Equivalent Circuits

In this section, we present an equivalent circuit modeling of cardiovascular diseases, including arteriosclerosis (rigid blood vessel model), and blood vessel leakage (leaky blood vessel model).

A blood vessel is considered as a cylindrical elastic tube with radius r_n and length l_n, and modeled as an electrical circuit, whose electrical components are related to the geometry of the blood vessels. A healthy blood vessel n possesses three electrical components. First, a resistance R_n, which is related to the blood viscosity and the diameter of the blood vessel. Second, an inductance L_n, which is related to the blood inertia, that is how a difference in blood pressure causes a difference in blood flow. Third, a capacitance C_n, which measures the blood vessel elasticity. We give below the expression of the electrical components based on their physiology [57].

The resistance of the blood vessel n is expressed as follows:

$$R_n = \frac{8\nu}{\pi l_n r_n^4} \,, \tag{131}$$

where ν is the blood viscosity.

The inductance of the blood vessel n is expressed as follows:

$$L_n = \frac{\eta}{\pi l_n r_n^2}\,, \tag{132}$$

where η is the blood density.

5.2.3.1 Rigid Vessel Model

The elasticity of a blood vessel is an important parameter in the success of drug delivery. There have been studies to show how abnormal elasticity affects drug propagation [90]. Blood blood vessels can become rigid because of aging and diseases such as arteriosclerosis [91].

For a rigid blood vessel, we model the change in elasticity using an *arterial elasticity factor*, which measures the ratio between normal elasticity and rigid elasticity. We retain the same electrical components as in the healthy blood vessel model, except for the capacitance, which is now equal to:

$$C_n = \frac{\pi {r_n}^2}{F_C(a_1 \exp(-a_2 r_n) + a_3)}\,, \tag{133}$$

where F_C is the arterial elasticity factor ($F_C = 1$ for a healthy blood vessel, $F_C = 0$ for a completely rigid blood vessel). $a_1 = 1.34 \times 10^7 g/(s^2.cm)$, $a_2 = 22.53 cm^{-1}$, and $a_3 = 5.77 \times 10^5 g/(s^2.cm)$ are statistical parameters obtained from physiological measurements [37].

5.2.3.2 Leaky Vessel Model

The leakage of a blood vessel is modeled by an equivalent conductance, which is related to how easy it is for a fluid to leak from the blood vessel. We retain the same electrical components as for the healthy blood vessel case, but we add an additional conductance G_n to model the blood vessel leakiness:

$$G_n = \frac{F_L}{R_n}\,, \tag{134}$$

where F_L is leakiness factor, which compares the leakage to the conductance of the healthy blood vessel (inverse of the resistance), and R_n is the resistance of the blood vessel.

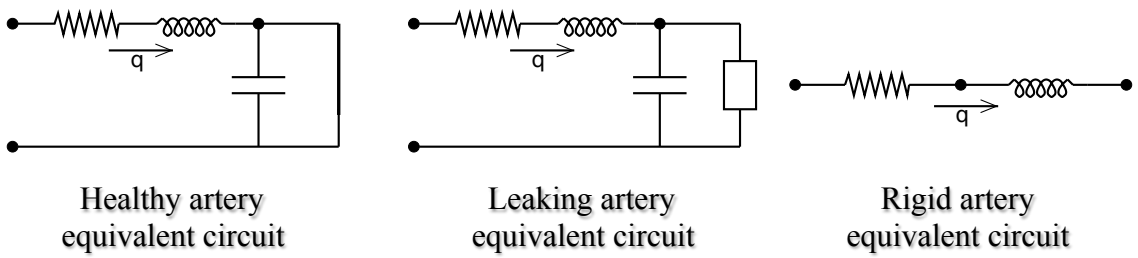

Figure 32. Equivalent electrical circuits for a blood vessel in different conditions.

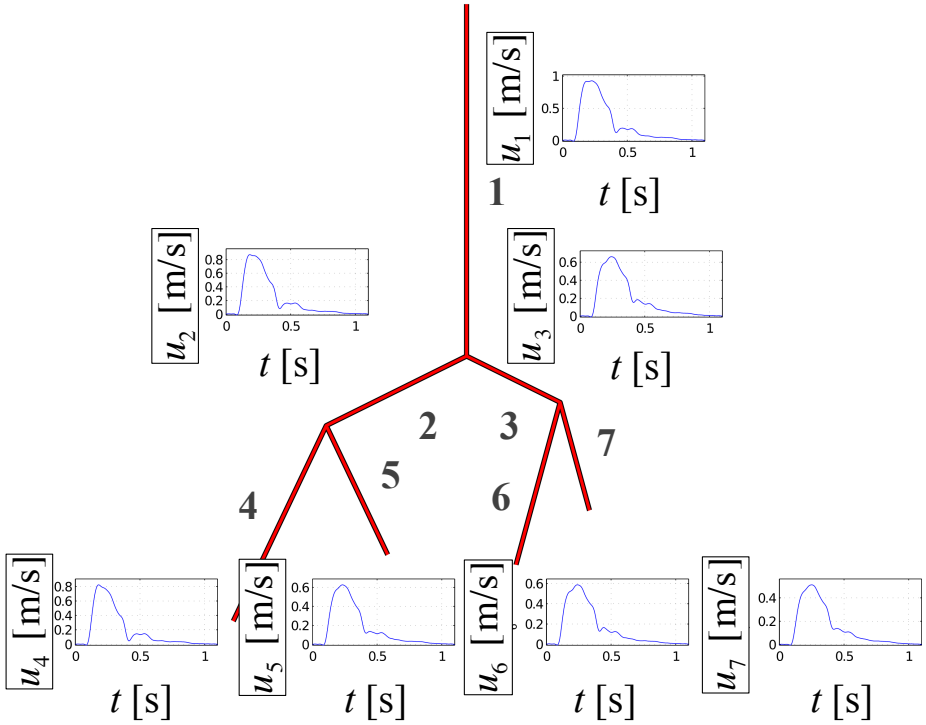

Figure 33. Blood velocities at a tree of small blood vessels in a healthy condition.

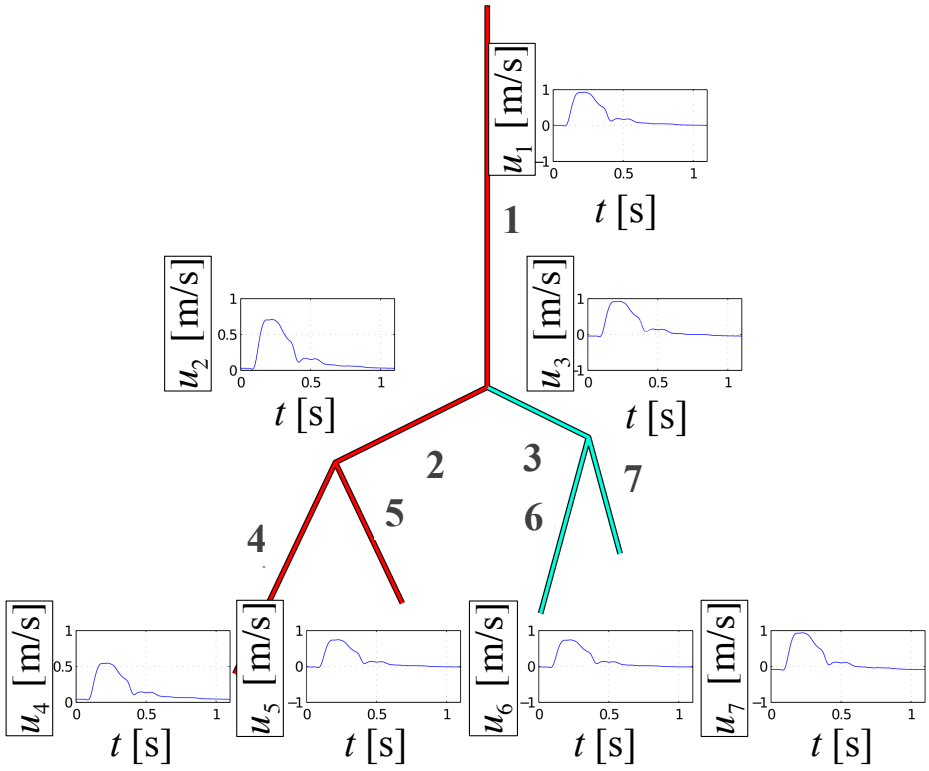

Figure 34. Blood velocities at a tree of small blood vessels with a branch suffering from blood vessel leakage.

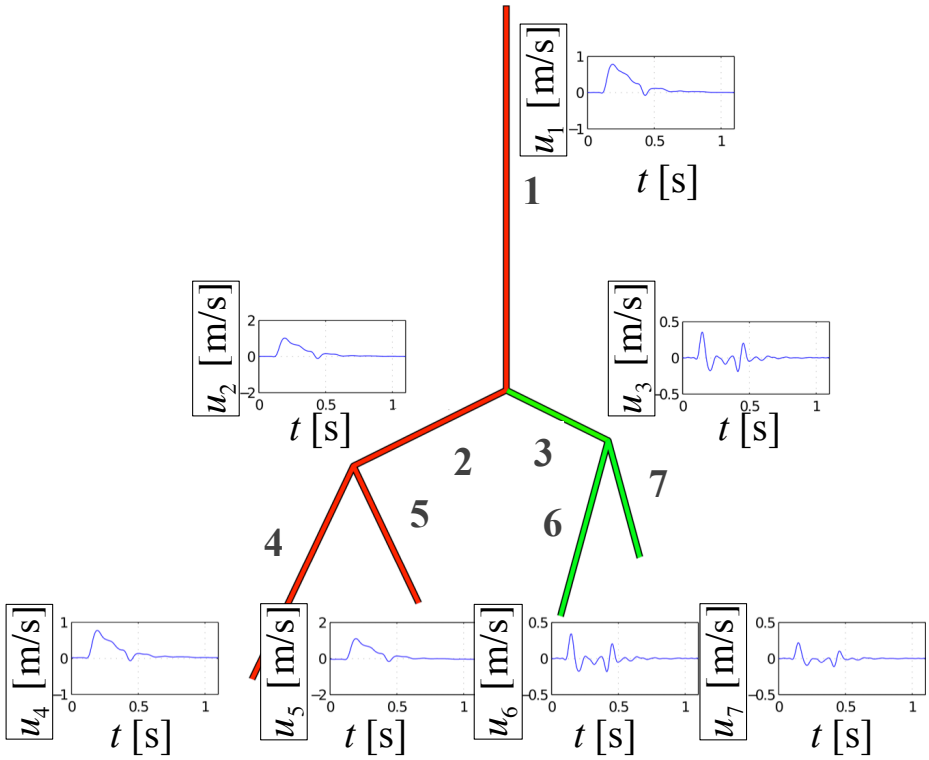

Figure 35. Blood velocities at a tree of small blood vessels with a branch suffering from arteriosclerosis.

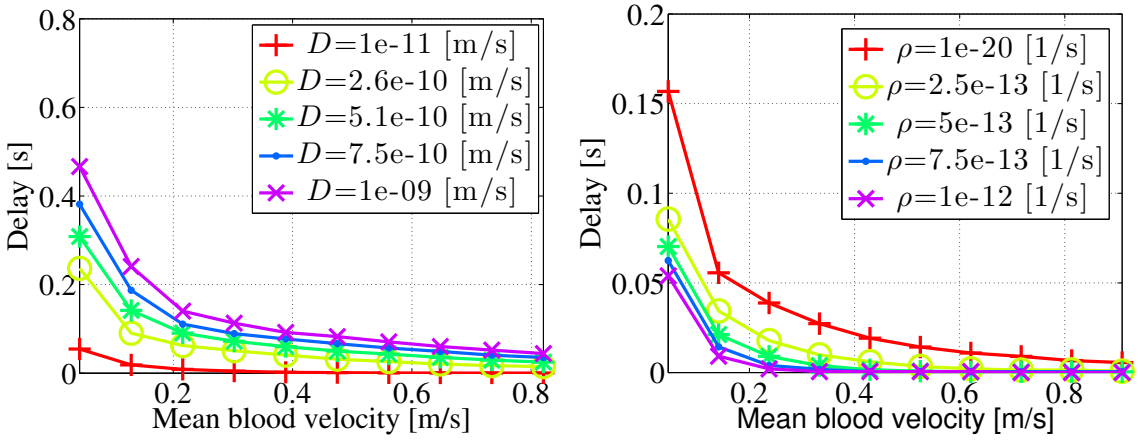

Figure 36. Effect of the diffusion coefficient D and the absorption rate ρ_n on the channel delay.

Fig. 32 shows the equivalent electrical circuit components for a blood vessel in different conditions such as a healthy condition, arteriosclerosis, and blood vessel leakage. By defining electrical equivalents of diseased blood vessels, the blood velocities are calculated by using the transmission line theory method presented in [57], after substituting the expressions of the conductances and the capacitances for healthy blood vessels with the expressions in (133) and (134), respectively. For the numerical results, the inner iliac blood vessel [55] was chosen, and the properties of three of its children blood vessels, denoted as $(3, 6, 7)$ in Fig. 33, Fig. 34, and Fig. 35, respectively, have been modified according to the considered disease condition.

In Fig. 33, we observe that in a healthy arterial tree, the blood velocity tends to dampen slowly as we go farther from the root of the blood vessel. In the case of a blood vessel leakage, as illustrated in Fig. 34, this trend is not observed, where we can see that the blood velocity may increase in some daughter blood vessels, since the resistance is reduced. Fig. 35 shows the extreme case where a portion of the arterial tree is affected by a severe arteriosclerosis. In that case, the diseased blood vessels exhibit a highly oscillatory blood flow.

The method introduced in this section can be applied to model the drug propagation in any location of the arterial network.

5.3 Biodistribution Estimation

The biodistribution is the study of the location and the quantity of the drug that is accumulated in the delivery location and the rest of the body, whether in the blood vessels, their surround tissues, or reacting with elements of the blood plasma. In this section, we estimate the biodistribution of TDDSs using the MC paradigm through the definition of two MC metrics, namely, the channel delay and the channel path loss. In Section 5.3.1, the channel delay is the time needed by the drug particles to reach their peak concentration at the delivery location after they are injected in the body. In Section 5.3.2, the channel path loss is the proportion of the injected particles that reach the delivery location despite the blood vessels branching, reaction, adhesion, and absorption. Finally, in Section 5.3.3, the drug accumulation in the rest of the body is expressed analytically using the MC model.

5.3.1 Channel Delay to the Delivery Location

We define the delay for a TDDS as the time required by injected molecules to reach their peak concentration at the delivery location, which is a definition typically used in biodistribution. Another definition of delay used in biodistribution studies is the half-life of a drug [92], which is only meaningful for drugs undergoing an exponential decay. The definition we choose is more general than half-life, and can provide more information about the toxicity, potency, and elimination rate of the drug, since these properties depend on the overall time spent by the majority of the molecules between the injection location and the delivery location.

We express the channel delay t_{delay} for the path $(n; n = 1 \dots N)$ as

$$t_{delay} = \frac{1}{T} \int_0^T \arg\max_{t>\tau} h^{(\rho_n,\mu_n;n=1\dots N)}_{(n;n=1\dots N)}(t+\tau,\tau)d\tau\,, \tag{135}$$

where $h^{(\rho_n,\mu_n)}_{(n;n=1\dots N)}(t,\tau)$ is the time-varying impulse response with injection starting at the time τ, and T is the heartbeat period.

Since the channel is time-varying and the blood flow changes periodically, the injected drug particles will be delivered with a different channel delay at the delivery location depending on the blood velocity that was experienced by the body when they were injected.

We consider the ambiguity in knowing the blood velocity at the time of injection by averaging over the channel delays for all possible blood velocity values that the body may experience.

The definition of the delay as the average is only acceptable for long propagation times. However, it is acceptable to use the delay as the average value to compare several drug delivery systems that are within the same flow, and propagation length conditions. The standard deviation (or error) in the delay calculation can be highly variable for the scenario where the propagation time is low. If the blood velocity period is higher than the time it takes for the molecules to reach the delivery location, then the error can be as much as in the order of 100%. However, if the blood velocity period is small compared with the delay, then the error is negligible, which means that the injection time is not critical.

5.3.2 Channel Path Loss at the Delivery Location

We define the channel path loss for the path $(n; n = 1 \dots N)$ as

$$L = 10 \log_{10} \left(1 - \int_0^{+\infty} h_{(n;n=1\dots N)}^{(\rho_n,\mu_n;n=1\dots N)}(t,0)dt \right), \tag{136}$$

where $h_{(n;n=1\dots N)}^{(\rho_n,\mu_n)}(t,0)$ is the time-varying impulse response, which we defined in Section 5.2.2 with injection starting at the time $\tau = 0$. This relationship comes from the fact that the impulse response is the probability density of a single particle arriving at a specific location and time. The log-scale is used because about half of the particles are lost at every blood vessel bifurcation, which makes the particle loss follow an exponential trend. In Fig. 36, we see the effect of the blood velocity, the drug diffusion coefficient and the reaction rate on the channel delay. In the numerically evaluated scenario in Fig. 37 , we observe that the increase in the drug diffusion coefficient contributes in increasing the delay of the channel, while the effect of the absorption rate contributes in decreasing the delay.

In Fig. 37, we observe that reaction and absorption have similar consequences on the channel path loss. For the absorption, we see that the higher the absorption rate the smaller

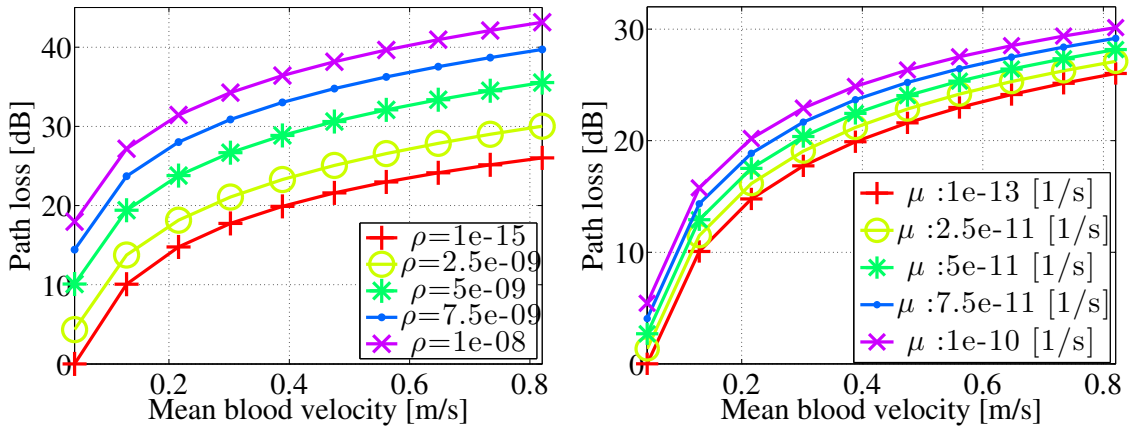

Figure 37. Effect of the absorption rate (ρ_n) and the reaction rate (μ_n) on the path loss.

the delay, which may seem counterintuitive. The reason behind the reduction in delay for increased absorption is that the absorption reduces the number of particles in the blood that are in proximity of the walls, which are the slowest moving particles, thus increasing the average velocity of all the particles.

5.3.3 Drug Accumulation in the Rest of the Body

Using the time-varying impulse response, we can calculate the proportions of the drug particles that are either still in the blood, have been absorbed by the surrounding tissues, or have reacted with the blood plasma.

We can express the proportion of drug particles that have been absorbed as follows:

$$d_{absorbed} = \frac{r_N^2}{r_1^2}\left(\int_0^{+\infty} h_{(n;n=1\ldots N)}^{(0,0;n=1\ldots N)}(t,0)dt - \int_0^{+\infty} h_{(n;n=1\ldots N)}^{(0,\mu_n;n=1\ldots N)}(t,0)dt\right). \tag{137}$$

Similarly, the proportion of drug particles that have reacted can be expressed as follows,

$$d_{reacted} = \frac{r_N^2}{r_1^2}\left(\int_0^{+\infty} h_{(n;n=1\ldots N)}^{(0,0;n=1\ldots N)}(t,0)dt - \int_0^{+\infty} h_{(n;n=1\ldots N)}^{(0,\mu_n;n=1\ldots N)}(t,0)dt\right). \tag{138}$$

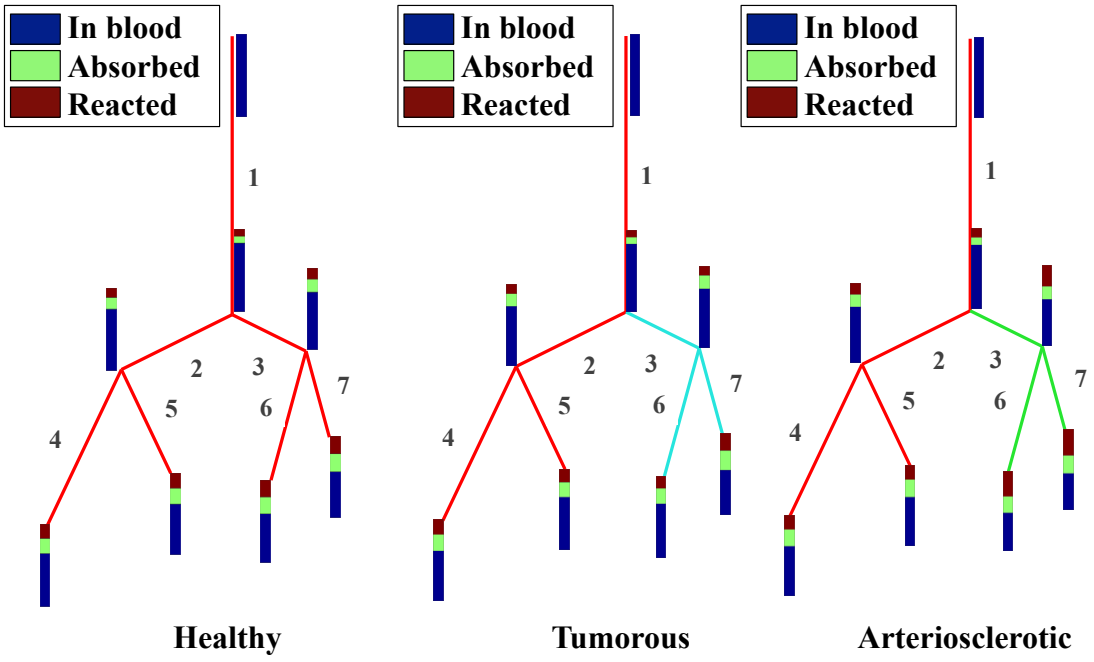

Figure 38. Effect of cardiovascular diseases on drug distribution.

Finally, the proportion of drug particles that remain in the blood is equal to the following:

$$d_{blood} = \frac{r_N^2}{r_1^2}\left(\int_0^{+\infty} h_{(n;n=1\ldots N)}^{(0,0;n=1\ldots N)}(t,0)dt \right. \tag{139}$$

$$\left. - \int_0^{+\infty} h_{(n;n=1\ldots N)}^{(\rho_n,\mu_n;n=1\ldots N)}(t,0)dt\right). \tag{140}$$

Therefore, we can use the MC paradigm to predict where the drug is going to accumulate based on the physiological parameters of the drug delivery system and the body. As presented in Fig. 38, the blood vessel conditions cause some variance in the biodistribution. This is moderately important in leaky blood vessels, but is very important in the case of blood vessels affected by arteriosclerosis.

5.4 Multiphysics Finite-Element Validation

In order to obtain a pharmacokinetic model of TDDSs, we made the following assumptions: continuous concentration at the bifurcation, Poiseuille flow, Taylor dispersion approximation, perfectly cylindrical geometry, and infinite-length blood vessels. Using finite-element

analysis, the developed model is validated realistically in a 3D geometry and assuming physical equations in their full forms. In this section, we present the validation of the MC model of TDDSs by simulation using finite-element analysis. We describe the geometry of the simulated system, its governing physical equations, and how the parameters of the analytical model have been mapped to parameters of the finite-element analysis.

Finite element analysis is a numerical method used to solve partial differential equations [9] that underlie the behavior of complex physical systems, including mechanical and chemical transport systems. Finite element analysis has several advan- tages compared with analytical models. First, finite element analysis allows to simulate objects of arbitrarily complex 3D geometry. This is especially required for biological objects such as blood vessels which have an imperfectly cylindrical shape and bifurcation shapes. Second, finite element analysis makes it possible to simulate the interaction of different physical phenomena, such as the interaction of the blood vessel walls, the blood flow, which is governed by fluid mechanics, and the chemical transport of drugs. The validation is carried out using COMSOL®[1], a finite element simulation software package.

The following aspects of a drug delivery systems are considered in the simulation as follows:

- *Blood flow:* the validation is performed using a 3D model of a blood arterial network under realistic conditions. The blood flow, which is the main driving force of the drug propagation, is simulated using the 3D Navier-Stokes equations in the stationary domain. In contrast with existing pharmacokinetic models which are based on unrealistic assumption of having a constant blood flow [93], the drug is propagated through a time-varying blood flow. The blood flow boundary conditions in the arterial networks are estimated based on the realistic transmission line theory which provides results in very good agreement with MRI measurements of blood flow in a human [57].

[1]COMSOL® is a registered trademarks of COMSOL AB.

- *Geometry:* in the simulation, we assume cylindrically-shaped small blood vessels, which is in agreement with the physiological observations [94]. Large blood vessels and anomalously shaped blood vessels can be considered with little modifications.

- *Drug transport:* Through the COMSOL simulation, we observe that the MC model based on Taylor dispersion is a good approximation of particle transport in blood and that, therefore, higher-order approximations [95] which will make the expression of the analytical solution more complex are not needed.

- *Drug kinetic interactions:* the binding is considered by adding a linear reaction term to the 3D advection-diffusion equation. The absorption is simulated as a boundary condition on the blood vessel walls where the particles are not perfectly bouncing but proportionally lost at the surface. The linear first order kinetics for binding and absorption are common for particles [96]. We assume that no other kind of binding occurs and that particles are at a sufficiently low concentration to avoid non-linear binding kinetics.

5.4.1 Topology

For the numerical evaluation of the model, the topology information was derived from the MRI scan of a young male individual, which is available from [55]. However, the available MRI scan anatomical information only covers the large blood vessels. An algorithm that represents the small blood vessels as a fractal tree rooted in the extremity of the large blood vessels was used to obtain the topology of the studied area, in a similar way as in [57]. The numerical values and structure of the topology are listed in this chapter and included in Table 2 to simplify the reproduction of the results. In fact, a blood network was considered, consisting of interconnected blood vessels n, where n is the blood vessel index ($n = 1 \ldots 7$). The *parent blood vessel* 1 bifurcates into two blood vessels, the *daughter blood vessel* 2 and the *daughter blood vessel* 3, and so on. The blood vessel n has a radius r_n and a length l_n, for $n = 1 \ldots 7$. We have $r_1 = 0.5\,mm$, $r_2 = 0.45\,mm$, $r_3 = 0.3\,mm$, $r_4 = 0.40\,mm$, $r_5 = 0.23\,mm$,

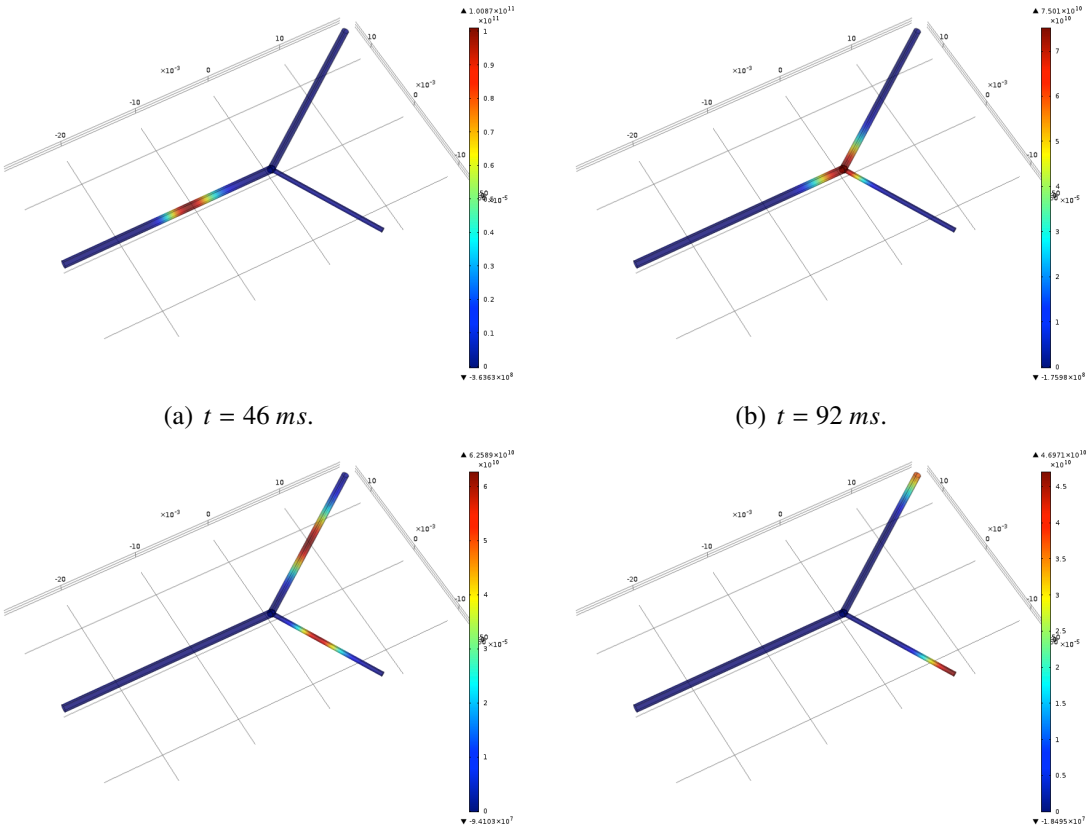

(a) $t = 46\ ms$.

(b) $t = 92\ ms$.

(c) $t = 138\ ms$.

(d) $t = 184\ ms$.

Figure 39. Evolution of the drug propagation in a tree of blood vessels showing the transport of the injected drug particles from the inlet of the tree of blood vessels to the outlets of the branches, at different times t.

$r_6 = 0.27\ mm$, and $r_7 = 0.18\ mm$ for the radii, and $l_1 = 25\ mm$, $l_2 = 22.5\ mm$, $l_3 = 15\ mm$, $l_4 = 20\ mm$, $l_5 = 11.5\ mm$, $l_6 = 13.5\ mm$, $l_7 = 9\ mm$. These dimensions are chosen to be physiologically plausible [55]. According to the physiological data about the size of blood vessels, all types of veins and blood vessels have an interior radius of the blood vessels that is very small compared to the length. This is supported quantitatively in the human and animal physiology literature such as in [55]. In particular, the work in [55] mentions that the length of blood vessels is 25 times the size of their diameters with a standard deviation equal to 5. This work also uses straight cylinders to model blood propagation in blood vessels, which occurs at a faster scale than drug diffusion.

Table 2. Blood network boundary conditions numerical values

k	0	1	2	3
$q_{k,1}$	$1.3 \cdot 10^{-4}$	$2.9 \cdot 10^{-3}$	$-1.8 \cdot 10^{-4}$	$1.6 \cdot 10^{-5}$
$p_{k,1}$	$1.3 \cdot 10^{-4}$	$1.7 \cdot 10^{-4}$	$5.0 \cdot 10^{-5}$	$-6.3 \cdot 10^{-5}$
$q_{k,1}$	$1.3 \cdot 10^{-4}$	$2.9 \cdot 10^{-3}$	$-1.8 \cdot 10^{-4}$	$1.6 \cdot 10^{-5}$
$p_{k,2}$	$1.3 \cdot 10^{-4}$	$1.7 \cdot 10^{-4}$	$4.9 \cdot 10^{-5}$	$-6.2 \cdot 10^{-5}$
$q_{k,2}$	$1.3 \cdot 10^{-4}$	$2.8 \cdot 10^{-3}$	$-1.7 \cdot 10^{-4}$	$1.6 \cdot 10^{-5}$
$p_{k,3}$	$7.3 \cdot 10^{-5}$	$9.6 \cdot 10^{-5}$	$2.8 \cdot 10^{-5}$	$-3.5 \cdot 10^{-5}$
$q_{k,3}$	$7.3 \cdot 10^{-5}$	$1.6 \cdot 10^{-3}$	$-9.8 \cdot 10^{-5}$	$8.8 \cdot 10^{-6}$
$p_{k,4}$	$1.3 \cdot 10^{-4}$	$1.7 \cdot 10^{-4}$	$4.9 \cdot 10^{-5}$	$-6.1 \cdot 10^{-5}$
$q_{k,4}$	$1.3 \cdot 10^{-4}$	$2.8 \cdot 10^{-3}$	$-1.7 \cdot 10^{-4}$	$1.5 \cdot 10^{-5}$
$p_{k,5}$	$7.2 \cdot 10^{-5}$	$9.5 \cdot 10^{-5}$	$2.7 \cdot 10^{-5}$	$-3.5 \cdot 10^{-5}$
$q_{k,5}$	$7.2 \cdot 10^{-5}$	$1.6 \cdot 10^{-3}$	$-9.6 \cdot 10^{-5}$	$8.6 \cdot 10^{-6}$
$p_{k,6}$	$7.2 \cdot 10^{-5}$	$9.5 \cdot 10^{-5}$	$2.7 \cdot 10^{-5}$	$-3.5 \cdot 10^{-5}$
$q_{k,6}$	$7.2 \cdot 10^{-5}$	$1.6 \cdot 10^{-3}$	$-9.6 \cdot 10^{-5}$	$8.6 \cdot 10^{-6}$
$p_{k,7}$	$4.0 \cdot 10^{-5}$	$5.3 \cdot 10^{-5}$	$1.5 \cdot 10^{-5}$	$-1.9 \cdot 10^{-5}$
$q_{k,7}$	$4.0 \cdot 10^{-5}$	$8.9 \cdot 10^{-4}$	$-5.4 \cdot 10^{-5}$	$4.9 \cdot 10^{-6}$

5.4.2 Blood Velocity Boundary Conditions

The multiphysics finite-element simulation requires the definition of boundary conditions, which are values defined at the surfaces of the blood network, to find the numerical solutions that satisfy the physical equations. We use five boundary conditions which are defined at the inlet ($n = 1$) and the outlets ($n = 4, 5, 6, 7$) of the blood network as shown in Fig 39. Thus, there are five boundary conditions which are the *blood velocity* $u_1(t)$ at the inlet of the network, and the blood velocities $u_n(t)$ for the blood vessels n, for $n = 4, 5, 6, 7$, respectively. The numerical values for the boundary conditions have been obtained using the transmission line model developed in [57]. Since the boundary conditions are time-varying and periodic, we express them in terms of their Fourier series decomposition as follows:

$$u_n(t) = \sum_{k=0}^{K-1} p_{k,n} \sin(k\omega_0 t) + q_{k,n} \cos(k\omega_0 t)\,, \tag{141}$$

where $\omega_0 = 2\pi/T$ is the radial sampling frequency, K is the number of samples, and the coefficients $\{p_{k,n}; k = 0 \ldots K-1\}$ and $\{q_{k,n}; k = 0 \ldots K-1\}$ are the even and odd Fourier coefficients, respectively.

5.4.3 Drug Propagation Initial Conditions

The drug propagation initial conditions describe the initial values of the drug concentration in the blood network at time t. We express the initial drug concentration $c(x_1, y_1, z_1, t)$ in the blood vessel n as a function of the Cartesian coordinates, with the origin at the center of the inlet of the blood vessel 1, and the $\vec{x_1}$ axis along the longitude of the blood vessel. We approximate the drug injection impulse with a Gaussian function with a very small variance, which we can write as follows:

$$c(x_1, y_1, z_1, t) = \frac{e^{-\frac{x_1^2}{2\sigma_1^2}}}{\sqrt{2\pi\sigma_1^2}} c_0 \,, \tag{142}$$

where x_1 is the Cartesian coordinate along the longitude of the blood vessel 1, σ_1 is the standard deviation of the impulse, and c_0 is the initial concentration of particles. The justification of a drug injection as a Gaussian function rather than a Dirac delta function is essential to obtain the resolution of partial differential equations using using a finite-element methods solver [97].

5.4.4 Validation Results

The impulse responses $h^{(\rho_n,\mu_n;n=1\ldots N)}_{(n;n=1\ldots N)}(t,\tau)$ are evaluated at the outlets of the blood vessels n where $n = 1 \ldots 3$. We evaluate the impulse response $h^{(\rho_n,\mu_n)}_{(n)}(t,\tau)$ as:

$$\begin{aligned} &h^{(\rho_n,\mu_n;n=1\ldots N)}_{(n;n=1\ldots N)}(t,\tau) \\ &= \frac{1}{S_{O_n}} \int_{M(x,y,z_n)\in O_n} c(x,y,z_n,t) dx dy dz \,, \end{aligned} \tag{143}$$

where O_n denotes the outlet of the blood vessel n, S_{O_n} is the surface area of O_n, $M(x, y, z_n)$ is a point in O_n, and $c(x, y, z_n, t)$ is the concentration at the time instant t and the point with the coordinates (x, y, z_n).

The simulations were performed using COMSOL on a desktop machine with a total computation time of $2\ h\ 57\ min$ to build the map of blood velocity and for the propagation of drug particles, for a simulation duration $T_{sim} = 0.25\ s$. Table 2 lists the Fourier coefficients that have been used in the multiphysics finite-element calculations.

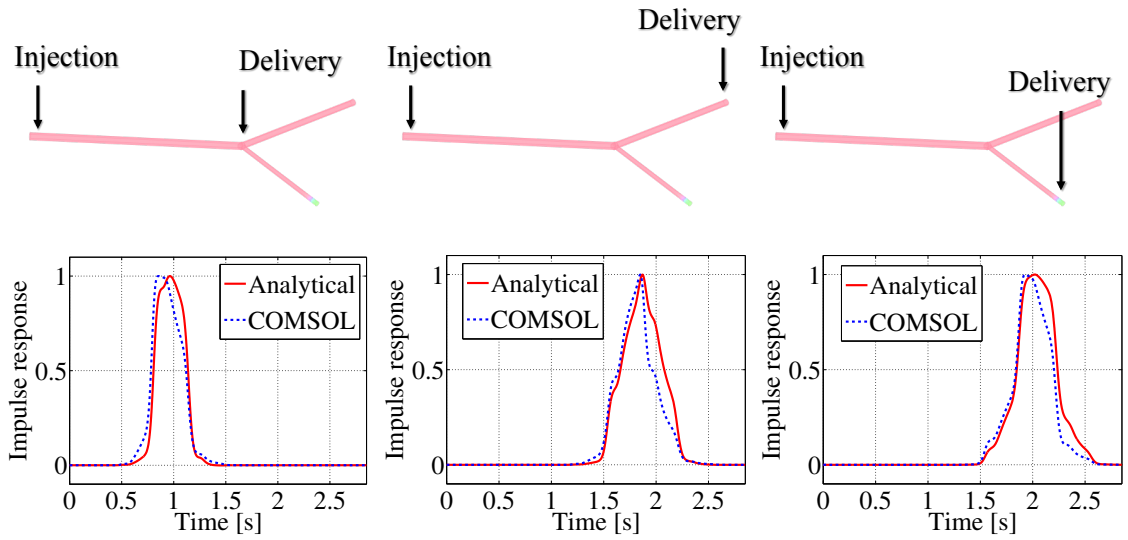

Figure 40. Comparison between the impulse responses obtained by the MC model and the impulse responses obtained by the multiphysics finite-element simulation technique for different delivery locations at the outlet of the blood vessels 1, 4, **and** 5, **respectively.**

In Fig. 40, we compare the impulse responses obtained by multiphysics finite-element simulation with the analytical results obtained using the MC model described in Section 5.2, where we use the following values for the diffusion coefficient $D = 10^{-8}\ m^2/s$ and the absorption rates ($\rho_n = 1e-5; n = 1 \ldots 7$). We compare the results for all three blood vessels 1, 4, and 5, and we notice in the three cases that there is good agreement between the values generated through the simulation and the model.

5.5 Drug Injection Optimization

In this section, we aim to propose a solution to the optimization of the drug injection in order to achieve a desired drug delivery rate, based on the MC-based pharmacokinetic model presented in Section 5.2. In order to obtain efficient drug delivery systems, the timing and location of the drug particles are crucial. The diseased region needs to receive the particles at the right time and in the right quantity. When the particles are injected by systemic administration, the drug particles can be lost in blood vessel bifurcations, absorbed by blood vessels, and mixed with the blood due to diffusion. Fig. 41 shows a scheme of the injection rate optimization, where, starting from the desired delivery rate, an optimal injection rate

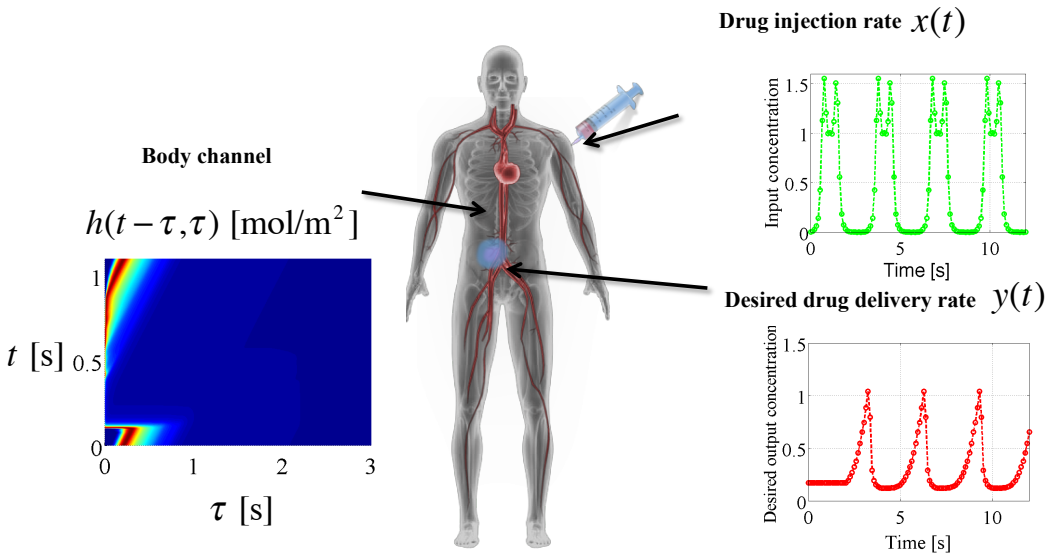

Figure 41. Scheme of the injection rate rate optimization for a desired drug delivery rate.

is found giving exactly the desired delivery rate with minimal error.

In the following, we present a method to find the optimal inject rate based on the desired drug delivery rate, the physiological parameters of the body, the drug properties, the injection location and the delivery location.

We consider a disease that requires a specific drug delivery rate that will make the healing effective, with just a minimal number of drug particles, and below the level that causes toxicity. We suppose that a desired drug injection rate is given by a time-varying function $x(t)$, which describes the drug concentration rate at every time t in the injection location.

Using the pharmacokinetic model in Section 5.2, we obtain a channel model characterized by a time-varying impulse response $h^{(\rho_n,\mu_n;n=1\ldots N)}_{(n;n=1\ldots N)}(t,\tau)$ which relates the drug injection rate $x(t)$ to the drug delivery rate $y(t)$, by the following relationship:

$$y(t) = \int_{-\infty}^{+\infty} h^{(\rho_n,\mu_n;n=1\ldots N)}_{(n;n=1\ldots N)}(t,\tau)x(\tau)d\tau\,. \tag{144}$$

Here, our objective is to find the optimal drug injection rate $x^*(t)$, such that the obtained drug delivery rate $y^*(t)$ is as close as possible to the drug delivery rate $y(t)$. This is expressed

by:

$$x^*(t) = \arg\min_{x(t)} \|y(t) - y^*(t)\| \ . \tag{145}$$

Using the time-varying impulse response, the previous expression becomes:

$$x^*(t) = \tag{146}$$
$$\arg\min_{x(t)} \left\| \int_{-\infty}^{+\infty} h_{(n;n=1\ldots N)}^{(\rho_n,\mu_n;n=1\ldots N)}(t,\tau)x(\tau)d\tau - y^*(t) \right\| ,$$

where $h_{(n;n=1\ldots N)}^{(\rho_n,\mu_n;n=1\ldots N)}(t,\tau)$ is the time-varying impulse response that characterizes the drug propagation from the injection location to the delivery location.

y_j is defined as follows:

$$y_j = \int_0^{jT_s} h_{(n;n=1\ldots N)}^{(\rho_n,\mu_n;n=1\ldots N)}(t_j,\tau)x(\tau)d\tau \, . \tag{147}$$

x_i is defined as:

$$x_i = x(iT_s) \, , \tag{148}$$

where $i, j = 1 \ldots K$, K is the number of samples, and T_s is the sampling period. With this notation, we can write:

$$y_j = \sum_{i=1}^{j} x_i \int_{(i-1)T_s}^{iT_s} h_{(n;n=1\ldots N)}^{(\rho_n,\mu_n;n=1\ldots N)}(jT_s,\tau)d\tau \, . \tag{149}$$

We define the channel coefficients $h_{i,j}^{(\rho_n,\mu_n;n=1\ldots N)}$ as follows:

$$h_{i,j}^{(\rho_n,\mu_n;n=1\ldots N)} = \int_{(i-1)T_s}^{iT_s} h_{(n;n=1\ldots N)}^{(\rho_n,\mu_n;n=1\ldots N)}(t_i,\tau)d\tau \, . \tag{150}$$

Therefore, we get the following expression:

$$y_j = \sum_{i=1}^{j} x_i h_{i,j}^{(\rho_n,\mu_n;n=1\ldots N)} \, . \tag{151}$$

Thus, the problem can be written in matrix notation as

$$\underline{\mathrm{y}} = \mathbf{H}_{(n;n=1\ldots N)}^{(\rho_n,\mu_n;n=1\ldots N)} \underline{\mathrm{x}} \, , \tag{152}$$

where $\underline{\mathrm{y}} = \left[y_j; j = 1 \ldots K \right]'$ is a K-dimensional vector whose elements are samples of the desired delivery rate, $\underline{\mathrm{x}} = [x_i; i = 1 \ldots K]'$ is a K-dimensional vector whose elements are

samples of the optimal injection rate, and $\mathbf{H}^{(\rho_n,\mu_n;n=1\ldots N)}_{(n;n=1\ldots N)}$ is the square matrix of size K-by-K, whose components are defined in (150), and $[.]'$ is the vector transpose operator.

The matrix $\mathbf{H}^{(\rho_n,\mu_n;n=1\ldots N)}_{(n;n=1\ldots N)}$ is supposed to be invertible. In case the matrix is not invertible, the linear matrix inequality approach as proposed in [98] can be directly adapted to the MC model to find the optimal injection rate.

We define the vector $\underline{\mathrm{x}}^* = [x_i; i = 1 \ldots K]'$ as follows:

$$\underline{\mathrm{x}}^* = \left\{\mathbf{H}^{(\rho_n,\mu_n;n=1\ldots N)}_{(n;n=1\ldots N)}\right\}^{-1} \underline{\mathrm{y}}, \tag{153}$$

where $\left\{\mathbf{H}^{(\rho_n,\mu_n;n=1\ldots N)}_{(n;n=1\ldots N)}\right\}^{-1}$ is the inverse of the matrix $\mathbf{H}^{(\rho_n,\mu_n;n=1\ldots N)}_{(n;n=1\ldots N)}$.

The desired drug injection rate is found by:

$$x^*(t) = \sum_{i=1}^{i=K} x_i^* \cdot \mathrm{sinc}\left(\frac{t - iT_s}{T_s}\right). \tag{154}$$

According to the Nyquist criterion [99], the sampling period should satisfy $T_s < \frac{1}{2B}$, where B is the bandwidth of the time-varying impulse response of the system. The sampling period depends on the blood velocity and the characteristic time scale of the advection-diffusion. For the simulations, a value of $T_s = 15.645$ ms, which is the sampling period of the measured blood cardiac flow input was chosen. This is much shorter than the characteristic time scale of the advection-diffusion.

5.6 Conclusions

In this chapter, we propose to apply the abstraction of the MC paradigm to address important problems in TDDSs, namely, modeling the drug pharmacokinetics, estimating the biodistribution, and optimizing the drug injection rate. The MC abstraction allowed to obtain an analytical pharmacokinetic model that accounts for various physicochemical processes in the particle propagation, and takes into account the impact of cardiovascular diseases. By stemming from the pharmacokinetic model, we proposed to use communication engineering metrics to estimate the drug biodistribution at the delivery location, while analytical expressions are obtained to estimate the drug accumulation in the rest of the body.

We have favorably compared our pharmacokinetic model with multiphysics finite-element simulations of the drug propagation in the arterial system, and provided numerical results for the drug biodistribution in different scenarios. We also proposed a procedure to optimize the drug injection rate according to a desired drug delivery rate through the pharmacokinetic model when the injection location and delivery are known.

The pharmacokinetic model presented in this chapter does not take into account particles that continue their propagation after having circulated the entire cardiovascular system. This is justified by the fact that heart and veins tend to significantly disperse the particles, therefore favoring their accumulation over their recirculation in the cardiovascular system. A possible future extension of this work could also include these effects in the pharmacokinetics through a stochastic model derived from an MC noise abstraction, as presented in [100].

The results presented in this chapter can support the future design of intra-body MC networks [101]. In fact, the developed pharmacokinetic model has the potential to be used to predict the propagation of MC signals in the human body undergoing several transport and kinetic processes. With regards to the communication performance of such a system, the theoretical limits of the amount information that can be reliably transmitted by MC over the blood vessels has been studied in [100]. By defining the encoding and modulation schemes for MC in the cardiovascular system, the achievable bit error rates can be evaluated.

In conclusion, the proposed abstraction of a TDDS with the MC paradigm provides a new way to model the TDDSs and support their engineering with tractable, yet complete, analytical models.

CHAPTER 6

MOLECULAR COMMUNICATION SYSTEM MODEL FOR ANTIBODY-MEDIATED DRUG DELIVERY SYSTEMS

6.1 Motivation and Related Work

Antibody-mediated Drug Delivery Systems (ADDS) are at the forefront of current therapeutic research [5]. The system uses artificial molecules that are constructed from biological materials to build and engineer drug delivery systems. They are inspired by the naturally occurring autoimmune mechanisms that enable the human body to diagnose itself and destroy the exact source of the disease, in an adaptive and constructive fashion. The versatility in engineering ADDS and their attested clinical success open up the possibility to develop sophisticated therapeutic strategies to effectively target diseases [102]. Fig. 2 illustrates the elements of the ADDS. The drug injection occurs in the blood vessels, and the drug delivery occurs in the extracellular matrix. The drug injection introduces antibodies which are transported by the blood flow and diffused through the tissues. The blood velocity field transports the antibodies and some of them diffuses through the vascular walls into the tissues. Upon arriving at the diseased cell, the antibodies bind with the antigens located on the surface of the diseased cell at the antigen-antibody binding site. The antigen-antibody kinetics promotes the selective targeting of the diseased cells without affecting the healthy cells. The interplay of these different transport and kinetic processes contributes to the performance of the ADDS in maximizing the delivery of the antibodies to the diseased cells.

In this chapter, Molecular Communication (MC) paradigm [2], where the information is conveyed through molecules, is proposed to model the ADDS while considering the unique properties of antibodies and the possibilities that they offer. This new model will address the short comings of *Physiologically-based Pharmacokinetics* (PB/PK) models that have been proposed for ADDS propagation in the literature. PB/PK methods suffer

from many limitations that make them inapplicable to helping the current state-of-the-art in nanomedicine [24] [25]. The issue with the PB/PK model is that the diseases that are meant to be targeted with ADDS, such as tumors, are highly localized and grow quickly, and this model does not provide enough spatial and temporal accuracy to assess the efficiency of the ADDS. Also, by modeling complex molecules for the first time in the area of MC, this work addresses the limitations in the existing MC modeling works [103] [12].

By using the MC-ADDS paradigm, a bottom-up approach of modeling the propagation of antibodies is proposed where the appropriate structure of the antibody is determined, and from that propagation around the body is predicted. The MC-ADDS model solves this problem by providing mechanistic models, based on the laws of biophysics instead of empirical observations, and minimizing the need for parameters estimation. This will provide higher spatial and temporal resolution tracking of the drug propagation in the micro and millisecond scale, while being scalable to lower and higher resolutions with small changes to the system model. In MC-ADDS, the human body is modeled as a complex network of blood vessels and tissues where the transmitted signal is modulated by the antibody concentration at the injection location, which is the location of the body where the syringe is injected, and the propagation in the body is represented with simple analytical models, directly derived from the physiology of the patient and the chemical and electrical structure of the antibody molecule. Sec. 6.7 will show that the MC-ADDS modeling allows the calculation of the end-to-end impulse response of the system, and evaluating which kinetic processes are impeding the drug delivery.

In particular, the main contributions of this work are as follows:

- **Modeling an end-to-end abstraction of ADDS as an MC channel:** The abstracted MC channels the ADDS into three different channels corresponding to different parts of the body. These three different channels include the vascular, extracellular, and antigen binding channels. Numerical evaluations are conducted for each channel to determine the influence on the delivery of the antibodies.

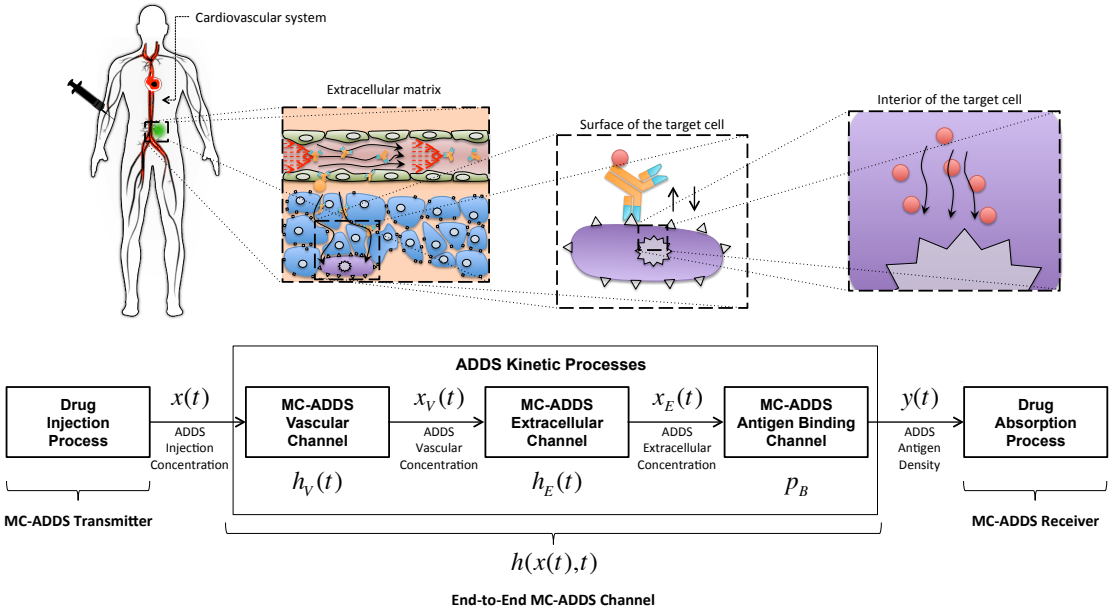

Figure 42. The MC abstraction of the ADDS.

- **Determining an optimized shape for the antibody molecular structure:** The movement of the antibodies with the blood flows is modeled based on their 3D structure. The optimized geometrical structure for the antibodies is determined based on the diffusion behavior, as well as their successful binding process to the diseased cells. The model considers the chemical components within the blood that affects the antibody, as well as the electrochemical properties of the antibody-antigen complex.

- **Validation of the end-to-end ADDS MC channel:** Validations of the ADDS is conducted using both analytical MC modeling and comparison to the COMSOL®[1], finite-element simulations. The comparison showed strong agreement between the MC models and the COMSOL® simulations.

The MC-ADDS modeling will provide a clearer understanding of the mode of operation of antibodies, and enable the development of innovative methods to guide the engineering of verifiable and safe antibody mediated therapies. This includes the design and engineering of the drug structure [104] [105], mode of administration, and dosage optimization [6].

[1]COMSOL® and COMSOL Multiphysics® are registered trademarks of COMSOL AB.

This opens up the possibility to optimize the properties of the ADDS to achieve a desired therapeutic effect, by determining the drug injection rate in terms of drug dosage concentration, the timing of the dosage, and the location of injection, thus maximizing the safety and success of ADDS and minimizing the costs [7]. The second motivation behind the use of MC-ADDS modeling, is to understand the physicochemical interactions between ADDS and the body, which are more complex than in PDDS. For example, ADDS undergo electrostatic forces within the *Extracellular Matrix* (ECM) due to negatively charged proteins [8]. These electric forces significantly affect the intercellular transport, antigen binding, and the absorption of the ADDS by the cells.

The rest of the paper is organized as follows: in Sec. 6.2, we explain the abstraction of the ADDS through the MC paradigm, the objectives, and principles of this approach. Sec. 6.3 presents the *MC-ADDS Vascular Channel Model*, which describes the MC analytical model of ADDS transport through the blood vessels, taking into account the roles of tissue absorption, and the plasma binding. Sec. 6.4 introduces the *MC-ADDS Extracellular Channel Model*, which is the MC analytical model of ADDS transport through the extracellular matrix (ECM), taking into account the role of ECM protein binding. Sec. 6.5 presents the *MC-ADDS Antigen Binding Channel Model* which is developed through the MC paradigm, by incorporating the electrochemical structure of the antibody molecule. Sec. 6.6 defines the realistic COMSOL® Multiphysics model that was simulated to validate the MC-ADDS model. Sec. 6.7 presents numerical results that were evaluated using the MC-ADDS model and the COMSOL® Multiphysics simulation model. Sec. 6.8 concludes the paper with the main outcomes of the MC-ADDS model and its prospective use for the design and engineering of optimal ADDS.

6.2 MC Abstraction of ADDS

In this section, we present the MC-ADDS framework which abstracts the kinetics processes that the antibody undergoes in different parts of the body as MC channels. In the context of

communication theory, a channel is a communication medium characterized by an input-output relationship. The combination of several channels together enables establishing a network between several transmitters and receivers. The concept of channels is useful for modeling, analyzing the performance, and optimizing a system regardless of the initial conditions and input signals. As illustrated in Fig. 42, cascading the MC-ADDS channels for each of these processes provides the *end-to-end MC-ADDS channel* from the location where the antibodies are injected to the location where they are absorbed by the cells. The drug injection is abstracted as a *MC-ADDS transmitter* and the drug absorption process is abstracted as a *MC-ADDS receiver*. The antibody concentrations at different phases of their propagation in the body are considered as MC signals, which are the inputs and outputs of the following MC-ADDS channels:

- **The MC-ADDS Vascular Channel** models the propagation of the antibodies by advection-diffusion through the force of the blood flow, the Brownian motion of the antibodies in the blood, and the chemical binding with the molecules present in the blood. The MC-ADDS vascular channel is characterized by a function $h_V(t)$. The input signal to the MC-ADDS Vascular Channel is the *ADDS Injection Concentration* $x(t)$, defined as the concentration of antibodies in the injection location, which is represented as follows:

$$x(t) = Ab(t)|_{\text{Injection location}} \,. \tag{155}$$

  $Ab(t)$ denotes the antibody concentration at the location of the injection at the time t. The output from the MC-ADDS Vascular Channel is the *Vascular ADDS Concentration* $x_V(t)$, which is defined as the concentration of antibodies in the blood as a function of time t, as follows:

$$x_V(t) = Ab(t)|_{\text{Blood}} = h_V(t) * x(t)\,, \tag{156}$$

  where $*$ denotes the application of the impulse response $h_V(t)$ to the signal $x(t)$.

- **The MC-ADDS Extracellular Channel** models the transport of the antibodies through the ECM. This channel is located between the vascular tissues and the surface of the target cells, and is driven by the interstitial pressure between the blood vessel walls and the target cells, the lymphatic flow, and the binding with the molecules of the ECM. The MC-ADDS extracellular channel is characterized by a function $h_E(t)$. The output signal of the MC-ADDS extracellular channel is the *ADDS Extracellular Concentration* $x_E(t)$, which is the concentration of antibodies in the ECM as a function of the time t as follows:

$$x_E(t) = Ab(t)|_{\text{ECM}} = h_E(t) * x_V(t)\,. \tag{157}$$

- **The MC-ADDS Antigen Binding Channel** models the antigen-antibody binding occurring at the surface of the target cell. The antigen-antibody binding is influenced by the chemical affinity between the antigens expressed by the cell and the antibody, as well as the physical forces exerted by the flow in the ECM. The MC-ADDS Antigen Binding Channel is characterized by a function p_B, which provides the output of the MC-ADDS Antigen Binding Channel as the *ADDS-Antigen Concentration* $y(t)$, which is the concentration of antibodies bound to the antigens as a function of the time t, given the ADDS extracellular concentration $x_E(t)$ as follows:

$$y(t) = AbAg(t)|_{\text{Cell surface}} = p_B x_E(t)\,. \tag{158}$$

  $AbAg(t)$ denotes the concentration of drug antibodies that are bound to antigens at the location of the injection at the time t. p_B is not time-varying because there is a scalar relationship between the antibodies around the diseased cells and the antibodies that bind to the antigens, in a steady state. $y(t)$ is determined from the number of antibodies that arrive around the surface of the diseased cells and the thermochemical properties of the antibody-antigen binding.

This study will allow the optimization of MC-ADDS systems by appropriately designing the antibody structure, shape, and chemical characteristics to maximize its ability to

deliver its therapeutic effect where it is needed in a timely and efficient way.

6.3 MC-ADDS Vascular Channel Model

In this section, we derive an analytical model of ADDS vascular transport using the MC paradigm. As illustrated in Fig. 43, the blood velocity field drives the transport of antibodies in the vascular region, and also the antibodies diffuse randomly by Brownian motion. The antibody molecule is characterized by two diffusion parameters, namely: the *translational diffusion coefficient* D_Z, and the *radial diffusion coefficient* D_R. D_Z is the parameter that characterizes the diffusion of antibodies along the axis of the blood vessels. It is formally defined as follows:

$$< z^2(t) >= 2D_Z t\,, \tag{159}$$

where the variable z is the translational coordinate of the antibody at the time t along the axis of the blood vessels. The rotational diffusion coefficient D_Θ is the parameter that characterizes the diffusion of antibodies around their center. It is formally defined as follows:

$$< \theta^2(t) >= 2D_\Theta t\,, \tag{160}$$

where the variable θ is the angle of rotation of the antibody around its center.

6.3.1 MC-ADDS Vascular Channel Impulse Response

In classical MC, only one parameter, namely the diffusion coefficient D, is involved in the transport of the molecules according to Ficks law by Brownian motion, but in the case of ADDS, we will consider two parameters, namely the *translational diffusion coefficient* D_Z, which depends on the shape of the molecule, and the *radial diffusion coefficient* D_R, which depends also on the structure of the diffusion medium. Based on the general theory of diffusion developed by Brenner [106], the irregular shape of molecules has an important effect on their transport. In fact, the irregularity causes coupling between the rotational and the translational diffusion parameters of complex molecules [107]. In addition, to the translational-rotational anisotropy due to molecule shape, there is a translational-radial

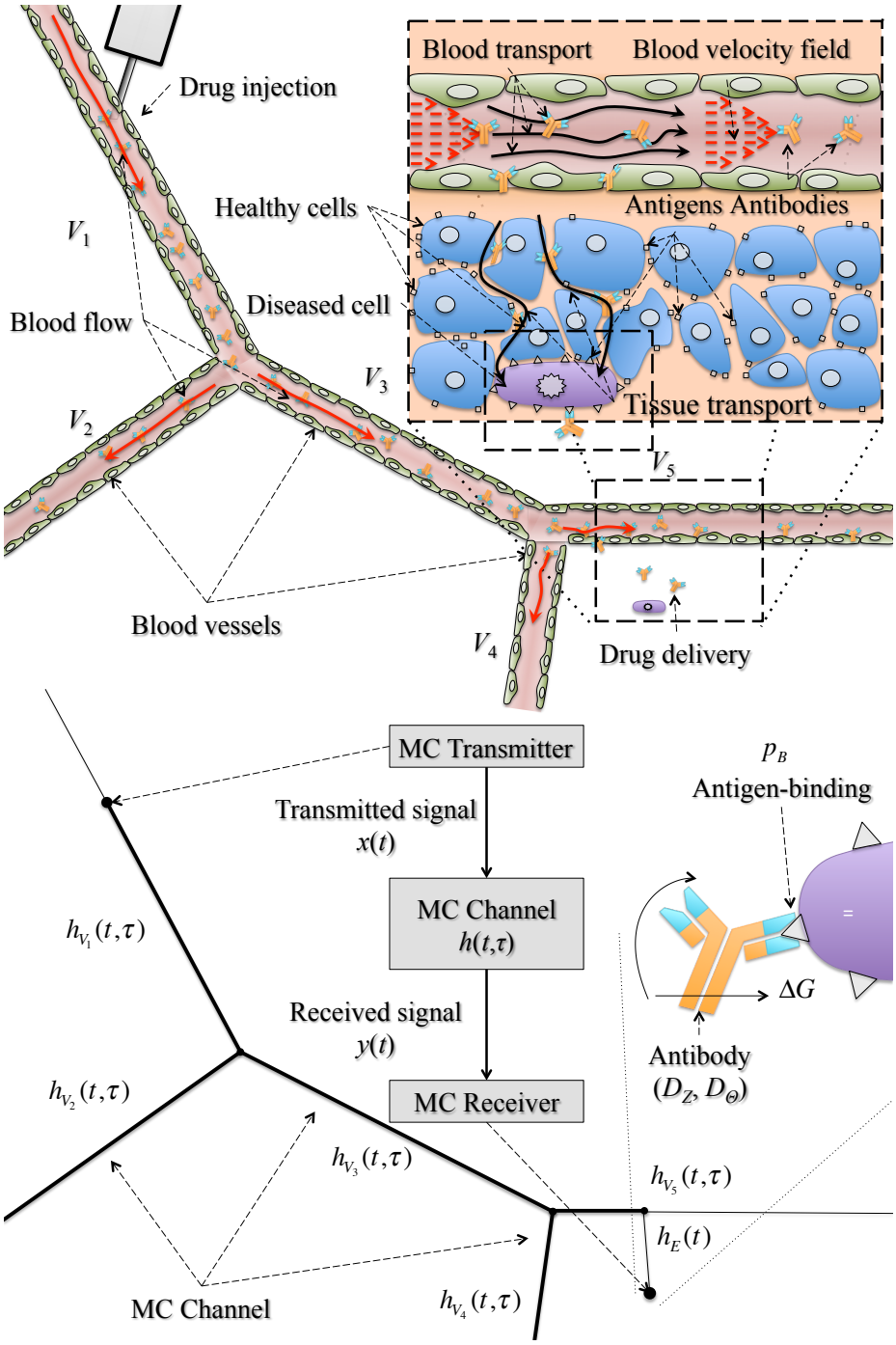

Figure 43. MC Abstraction of the ADDS

anisotropy owed to the non-homogeneity of cells matrices where one direction is more conducive to diffusion than the perpendicular direction. Examples of translational-radial anisotropy include the transport of molecules in blood vessels, where the non-uniform distribution of red blood cells affects the diffusion in the radial direction [108], and the anisotropy in the ECM, where the cells are organized in a preferential direction, due to the direction of mechanical forces, especially the ones involving connective tissues [109].

An MC-ADDS transport model is developed, enabling the prediction of the propagation of antibodies in the vascular channel. This model is deterministic, but it should be noted that there are many fluctuations in drug delivery systems in general owing to blood turbulence, Brownian motion, and ligand-binding noise. These noise effects are explained in a previous work [110], and can be applied to ADDS with little modifications. The impulse response $h_V(t, \tau)$ is obtained by cascading the impulse responses of each channel between the drug injection site and the drug delivery site, which can be expressed as follows:

$$h_V(t, \tau) = h_{V_1}(t, \tau) \otimes \ldots h_{V_i}(t, \tau) \cdots \otimes h_{V_L}(t, \tau)\,, \tag{161}$$

where $\otimes$ denotes the operator for cascading the periodically time-varying impulse responses of two systems as described in [57], $h_{V_i}(t, \tau)$ is the impulse response of the i-th MC vascular channel, and L is the number of blood vessels located between the drug injection site and the drug delivery site.

The transport process in the ECM is dominated by diffusion, although there is an advective transport due to the plasma excudating drug particles from blood vessels to the lymphatic system in a directed way. However, the flow rate is so slow that the dispersion due to advection is negligible. This coincides with clinical observation of antibody transport [111]. The impulse response $h_{V_i}(t, \tau)$ is expressed for each MC vascular channel based on the generalized anisotropic Taylor dispersion equation with absorption [112], with the

assumption of diffusion-dominated transport around the blood vessels, as follows:

$$h_{V_i}(t,\tau) = \frac{1}{\sqrt{2\pi\sigma_i^2(t,\tau)}} \exp\left(-\frac{(l - m_i(t,\tau))^2}{2\sigma_i^2(t,\tau)}\right), \tag{162}$$

where:

- The mean antibody velocity varies with time and is expressed as follows:

$$m_i(t,\tau) = \int_\tau^t v_i(r,t)\, dt', \tag{163}$$

- The variance of the antibody concentration increases with time and is expressed as follows:

$$\sigma_i^2(t,\tau) = 2\int_\tau^t D_i(t')\, dt', \tag{164}$$

where t and t' are time parameters, The effective diffusion coefficient of the antibodies $D_i(t)$ is expressed as follows [112]:

$$D_i(t) = D_Z P_f + D_E P_w + P_f^3 v_i^2(t)\left(\frac{K_V}{K_E} + \frac{r_i^2}{48 D_R}\right), \tag{165}$$

where D_Z is the translational diffusion coefficient of the ADDS in the blood expressed in (168), D_E is the diffusion coefficient in the ECM, which is defined in Sec. 6.4, D_R is the radial diffusion coefficient due to anisotropy [108], r_i is the radius of the vessel i, K_V is the non-specific binding equilibrium constant in the vascular channel, K_E is the non-specific binding equilibrium constant in the ECM, $P_f = \frac{1}{1+K_V}$ is a kinetic ratio, and the effective blood velocity $v_i(t)$ is expressed as follows:

$$v_i(t) = P_f u_i(t), \tag{166}$$

The non-specific binding equilibrium constant in the vascular channel can be calculated from the non-specific binding energy ΔG_V. This is calculated between the antibody and the proteins contained in the blood in a similar way to the calculation of the specific binding

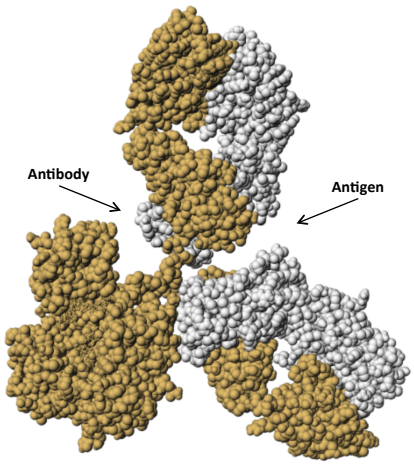

Figure 44. 3D structure of the antibody-antigen complex from the Protein Data Bank.

energy ΔG between the antibody and the antigens in (178) (Sec. 6.5), and is represented as follows:

$$K_V = \exp\left[-\frac{\Delta G_V}{RT}\right], \tag{167}$$

where ΔG_V is the non-specific binding free energy between the antibody and the proteins in the vascular channel, and R is the ideal gas constant. Finally, from (161) and (162), we obtain the MC end-to-end impulse response of the ADDS.

6.3.2 MC-ADDS Vascular Channel Diffusion Coefficients

Here we introduce the model of the structure of the antibody which provides the reference geometrical and electrochemical properties of the ADDS. These properties will be used to derive the transport diffusion coefficients. The structural information is obtained from the *Protein Data Bank* (PDB) [113], which hosts the tridimensional structural data of a large number of biological molecules, including antibodies and their antigens. A visualization of such a structure is presented in Fig. 44 which represents the atomic structure of the antibodies as an assortment of balls occupying the volume of the atoms and their bonds with other atoms. The PDB also includes the constituting chemical elements of the antibodies and their electric charges. Among all the information provided by the PDB, in this chapter we focus on the geometry of a molecule and its charges. Each element of the antibody is

denoted as n, and the total number of elements constituting the antibody as N. An element n possesses the following information:

- *Cartesian coordinates*, denoted by the vector (x_n, y_n, z_n) with a given Cartesian center O.
- *Radius*, denoted by the scalar value ρ_n, which measures half the distance between one atom and its closest element.
- *Charge*, denoted by the value q_n, which is the electric charge born by the element n.

These three types of information are sufficient to describe the kinetic parameters of the antibody. In the following, we explain how these parameters are derived directly from the PDB information.

In the literature [114] [115] [116], all MC and pharmacokinetic models contain information on the basic shapes for the molecules such as spheres, and rarely ellipsoids and rods, to capture the antibody propagation. Therefore, there is a need for a model that takes into account the antibody shape and structure to predict the diffusion parameters of this small molecule without any empirical choices. The antibodies come in different arbitrary shapes and structures as can be seen in X-Ray structure analysis of this type of molecules [117]. As illustrated in Fig. 45, the antibody-antigen is composed of several beads. In general, the antibodies are roughly Y-shaped molecules and consist of different heterogeneous regions (light chain and heavy chain). The geometry of the antibody has an important effect on its motion in the blood and tissues. The irregular shape can create arbitrary motions and fluctuations that are different from the case of spherical nanoparticles that were considered in PDDS.

The translational diffusion coefficient D_Z and the rotational diffusion coefficient D_Θ are calculated as follows [118]:

$$\begin{cases} D_Z = \frac{k_B T}{3\eta} tr(A_Z)\,, \\ D_\Theta = \frac{k_B T}{3\eta} tr(A_\Theta)\,, \end{cases} \tag{168}$$

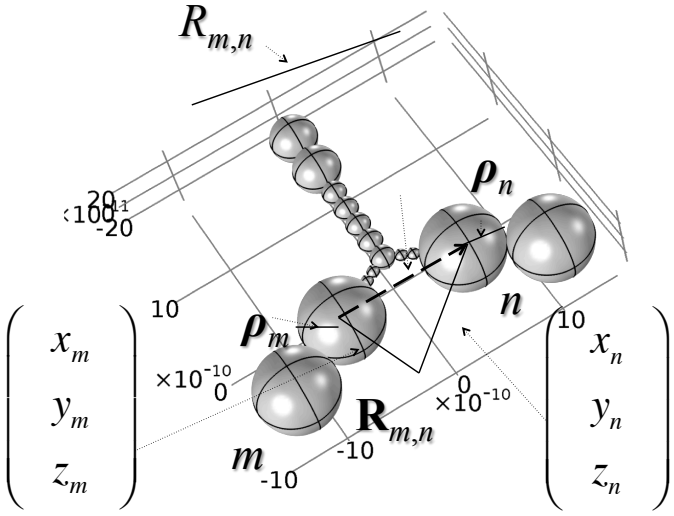

Figure 45. Bead model of an antibody.

where k_B is Boltzmann coefficient, T is the temperature of the blood, η is the fluid viscosity, $tr(\cdot)$ is the trace function of the matrices A_Z and A_Θ, which represent the *translational mobility tensor matrix* and the *rotational mobility tensor matrix* [107]. These matrices A_Z and A_Θ are expressed as follows [119]:

$$\begin{cases} A_Z = & \sum_{m=1}^{N}\sum_{n=1}^{N}\left[\frac{\delta_{m,n}\mathbf{I}}{6\pi\eta R_{m,n}} + (1-\delta_{m,n})\,\mathbf{T}_{m,n}\right]^{-1}, \\ A_\Theta = & -\sum_{m=1}^{N}\sum_{n=1}^{N} U_m\left[\frac{\delta_{m,n}\mathbf{I}}{6\pi\eta R_{m,n}} + (1-\delta_{m,n})\,\mathbf{T}_{m,n}\right]^{-1} U_n \\ & +8\pi\eta\left(\sum_{n=1}^{N}\rho_n^3\right)\mathbf{I}, \end{cases} \tag{169}$$

where m and n are the indices of two beads m and n in the molecular compound, as illustrated in Fig. 45, N is the total number of beads in the molecular compound, η is the fluid viscosity, $R_{m,n}$ is the center-to-center distance between two beads m and n, ρ_n is the radius of the bead n, $\delta_{m,n}$ is the Kronecker delta function, $\mathbf{T}_{m,n}$ is the hydrodynamic tensor of the antibody calculated as follows from the geometric parameters of the antibody molecule:

$$\mathbf{T}_{m,n} = \frac{1}{8\pi\eta R_{m,n}}\left[\left(\mathbf{I} + \frac{\mathbf{R}_{m,n}\mathbf{R}_{m,n}^{\dagger}}{R_{m,n}^2}\right) + \frac{\rho_m^2+\rho_n^2}{R_{m,n}^2}\left(\frac{\mathbf{I}}{3} - \frac{\mathbf{R}_{m,n}\mathbf{R}_{m,n}^{\dagger}}{R_{m,n}^2}\right)\right], \tag{170}$$

where $\mathbf{R}_{m,n}$ is the distance vector between the beads m and n, $\{\cdot\}^{\dagger}$ is the transpose function of the vector $\mathbf{R}_{m,n}$, $R_{m,n}$ is the center-to-center distance between two beads m and n, ρ_n is

the radius of the bead n, ρ_m is the radius of the bead m, and $\mathbf{U}_m$ is the skew matrix of the bead m and is expressed as follows:

$$\mathbf{U}_m = \begin{pmatrix} 0 & -z_m & y_m \\ z_m & 0 & -x_m \\ -y_m & x_m & 0 \end{pmatrix}. \tag{171}$$

where (x_m, y_m, z_m) are the Cartesian coordinates of the bead with index m from an arbitrary origin O. Similarly, $\mathbf{U}_n$ is the skew matrix of the bead n expressed as follows:

$$\mathbf{U}_n = \begin{pmatrix} 0 & -z_n & y_n \\ z_n & 0 & -x_n \\ -y_n & x_n & 0 \end{pmatrix}. \tag{172}$$

where (x_n, y_n, z_n) are the Cartesian coordinates of the bead with index n from the origin O.

6.4 MC-ADDS Extracellular Channel Model

In this section, we present how the transport of ADDS in the ECM is modeled. Due the differences between tissues in the body in terms of geometry, arrangement, tortuosity, and density, the transport of ADDS is going to vary greatly in different parts of the body. The parameter D_E denotes the diffusion coefficient in a tissue surrounding a blood vessel. The structure of the ECM is similar to foam. The antibodies will perform random motions and collide with the membranes of the cells, thus affecting the distribution of their concentration. Using the theory of transport in porous media [120] [121], it is possible to derive an expression for D_E based on the characteristics of the tissue. In practice, it has been observed that the transport in the ECM is largely dominated by the diffusion, therefore, we neglect the transport due to interstitial pressure differences.

The MC-ADDS model of extracellular transport becomes a diffusion MC channel [103] with a diffusion coefficient D_E and a non-specific binding equilibrium constant K_E in the ECM, as follows:

$$h_E(t) = \frac{1}{\sqrt{2\pi D_E t}} \exp\left[\frac{-z^2}{(4D_E + K_E)\, t}\right], \tag{173}$$

where z is the coordinate towards the target cell, K_E is the non-specific binding equilibrium constant in the ECM, and D_E is the diffusion coefficient in the ECM. The non-specific binding equilibrium constant is a value that characterizes the rate of the first-order linear reaction between two reactants such as the antibody and other molecules.

$$D_E = \frac{\phi}{\kappa} D_Z \,. \tag{174}$$

As shown in Fig. 46, the diffusion coefficient D_E is a function of following parameters which can be estimated from the shape of the ECM:

- *The porosity* ϕ measures the propensity of the tissue components to allow the antibodies to pass.

- *The tortuosity* κ is the arc length of the path over the geometric distance between the input and the output locations of the channel. Typical values for the tortuosity are measured experimentally from cellular imaging. The work in [122] cites values between $\kappa = 1.55$ and $\kappa = 1.65$ in the human adult brain. The work in [123] cites values between $\kappa = 2$ and $\kappa = 3$, and the work in [123], mentions that the tortuosity can be as high as $\kappa = 9$ in crowded protein-loaded environments.

- *The free fluid coefficient* D_Z is the translational diffusion coefficient of the antibodies in the fluid, which is calculated using the result in (168).

It is noted that extracellular transport may also be subject to protein binding [124], in which case, the model of the following section could supplement the binding of antibodies with gels and ECM proteins. In fact, the non-specific binding equilibrium constant in the ECM K_E can be calculated from the non-specific binding energy ΔG_E, which is calculated between the antibody and the proteins of the ECM (such as collagens) in a similar way to

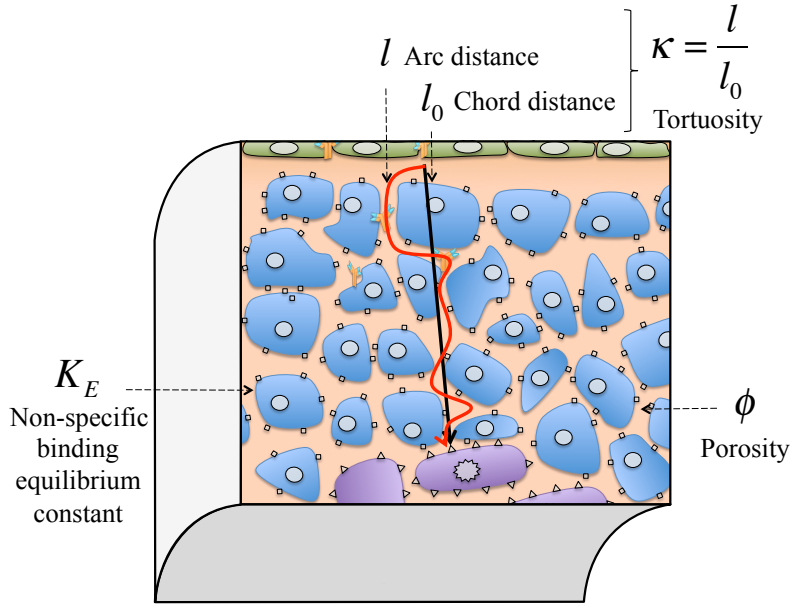

Figure 46. Parameters of the MC-ADDS extrallelular transport model.

the computation of the specific binding energy ΔG between the antibody and the antigens in (178) (Sec. 6.5), as is represented in the following:

$$K_E = \exp\left[-\frac{\Delta G_E}{RT}\right], \tag{175}$$

where ΔG_E is the non-specific binding free energy between the antibody and the ECM proteins. For simplicity, we assume that the environment around the blood vessel is homogeneous, but, technically, the different heterogeneous layers of cell types around the blood vessels could be accounted for by cascading the impulse response for each layer from the plasma to the target diseased cells, based on their own tortuosity and porosity.

6.5 ADDS Antigen Binding Channel Model

In this section, we derive the characteristic function p_B of the MC-ADDS Antigen Binding Channel, as a function of the geometry and charge of the antibody, and the number of antigens in the surface of the diseased cells. This function allows to obtain the distribution of the ADDS antigen-antibody density at the surface of the cell $y(t)$ as a function of the

ADDS extracellular concentration $x_E(t)$ as follows:

$$y(t) = p_B x_E(t)\,. \tag{176}$$

The antigen binding probability p_B is found to be expressed as [69]:

$$p_B = \frac{C_{ag}}{RT} \exp\left[-\frac{\Delta G}{RT}\right], \tag{177}$$

where C_{ag} is the concentration of antigens on the surface of the diseased cells, and T is the temperature. In the following, we derive the expression for the antigen-antibody binding free energy ΔG, the binding probability, and the kinetic rates of the antibodies in reaction with other proteins including extracellular matrix proteins and antigens. The antigen-antibody binding free energy ΔG is calculated as follows [125]:

$$\Delta G = G^+ - G^-\,, \tag{178}$$

where G^- is the unbound free energy defined as:

$$G^- = \sum_{\substack{m,n=1 \\ n\neq m}}^{N} \left(S_{m,n} + V_{m,n} + E_{m,n}\right) + \sum_{\substack{m,n=N+1 \\ n\neq m}}^{M+N} \left(S_{m,n} + V_{m,n} + E_{m,n}\right)\,, \tag{179}$$

where M is the total number of beads in the antigen, N is the total number of beads in the antibody, m and n are the indices of the beads, $S_{m,n}$ is the *pair solvent free energy* for two beads m and n, $V_{m,n}$ is the *pair van der Waals energy* for two beads m and n, $E_{m,n}$ is the *pair electrostatic potential* for the two beads m and n. The equation in (179) consists of the addition of the total energies for the antibody and the antigen, each taken individually, where the first sum is the free energy for the individual antibody, and the second sum is the free energy for the individual antigen. G^+ is the bound free energy defined as:

$$G^+ = \sum_{\substack{m,n=1 \\ n\neq m}}^{M+N} \left(S_{m,n} + V_{m,n} + E_{m,n}\right)\,, \tag{180}$$

where $S_{m,n}$ is the *pair solvent free energy* for two beads m and n, $V_{m,n}$ is the *pair van der Waals energy* for two beads m and n, $E_{m,n}$ is the *pair electrostatic potential* for two beads m

and n. The equation in (180) consists of the free energy of the antigen-antibody compound joined together. The PDB database provides the antigen-antibody bead coordinates in their joined state, therefore the bound free energy is directly computable from the database.

The pair energies used in the expressions of the unbound and bound free energies, in (179) and (180), respectively are expressed as follows:

- The *pair solvent energy* $S_{m,n}$ for the beads m and n is expressed as follows [126]:

$$S_{m,n} = \frac{1}{8\pi}\left(\frac{1}{\epsilon_0} - \frac{1}{\epsilon}\right)\frac{q_m q_n}{f_{m,n}}\,, \tag{181}$$

  where q_m is the charge on the bead m, q_n is the charge on the bead n, ϵ_0 is the free space permittivity, ϵ is the dielectric constant of interstitial fluid, and $f_{m,n}$ is given by:

$$f_{m,n} = \sqrt{R_{m,n}^2 + \rho_m \rho_n e^{-g_{m,n}}}\,, \tag{182}$$

  where $R_{m,n}$ is the distance between two elements m and n, ρ_n and ρ_m are respectively the radii of the two elements m and n, and $g_{m,n}$ is a ratio defined as follows:

$$g_{m,n} = \frac{R_{m,n}}{4\rho_m \rho_n}\,. \tag{183}$$

  This model is based on the generalized Born salvation free energy [126] which is an approximation of the solution to the Poisson-Boltzmann equation.

- The *pair van der Waals energy* $V_{m,n}$ for the beads m and n is calculated as follows [127]:

$$V_{m,n} = -\frac{A}{6}\left(\frac{2\rho_m\rho_n}{R_{m,n}^2 - (\rho_m+\rho_n)^2} + \frac{2\rho_m\rho_n}{R_{m,n}^2 - (\rho_m-\rho_n)^2} + \ln\left[\frac{R_{m,n}^2 - (\rho_m+\rho_n)^2}{R_{m,n}^2 - (\rho_m-\rho_n)^2}\right]\right), \tag{184}$$

  where A is the Hamaker coefficient [127] which depends on the properties of the material, and $R_{m,n}$ is the center-to-center distance between two beads m and n.

- The *pair electrostatic potential* $E_{m,n}$ for the beads m and n is calculated as follows:

$$E_{m,n} = \frac{q_m q_n}{8\pi\epsilon R_{m,n}}\,, \tag{185}$$

where q_m is the charge on the bead m, q_n is the charge on the bead n, and ϵ is the dielectric constant of interstitial fluid.

Finally, based on the structure data of the antigen and antibody from the PDB, namely the charges $\{q_n; n = 1 \dots M + N\}$, the radii $\{\rho_n; n = 1 \dots M + N\}$, the beads center-to-center distances $\{R_{m,n}; m, n = 1 \dots M + N\}$, the medium parameters $\{A, \epsilon\}$ we have derived the relationship between the ADDS antigen-antibody density at the surface of the cell $y(t)$ and the ADDS extracellular concentration $x_E(t)$ as expressed in (176) and (177).

6.6 COMSOL® Multiphysics Simulation

In this section, we present the simulation scheme used to validate the MC-ADDS model in a realistic 3D environment. COMSOL® Multiphysics is a finite-element modeling (FEM) software package which helps to set up complex 3D simulations involving different physical laws and models. In the interest to accurately capture the complexity of MC-ADDS systems, COMSOL® is used here to simulate two important physical laws involved in the propagation of antibodies. First, the *fluid dynamics* (Sec. 6.6.1) provide the time-varying blood velocity field in the blood vessels. Second, the *advection-diffusion* physics (Sec. 6.6.2) provide the time-varying concentration of the antibodies transported in an anisotropic manner through the blood vessels and their surrounding tissues. By combining these two physical laws, COMSOL® provides a realistic reference model for the spatio-temporal evolution of the antibody through the body.

6.6.1 COMSOL® Fluid Dynamics

The blood flow is simulated by COMSOL fluid dynamics simulations to predict the blood velocity field in the tridimensional coordinates inside the blood vessels. The blood flow is important since it is the main driving force transporting antibodies throughout the body. This realistic simulation is utilized to demonstrate that the assumption of uniform blood velocity in each blood vessel is valid for the analytical model. The uniform blood velocity allowed us to derive the simple expressions of time-varying impulse responses.

The COMSOL® fluid dynamics is based on the Navier-Stokes equation. Blood is supposed to be an incompressible fluid in laminar flow with a density $\rho = 1060\ \mathrm{kg \cdot m^{-3}}$ and a fluid viscosity $\eta = 0.005\ \mathrm{Pa \cdot s}$. The Navier-Stokes equation is written as follows:

$$\rho\left(\frac{\partial \mathbf{v}}{\partial t} + \mathbf{v} \cdot \nabla \mathbf{v}\right) = -\nabla p + f\,, \tag{186}$$

where p is the blood pressure, v is the blood velocity, ρ denotes the blood density, ∇ is the vector differential operator, η is the fluid viscosity, and f represents forces applies by the blood vessel walls.

The geometry of the blood vessels network is presented in Fig. 47. The networks consists of 9 curved blood vessels. The 3D data was obtained from the COMSOL® simulation library and scaled down by a 100 factor to have the typical size of arterioles. The dimensions of the blood vessels are given in Table 4.The blood vessels are surrounded by elastic vascular walls and muscles that apply stress on the surface of the blood vessels. The outlets and inlets of the blood vessel network are assumed to be open with a predefined blood pressure. The objective of the simulation is to verify that the MC analytical model properly predicts the diffusion through the walls and the diffusion along the radial dimension by comparing the end-to-end impulse response with the concentration at the output of the COMSOL simulated network given an initial concentration at the inlet of the network. The surrounding tissue is simulated as a thin diffusion layer in COMSOL with a porosity of 1.6.

The boundary conditions for COMSOL® fluid dynamics consist of the time-varying pressure applied at the inlets and outlets of the blood vessel network. The pressure at a vessel i is denoted by $p_i(t)$ where t is the time-variable. The heartbeat period is supposed to be constant and equal to $1s$. The function $p_i(t)$ is expressed as follows:

$$\begin{cases} p_i(t) = p_{i,0}\sin(\pi t) & 0 \le t \le 0.5\ \mathrm{s} \\ p_i(t) = p_{i,0}\left(1.5 - 0.5\cos(-2\pi(0.5 - t))\right) & 0.5 \le t \le 1\ \mathrm{s} \end{cases} \tag{187}$$

Table 3. Numerical values of the blood pressure at the inlets and outlets of the blood vessels network.

i	0	1	2	3	4	5
$p_{i,0}$	11208	11148	11148	11148	11148	11148

Table 4. Physiological lengths and radii of the blood vessels.

Vessels	V_1	V_2	V_3	V_4	V_5	V_6	V_7	V_8	V_9
Length [mm]	81	17	16	18	11	14	17	11	6
Radius [mm]	2.8	2.5	2.8	2.5	2.8	2.5	2.8	2.5	2.8

where $p_{i,0}$ are pressure constants in (Pa) for which the numerical values are available in Table 3.

6.6.2 COMSOL® Advection-Diffusion

The COMSOL® advection-diffusion physics are modeled using the time-varying advection-diffusion equation in different domains of the simulated geometry. The geometry consists of two domains, namely the blood vessels and the ECM that surrounds it. Each domain is denoted by the index i. The advection-diffusion equation is expressed as follows:

$$\frac{\partial c}{\partial t} = \nabla \cdot (D\nabla c) - \nabla \cdot (\vec{v}c) + K_V c\,, \tag{188}$$

where c_i is the antibody concentration in the domain i, D_i is the diffusion coefficient or matrix in the domain i and v is the blood velocity calculated from the COMSOL® fluid dynamics physics, K_V is the non-specific binding equilibrium constant between the antibody and the blood.

Between two domains, there is a molecular flux discontinuity, expressed by the following equation:

$$\begin{cases} -\mathbf{n} \cdot D_i = \frac{D_i}{D_j}(c_i - c_j) \\ -\mathbf{n} \cdot D_j = \frac{D_i}{D_j}(c_j - c_i)\,, \end{cases} \tag{189}$$

where D_i and D_j are the diffusion coefficients or matrices for the domains i and j respectively, c_i and c_i are the antibody concentrations in the domains i and j respectively, and $\mathbf{n}$ is the unit vector normal to the surface boundary delimiting the two domains i and j.

The following equation describes the initial concentration antibodies at the time $t = 0$:

$$\begin{cases} c_0(x,y,z) = \dfrac{e^{-\frac{z^2}{2\sigma_0^2}}}{\sqrt{2\pi\sigma_0^2}} C_0 & x \geq x_0 \text{ and } z \leq z_0 \\ c_0(x,y,z) = 0 & \text{otherwise}\,, \end{cases} \tag{190}$$

where $\sigma_0 = 0.25$ mm, $C_0 = 1$ mol $\cdot$ L^{-1}, and $\sigma_0 = 0.35$ mm, $x_0 = 50$ mm, and z is the third Cartesian axis as shown in Fig. 47. A Gaussian function is used to have a smooth impulse, which helps to avoid numerical problems.

The inlets and outlets of the blood vessel network are assumed as open extremities, which is expressed by the following equation:

$$\mathbf{n} \cdot D\nabla c = 0\,. \tag{191}$$

The anisotropic diffusion matrix is defined in the curvilinear coordinates along the axis of the blood vessels.

Finally, the equations in (188), (189), (190), and (191) are applied to the geometry of the vascular channel in Fig. 47. COMSOL® calculates the concentration $c(x, y, z, t)$ of the antibodies in the Cartesian coordinates $(x, y, z,)$ and time t.

6.7 Numerical Results

In this section, we show numerical results which compare the MC-ADDS analytical model with a finite-element methods simulation model in a realistic 3D geometry and show the significance of anisotropy. COMSOL® was used to simulate the propagation of antibodies using the complete advection-diffusion equation in a 3D setting, and the effect of anisotropy on the impulse response of the system was evaluated.

Fig. 48 compares the mathematical model, derived in (161) and (162) from Sec. 6.3, from the MC-ADDS paradigm incorporating the effect of anisotropy and the complete 3D

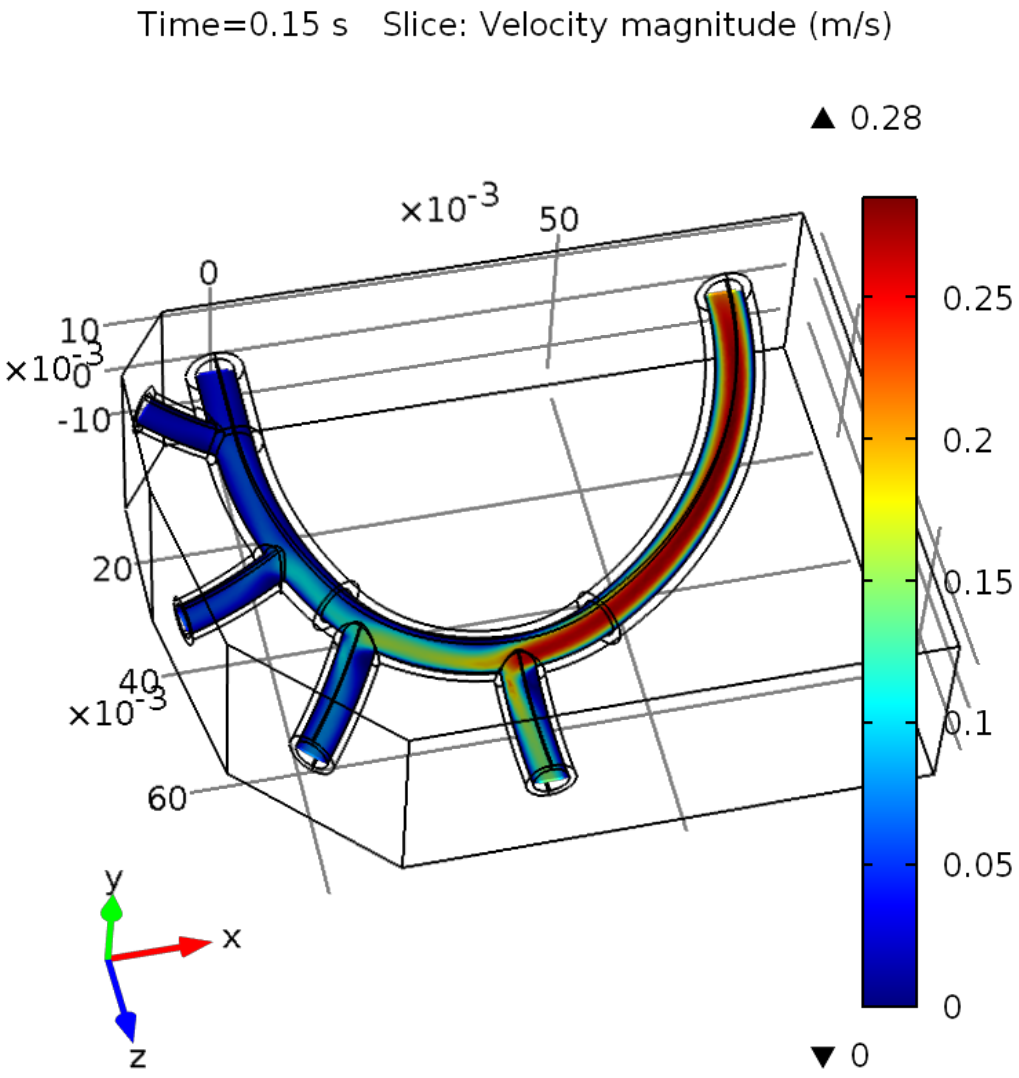

Figure 47. COMSOL® simulation of ADDS propagation in the vascular channel.

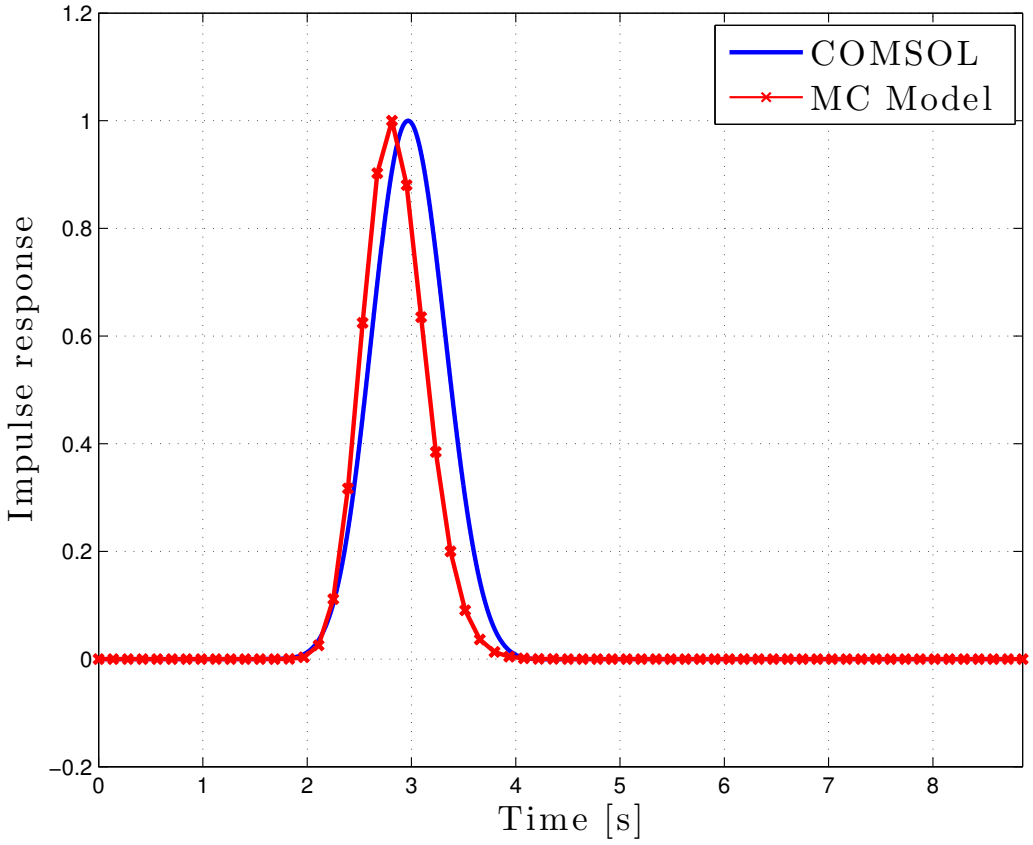

Figure 48. Validation of the analytical impulse response with COMSOL simulation results.

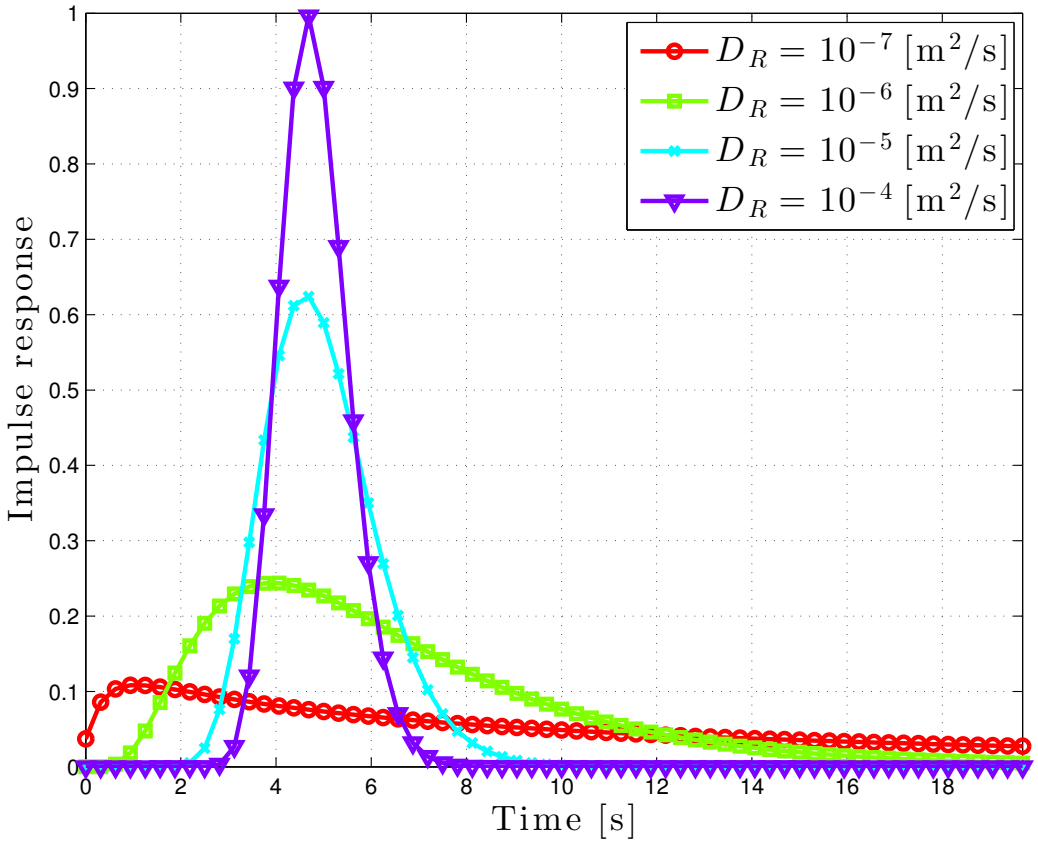

Figure 49. MC Vascular Channel impulse responses for different radial diffusion coefficient D_R.

simulation with COMSOL® on one blood artery. The translational and radial diffusion coefficients, calculated based on the bead model, have been used in both COMSOL® and the MC-ADDS model. An excellent agreement between the two results is shown in the figure. This is to our knowledge the first work to validate through FEM the anisotropic transport of molecules undergoing advection and diffusion. The anisotropic diffusion coefficient was specified in COMSOL® in matrix form in the cartesian coordinates, where the x and y represented the radial diffusion, and z represents the translational diffusion. The results show that MC anisotropic model will allow taking into account realistic diffusion environments that occur in biology.

Fig. 49 illustrates how the normalized impulse response from (162) presented in Sec. 6.3, varies highly depending on the radial diffusion coefficient. For a fixed translational diffusion coefficient, the radial diffusion coefficient was varied from $D_R = 10^{-7}$ m^2/s to

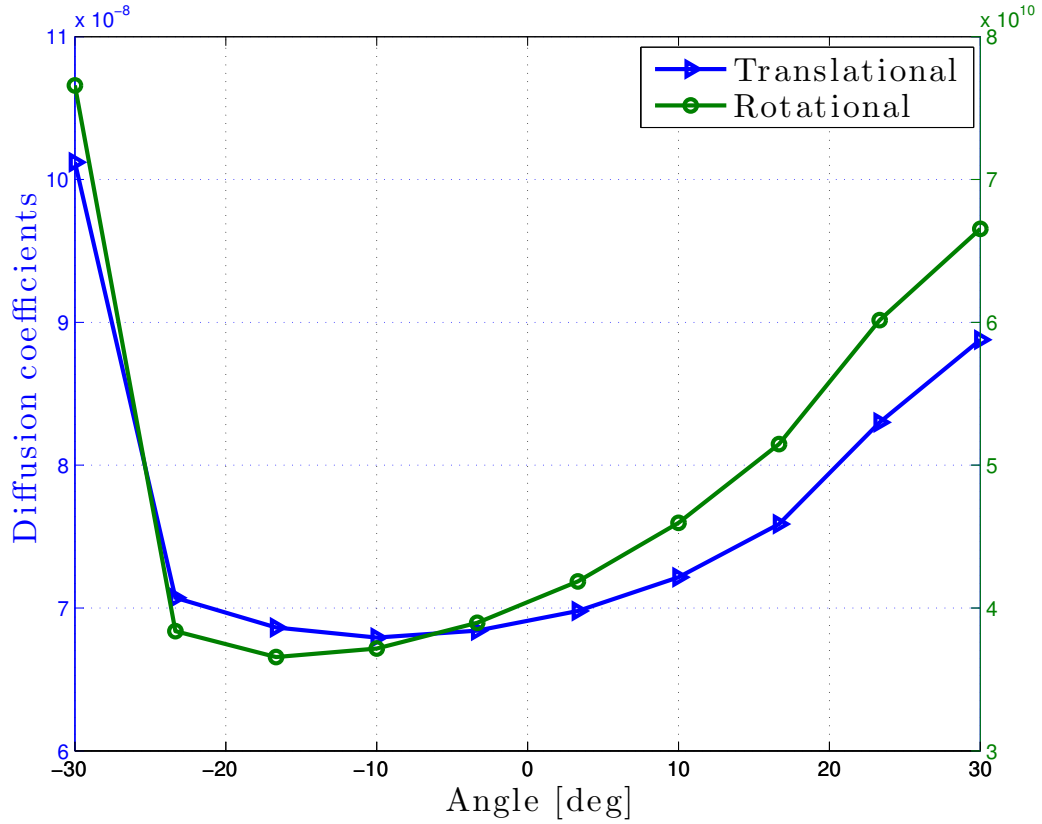

Figure 50. Translational diffusion coefficient and rotational diffusion coefficients as functions of the angle between antibody arms.

$D_R = 10^{-4}$ m^2/s. The numerical evaluations of the MC-ADDS extracellular impulse response for these different values show that the anisotropic transport due to a radial diffusion that is different from translational diffusion can have an important effect on the transport of antibodies. It can be seen that the impulse response is attenuated exponentially as a function of the radial diffusion coefficient. Therefore, radial diffusion coefficient is a critical parameter for the computational and numerical evaluation of MC-ADDS systems.

Fig. 50 shows the dependence of the anisotropic diffusion parameters on the angle between the arms of the antibody given by (168). from Sec. 6.3.2. In this figure, our objective is to quantify the effect of changing the shape of the antibody on the diffusion parameters. The bead model of the antibody illustrated in Fig. 45 at Sec. 6.5 has been considered, and we have varied the angle between the two long arms of the antibody from -30 degrees to 30 degrees, and we have plotted the rotational diffusion coefficient D_Θ and the translational

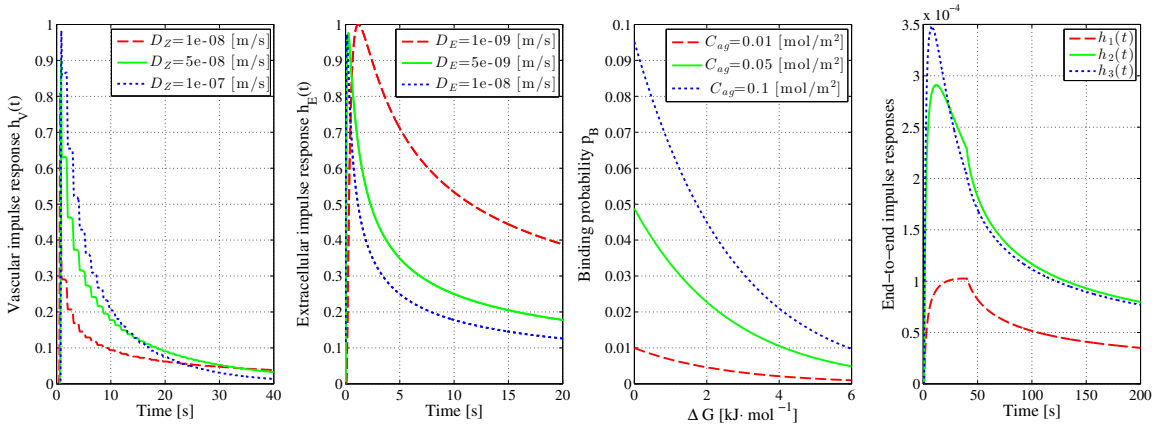

Figure 51. Numerical evaluation of the MC-ADDS end-to-end response.

diffusion coefficient D_Z for these different shapes. Note that the change in shape can have a considerable effect on these two diffusion coefficient in a similar way. The more the molecule resembles a rectangular shape the higher the diffusion coefficient is, and the more the molecule resembles a spherical shape, the lower is the diffusion coefficient. This can be explained by the fact that a spherical shape maximizes the contact surface area of the antibodies, which causes more collisions, and therefore a higher diffusion coefficient due to Brownian motion.

Fig. 51 shows the effect of the different kinetic processes on the MC-ADDS end-to-end response by cascading the impulse responses of the different transport and kinetic processes through (161) . The end-to-end impulse response is calculated for three different sets of parameters, each corresponding to either the color red, green, or blue, i.e. the end-to-end impulse response $h_1(t)$ is for $D_Z = 10^{-8}$ m^2/s, $D_E = 10^{-9}$ m^2/s, $C_{ag} = 0.01$ mol/m^2, and $\Delta G = 5$ kJ $\cdot$ mol^{-1}, the end-to-end impulse response $h_2(t)$ is for $D_Z = 5 \cdot 10^{-8}$ m^2/s, $D_E = 0.5 \cdot 10^{-9}$ m^2/s, $C_{ag} = 0.05$ mol/m^2, and $\Delta G = 5$ kJ $\cdot$ mol^{-1}, and the end-to-end impulse response $h_3(t)$ is for $D_Z = 10^{-7}$ m^2/s, $D_E = 10^{-8}$ m^2/s, $C_{ag} = 0.1$ mol/m^2, and the antigen-antibody binding free energy $\Delta G = 5$ kJ $\cdot$ mol^{-1} obtained through (178) in Sec. 6.5. For the vascular impulse response, we observe that increasing the translation diffusion coefficient of the antibodies increases the delay and the dispersion of the impulse response.

The figures for the vascular and extracellular impulse response are normalized with regard to the maximum value of the impulse responses. The vascular impulse response $h_V(t)$ shows some periodic sharp drops due to the periodicity of the heartbeat. For the extracellular impulse response $h_E(t)$, at a fixed association and dissociation kinetic set of parameters, the extracellular impulse response shows increased delay but decreased dispersion, due to the interplay of kinetic and diffusion parameters in the ECM. For the binding probability function p_B, we see that the concentration of antigens in the surface of the cells is a determining factor for the binding rate, and the higher the binding energy, the lower is the binding probability. This is explained by the fact that a high binding probability is more likely if the required energy for the antibody-antigen binding is low. The end-to-end impulse responses use the average values for the binding probability. The figure shows that the binding probability for these specific numerical values is the most significant factor in the end-to-end impulse response, and that although the vascular and extracellular parameters are very dissimilar for the green and blue end-to-end impulse response, the difference in the binding probability makes the two end-to-end impulse responses mostly the same.

MC-ADDS systems are remarkably complex due to the interplay of different kinetic and transport processes. The MC modeling approach allows capturing all the important kinetic parameters in a simple analytical expression and combining them together. The MC-ADDS approach makes it possible to evaluate numerically the effect of each of these kinetic parameters as well as the geometry of the disease and the physiology of the patient. Fig. 51 has shown that diffusion in the vascular space can exhibit a trend that is opposite to the one in the extracellular space. This means that values for the diffusion coefficient that are beneficial for the transport in the vascular channel may be detrimental in the extracellular channel. Therefore, there is a trade-off value for the diffusion coefficient that improves transport in the vascular channel without sacrificing the transport in the extracellular transport. This is important for appropriate engineering the diffusion properties of the antibodies. The figure also shows the importance of the binding parameters, which remain

the most critical barrier for the efficiency of ADDS. The numerical evaluation of these impulse responses and functions does not require important computational resources, which makes the optimization of MC-ADDS for a specific clinical scenario very tractable using this approach.

6.8 Conclusions

The Molecular Communication (MC) framework was used as an abstraction of antibody-mediated Drug Delivery Systems (ADDS), which is one of the therapeutic methods at the forefront of pharmacological research. The proposed MC model is based on the biophysical equations which govern antibody transport and kinetics in the human body. Analytical expressions of the impulse responses and drug delivery probabilities for the vascular transport, propagation in the ECM, and antigen binding were derived to mathematically capture ADDS. The transport and antigen-binding kinetics of ADDS are predicted based on the geometry of the human body, and the shape and electrochemical structure of the antibody-antigen compound.

The aim is to provide a novel model for ADDS based directly on the chemical and structural information about the antibody molecule. Based on the geometry and the charge of the ADDS constituting elements, we have derived the transport and binding parameters of the ADDS based on the theory of anisotropic diffusion and the thermodynamics of antibody-antigen interactions.

The derived MC model is based on the recent advances in mass transport theory to provide an analytical solution to the problem of ADDS transport. In the frame of the current, often over-complicated models of system biology, the proposed MC approach models the complex behavior of ADDS with a straight-forward model. Using the MC paradigm, the ADDS transport from the point of injection to the interior of a cell has been abstracted as a cascade of MC channels, each characterized by an analytical impulse response. The MC-ADDS model studies the ADDS transport in the blood vessels, in the ECM, and through the

ligand binding. Compared with existing models, the majority of the systems parameters are directly related to the physiology, instead of using empirical values that involve statistical estimations from experiments.

There are several important issues that remain to be investigated on the modeling of ADDS systems. First, an optimization framework should be devised to take advantage of the possibilities offered by the MC approach. Second, the interference from the immune system and the endocrine system should be added to the model as a feedback process to improve the targeting of the disease. Finally, the toxicity of ADDS should be quantified mathematically in this framework.

The MC-ADDS model allowed determining the parts of the human body which influence the efficiency of the drug delivery, and the ADDS molecule parameters that are critical to overcome the obstacles posed by these limiting parts. Moreover, the MC model showed how the shape and electrochemical structure simultaneously affects the transport and antigen-binding kinetics of the ADDS. Finally, the validation of the MC-ADDS model against finite-element simulations in a realistic 3D geometry has shown that the model is a good approximation for the anisotropic advection-diffusion in the complex geometry of the body. This analytical model can be readily used to predict, design, and optimize advanced drug delivery systems in a versatile and accurate manner, and to simulate sophisticated therapeutic scenarios.

CHAPTER 7

CONCLUSIONS

Molecular communication (MC) is a novel communication paradigm where the transfer of molecules is abstracted as a transfer of information. It has promised to have a wide range of applications particularly in the biomedical field. In this thesis, the potential of the MC paradigm is harnessed to model an important area of biomedical engineering that is the modeling of drug delivery systems (DDS). The suitability of the MC paradigm comes from a direct identification between the elements of a communication system and the elements of a DDS. In fact, the injection of particles can be viewed as the transmission part of a communication scheme, the propagation of particles as the communication channel, and the delivery of particles as the reception part of the communication scheme. However, the reality is that under this simplifying system view lies an important complexity in terms of the governing physics of particle emission, propagation, and delivery. As examples, the particles are carried by the blood flow governed by the Navier-Stokes equation, delivered to tissues with porous material properties, and reacts according to stochastic properties. In this thesis, a unifying framework is provided to model DDS as a communication system. The framework is analytical, and compared with alternative methods for studying DDS's such as finite-element simulation and kinetic Monte-Carlo simulation.

The objectives of this thesis are as follows. First, we devise a system model that enables the prediction of time and space evolution of drug propagation in the cardiovascular system. The system model is based on a one-dimensional reduction of Navier-Stokes equations, the advection-diffusion equation through Taylor dispersion, conservation laws, and topological properties of the cardiovascular system. The system model is linked with the classical measurements used in classical DDS systems such as pharmacokinetics and biodistribution. Second, we develop a model to study the performance of a DDS through the concept of information theoretical capacity. After evaluating the properties of noise in a DDS as well

as the constraints that limits it, the information theoretical capacity of a DDS is defined and used to measure the success of a DDS. Third, antibody-mediated DDS are considered in the MC framework. We propose modifications to the basic framework in order to capture the peculiarities of antibody-antigen dynamics. This enables to study the end-to-end response of an antibody-mediated DDS.

Chapter 3 is devoted to present a molecular communication system model for particulate drug delivery systems. The main contributions are as follows:

- We define the basic elements of system modeling approach of particulate drug delivery systems using molecular communication, which consist of the topology of the cardiovascular system, the drug injection, the drug delivery rate, the drug propagation channel, and the blood velocity network.

- We model the blood velocity in every blood vessel of the cardiovascular system through the definition of a *blood velocity network*. The calculation of the blood velocity is based on a one-dimensional simplification of the network of blood vessels and an analogy with transmission line networks for large and small arteries. The inputs to the blood velocity network are the topology (lengths and arrangement of the blood vessels), the cardiac inflow, and the index of the target artery.

- We model the evolution of the drug concentration using harmonic transfer matrices (HTM). Given the fact that the blood velocity is time-varying, a *drug propagation network* is defined as a composition of HTMs with a equivalent linear periodically time-varying (LPTV) link or node. The time-varying impulse response for a blood vessel is analytically derived given the blood velocity, the length, and the radius of the blood vessels. The HTM's are combined using basic arithmetic rules.

Through the results of this novel approach in modeling particulate drug delivery systems, we learn that molecular communication provides a low-complexity and physiology-based modeling framework for this type of systems. This opens up the possibility to study

optimization techniques for particulate DDSs which could allow a careful selection of the location of injection and drug injection profile with the goal of obtaining a desired drug delivery profile at a targeted site while minimizing the drug presence in the rest of the cardiovascular system. In addition, the models developed in this research work could potentially serve to investigate novel communication techniques for Intra-Body Communication (IBC) networks.

Chapter 4 is devoted to the noise and capacity analysis of particulate drug delivery systems. The main contributions are as follows:

- We present an end-to-end system model of particulate drug delivery systems that includes not only the drug propagation but also the drug emission process and the drug reception process. The drug emission process is characterized with several design parameters and constraints and the drug reception process is derived based on the interaction of blood flow with the binding of drug particles.

- We show that the noise in a particulate drug delivery system can be modeled through an inhomogeneous Poisson process which is a function of the drug propagations time-varying impulse response and the probability of drug reception. The results stems from identifying the advection-diffusion equation with a Fokker-Planck equation describing the motion of one particle traveling through the several compartments of the cardiovascular system.

- We compare the results of analytical noise model with the results of kinetic Monte-Carlo simulations of drug particle propagation.

- We define the capacity in a particulate drug delivery systems as the maximum mutual information between the drug injection rate and the drug reception rate. We prove that the capacity of a particulate drug delivery systems is limited by several factors. These include the distance, the characteristics of the emission device, and the blood flow condition in the target location.

Through the results of the noise and capacity analysis of particulate drug delivery systems, we establish the first work to propose the use of information theory in PDDS design. Other works were mainly based on deterministic and probabilistic analysis of the long-term and steady-state drug distribution throughout the body. Our information-theoretical approach can be applied to put into use high precision nanomedicine delivery, in contrast with traditional medicine where the drug injection is not optimized with respect to the body variabilities such as the blood flow, the ligand-binding kinetics, and their interaction.

Chapter 5 is devoted to pharmacokinetic modeling using molecular communication. The main contributions are as follows

- We describe the several processes that a drug particle may undergo during the propagation in the human body. These include absorption, adsorption, reaction, diffusion, and advection. We define parameters for each of these processes.

- We study the performance of a particulate drug delivery system through the analytical definition of the path loss and the delay. These two measures are related to the pharmacokinetics and biodistribution of a drug particle.

- We model biodistribution through the novel molecular communication-based paradigm. We present formulas for directly calculating the amount of drug particles that effectively attain their target under several system conditions.

- We present a method to optimize the drug injection in order to obtain a desired a drug reception rate through the discretization of the time-varying impulse response of the system.

- We compare the results of the analytical molecular communication frameworks with the results of the finite-element-based COMSOL simulations.

Through the results of this pharmacokinetic modeling approach, we learn that the MC abstraction allows to obtain an analytical pharmacokinetic model that accounts for various

physicochemical processes in the particle propagation, and takes into account the impact of cardiovascular diseases. By stemming from the pharmacokinetic model, we proposed to use communication engineering metrics to estimate the drug biodistribution at the delivery location, while analytical expressions are obtained to estimate the drug accumulation in the rest of the body. We have favorably compared our pharmacokinetic model with multiphysics finite-element simulations of the drug propagation in the arterial system, and provided numerical results for the drug biodistribution in different scenarios. We also proposed a procedure to optimize the drug injection rate according to a desired drug delivery rate through the pharmacokinetic model when the injection location and delivery are known.

Chapter 6 is devoted to present a molecular communication system model for antibody-mediated drug delivery systems. The main contributions are as follows

- We present a system model that links the intrinsic properties of antibody-antigen compounds with their molecular communication parameters.
- We analytically derive impulse responses for the propagation in the extracellular matrix.
- We derive the end-to-end time-varying impulse response linking the emission of antibody-mediated drugs with their specific binding to antigens located at the target site.

Through the results of this modeling framework of antibody-mediated drug delivery systems, we learn that the MC-ADDS model enables the determination of the parts of the human body which influence the efficiency of the drug delivery, and the ADDS molecule parameters that are critical to overcome the obstacles posed by these limiting parts. Moreover, the MC model showed how the shape and electrochemical structure simultaneously affects the transport and antigen-binding kinetics of the ADDS. Finally, the validation of the MC-ADDS model against finite-element simulations in a realistic 3D geometry has

shown that the model is a good approximation for the anisotropic advection-diffusion in the complex geometry of the body. This analytical model can be readily used to predict, design, and optimize advanced drug delivery systems in a versatile and accurate manner, and to simulate sophisticated therapeutic scenarios.

We propose several future direction to extend on this work. First, to develop channel coding techniques inspired by the naturally-occurring biological quality check of drug delivery agents. Second, to study the ability of drug delivery systems to target several types of antigens simultaneously as a multiple-input multiple-output system. Third, to develop non-linear models of the blood velocity network and drug propagation network with robust drug delivery strategies.

PUBLICATIONS

Journal

1. Y. Chahibi, I. Akyildiz, and I. Balasingham, "Propagation Modeling and Analysis of Molecular Motors in Molecular Communication," submitted for journal publication, July 2016.

2. M. Veletic, P. A. Floor, Y. Chahibi, and I. Balasingham, "On the Upper Bound of the Information Capacity in Neuronal Synapses," submitted for journal publication, March 2016.

3. J. Beal , T. Haddock-Angelli , M. Gershater, K. de Mora, M. Lizarazo, J. Hollenhorst, et al., "Reproducibility of Fluorescent Expression from Engineered Biological Constructs in E. coli," PLoS ONE 11(3): e0150182, February 2016.

4. Y. Chahibi, M. Pierobon, and I. F. Akyildiz, "A Molecular Communication System Model for Particulate Drug Delivery Systems," IEEE Transactions on Biomedical Engineering, vol. 60, no. 12, pp. 3468,3483, December 2013.

5. Y. Chahibi and I. F. Akyildiz, "Molecular Communication Noise and Capacity Analysis for Particulate Drug Delivery Systems," IEEE Transactions on Communications, vol. 62, no. 11, pp. 3891-3903, November 2014.

6. Y. Chahibi, M. Pierobon, and I. F. Akyildiz, "Pharmacokinetic Modeling using the Molecular Communication Paradigm," IEEE Transactions on Biomedical Engineering, vol. 62, no. 10, pp. 2410-2420, October 2015.

7. Y. Chahibi, I. F. Akyildiz, S. Balasubramaniam, and Y. Koucheryavy, "Molecular Communication Modeling of Antibody-mediated Drug Delivery System," IEEE Transactions on Biomedical Engineering, vol. 62, no. 7, pp. 1683-1695, July 2015.

Conference

1. Y. Chahibi, and I. Balasingham, "An Intra-body Molecular Communication Networks Framework for Continuous Health Monitoring and Diagnosis," in Proc. of IEEE EMBC 2015, Milan, Italy, August 2015.

2. Y. Chahibi, and I. Balasingham, "Channel Modeling and Analysis for Molecular Motors in Nano-scale Communications," in Proc. of ACM NANOCOM 2015, Boston, MA, USA, September 2015.

3. Y. Chahibi and M. Pierobon , "Molecular Communication Analysis of Particulate Drug Delivery Systems and Body Interactions," in Proc. of the 47th Asilomar Conference on Signals, Systems and Computers, Pacific Grove, CA, November 2013.

4. Y. Chahibi, M. Pierobon, S. O. Song, and I. F. Akyildiz, "Antibody-Mediated Molecular Communication for Targeted Drug Delivery Systems," in Proc. of IEEE EMBC 2014, Chicago, USA, August 2014.

REFERENCES

[1] N. Kumar, *Handbook of Particulate Drug Delivery*. No. v. 1 in Nanotechnology book series, American Scientific Publishers, 2008.

[2] I. F. Akyildiz, F. Brunetti, and C. Blazquez, "Nanonetworks: a new communication paradigm at molecular level," *Computer Networks (Elsevier) Journal*, vol. 52, pp. 2260–2279, August 2008.

[3] D. L. Nelson and M. M. Cox, *Lehninger Principles of Biochemistry*, ch. 12.2, pp. 425–429. W. H. Freeman, 2005.

[4] L. Zhao, N. Li, and H. Yang, "A new stochastic approach to multi-compartment pharmacokinetic models: probability of traveling route and distribution of residence time in linear and nonlinear systems," *Journal of pharmacokinetics and pharmacodynamics*, vol. 38, no. 1, pp. 83–104, 2011.

[5] A. M. Scott, J. D. Wolchok, and L. J. Old, "Antibody therapy of cancer," *Nature Reviews Cancer*, vol. 12, no. 4, pp. 278–287, 2012.

[6] A. R. Tzafriri, E. I. Lerner, M. Flashner-Barak, M. Hinchcliffe, E. Ratner, and H. Parnas, "Mathematical modeling and optimization of drug delivery from intratumorally injected microspheres," *Clinical Cancer Research*, vol. 11, no. 2, pp. 826–834, 2005.

[7] L. Hu and R. J. Hansen, "Issues, challenges, and opportunities in model-based drug development for monoclonal antibodies," *Journal of pharmaceutical sciences*, vol. 102, no. 9, pp. 2898–2908, 2013.

[8] C. A. Boswell, D. B. Tesar, K. Mukhyala, F.-P. Theil, P. J. Fielder, and L. A. Khawli, "Effects of charge on antibody tissue distribution and pharmacokinetics," *Bioconjugate chemistry*, vol. 21, no. 12, pp. 2153–2163, 2010.

[9] M. Pierobon and I. F. Akyildiz, "A physical end-to-end model for molecular communication in nanonetworks," *IEEE Journal on Selected Areas in Communications (JSAC)*, vol. 28, pp. 602–611, May 2010.

[10] I. F. Akyildiz, J. M. Jornet, and M. Pierobon, "Nanonetworks: A new frontier in communications," *Communications of the ACMs*, vol. 54, pp. 84–89, November 2011.

[11] M. Pierobon and I. F. Akyildiz, "A physical end-to-end model for molecular communication in nanonetworks," *Selected Areas in Communications, IEEE Journal on*, vol. 28, no. 4, pp. 602–611, 2010.

[12] M. Pierobon and I. F. Akyildiz, "Noise analysis in ligand-binding reception for molecular communication in nanonetworks," *Signal Processing, IEEE Transactions on*, vol. 59, no. 9, pp. 4168–4182, 2011.

[13] M. Pierobon and I. Akyildiz, "Capacity of a diffusion-based molecular communication system with channel memory and molecular noise," *Information Theory, IEEE Transactions on*, vol. 59, no. 2, pp. 942–954, 2013.

[14] L. Parcerisa and I. F. Akyildiz, "Molecular communication options for long range nanonetworks," *Computer Networks (Elsevier) Journal*, vol. 53, pp. 2753–2766, August 2009.

[15] M. Moore, A. Enomoto, T. Nakano, R. Egashira, T. Suda, A. Kayasuga, H. Kojima, H. Sakakibara, and K. Oiwa, "A design of a molecular communication system for nanomachines using molecular motors," in *Proc. of Fourth Annual IEEE International Conference on Pervasive Computing and Communications Workshops*, pp. 6–12, March 2006.

[16] M. Gregori and I. F. Akyildiz, "A new nanonetwork architecture using flagellated bacteria and catalytic nanomotors," *IEEE Journal on Selected Areas in Communications (JSAC)*, vol. 28, pp. 602–611, May 2010.

[17] P. Charoenphol, R. B. Huang, and O. Eniola-Adefeso, "Potential role of size and hemodynamics in the efficacy of vascular-targeted spherical drug carriers," *Biomaterials*, vol. 31, no. 6, pp. 1392–1402, 2010.

[18] M. Li, K. T. Al-Jamal, K. Kostarelos, and J. Reineke, "Physiologically based pharmacokinetic modeling of nanoparticles," *ACS nano*, vol. 4, no. 11, pp. 6303–6317, 2010.

[19] D. E. Mager and W. J. Jusko, "General pharmacokinetic model for drugs exhibiting target-mediated drug disposition," *Journal of pharmacokinetics and pharmacodynamics*, vol. 28, no. 6, pp. 507–532, 2001.

[20] M. Dostalek, I. Gardner, B. M. Gurbaxani, R. H. Rose, and M. Chetty, "Pharmacokinetics, pharmacodynamics and physiologically-based pharmacokinetic modelling of monoclonal antibodies," *Clinical pharmacokinetics*, vol. 52, no. 2, pp. 83–124, 2013.

[21] R. S. Yang, L. W. Chang, C. S. Yang, and P. Lin, "Pharmacokinetics and physiologically-based pharmacokinetic modeling of nanoparticles," *Journal of nanoscience and nanotechnology*, vol. 10, no. 12, pp. 8482–8490, 2010.

[22] W. Wang, E. Wang, and J. Balthasar, "Monoclonal antibody pharmacokinetics and pharmacodynamics," *Clinical Pharmacology & Therapeutics*, vol. 84, no. 5, pp. 548–558, 2008.

[23] J. P. Davda, M. Jain, S. K. Batra, P. R. Gwilt, and D. H. Robinson, "A physiologically based pharmacokinetic (pbpk) model to characterize and predict the disposition of monoclonal antibody cc49 and its single chain fv constructs," *International immunopharmacology*, vol. 8, no. 3, pp. 401–413, 2008.

[24] A. Garg and J. P. Balthasar, "Physiologically-based pharmacokinetic (pbpk) model to predict igg tissue kinetics in wild-type and fcrn-knockout mice," *Journal of pharmacokinetics and pharmacodynamics*, vol. 34, no. 5, pp. 687–709, 2007.

[25] G. Z. Ferl, A. M. Wu, and J. J. DiStefano III, "A predictive model of therapeutic monoclonal antibody dynamics and regulation by the neonatal fc receptor (fcrn)," *Annals of biomedical engineering*, vol. 33, no. 11, pp. 1640–1652, 2005.

[26] L. L. M. Heaton, E. López, P. K. Maini, M. D. Fricker, and N. S. Jones, "Advection, diffusion, and delivery over a network," *Phys. Rev. E*, vol. 86, pp. 021905–1 – 021905–10, Aug 2012.

[27] P. K. Watkins, A. B. Walker, and G. L. B. Verschoor, "Dynamical monte carlo modelling of organic solar cells: The dependence of internal quantum efficiency on morphology," *Nano Letters*, vol. 5, no. 9, pp. 1814–1818, 2005. PMID: 16159229.

[28] M. Pierobon and I. Akyildiz, "Capacity of a diffusion-based molecular communication system with channel memory and molecular noise," *Information Theory, IEEE Transactions on*, vol. PP, no. 99, p. 1, 2012.

[29] M. Potter and D. Wiggert, *Fluid Mechanics*. Schaum's Outlines, McGraw-Hill (USA), 2008.

[30] C.-W. Chen, Y.-W. Shau, and C.-P. Wu, "Analog transmission line model for simulation of systemic circulation," *Biomedical Engineering, IEEE Transactions on*, vol. 44, pp. 90 –94, jan. 1997.

[31] J. Siepmann, R. Siegel, and M. Rathbone, *Fundamentals and Applications of Controlled Release Drug Delivery*. Advances in Delivery Science and Technology, Springer, 2011.

[32] F. N. van de Vosse and N. Stergiopulos, "Pulse wave propagation in the arterial tree," *Annual Review of Fluid Mechanics*, vol. 43, no. 1, pp. 467–499, 2011.

[33] N. Westerhof, F. Bosman, C. J. D. Vries, and A. Noordergraaf, "Analog studies of the human systemic arterial tree," *Journal of Biomechanics*, vol. 2, no. 2, pp. 121 – 143, 1969.

[34] M. S. Olufsen and A. Nadim, "On deriving lumped models for blood flow and pressure in the systemic arteries," *Math Biosci Eng*, vol. 1, pp. 61–80, Jun 2004.

[35] P. Vanassche, G. Gielen, and W. Sansen, "Symbolic modeling of periodically time-varying systems using harmonic transfer matrices," *Computer-Aided Design of Integrated Circuits and Systems, IEEE Transactions on*, vol. 21, pp. 1011 – 1024, sep 2002.

[36] H. Cao, V. Leung, C. Chow, and H. Chan, "Enabling technologies for wireless body area networks: A survey and outlook," *IEEE Communications Magazine*, vol. 47, pp. 84–93, December 2009.

[37] J. Ottesen, M. Olufsen, and J. Larsen, *Applied Mathematical Models in Human Physiology*. Siam Monographs on Mathematical Modeling and Computation, Society for Industrial and Applied Mathematics, 2004.

[38] B. Kirby, *Micro- And Nanoscale Fluid Mechanics: Transport in Microfluidic Devices*. Cambridge University Press, 2010.

[39] B. Davies, *Integral transforms and their applications*. Springer, New York, 2002.

[40] M. S. Olufsen, "Structured tree outflow condition for blood flow in larger systemic arteries," *American Journal of Physiology - Heart and Circulatory Physiology*, vol. 276, no. 1, pp. H257–H268, 1999.

[41] J. Irwin and R. Nelms, *Basic Engineering Circuit Analysis*. John Wiley & Sons, 2010.

[42] Á. Baricz, *Generalized Bessel Functions of the First Kind*. No. no. 1994 in Lecture Notes in Mathematics, Springer, 2010.

[43] C. Paul, *Fundamentals of electric circuit analysis*. John Wiley & Sons, 2001.

[44] A. Cheer and C. Van Dam, *Fluid Dynamics in Biology: Proceedings of an AMS-IMS-SIAM Joint Summer Research Conference Held July 6-12, 1991 with Support from the National Science Foundation and NASA Headquarters*. Contemporary Mathematics, American Mathematical Society, 1993.

[45] T. Esmailian, F. R. Kschischang, and P. Glenn Gulak, "In-building power lines as high-speed communication channels: channel characterization and a test channel ensemble," *International Journal of Communication Systems*, vol. 16, no. 5, pp. 381–400, 2003.

[46] P. L. D. Peres, I. S. Bonatti, and A. Lopes, "Transmission line modeling: A circuit theory approach," *SIAM Rev.*, vol. 40, pp. 347–352, June 1998.

[47] J. T. Ottesen, M. S. Olufsen, and J. K. Larsen, *Applied Mathematical Models in Human Physiology*. Society for Industrial and Applied Mathematics, 2004.

[48] K. Azer, "Taylor diffusion in time-dependent flow," *International Journal of Heat and Mass Transfer*, vol. 48, no. 13, pp. 2735 – 2740, 2005.

[49] D. Basmadjian, *Mass Transfer: Principles and Applications*. CRC PressI Llc, 2004.

[50] K. Dill and S. Bromberg, *Molecular Driving Forces: Statistical Thermodynamics in Chemistry, Physics, Biology, and Nanoscience*. Taylor & Francis Group, 2003.

[51] K. Howell, *Principles of Fourier Analysis: A Text and Reference for Scientists, Engineers, and Mathematicians*. Studies in Advanced Mathematics Series, CRC Press-INC, 2001.

[52] A. Mandelis, *Diffusion-wave fields: mathematical methods and Green functions*. Springer-Verlag, 2001.

[53] R. Hoskins and J. Pinto, *Theories Of Generalised Functions: Distributions, Ultradistributions and Other Generalised Functions*. Horwood Pub., 2005.

[54] R. Müller and H.-J. Jentschel, "Determination of Harmonic-Transfer-Matrices by Simulation," *Advances in Radio Science*, vol. 3, pp. 349–354, May 2005.

[55] M. S. Olufsen, C. S. Peskin, W. Y. Kim, E. M. Pedersen, A. Nadim, and J. Larsen, "Numerical simulation and experimental validation of blood flow in arteries with structured-tree outflow conditions," *Annals of biomedical engineering*, vol. 28, no. 11, pp. 1281–1299, 2000.

[56] A. R. Tzafriri and E. R. Edelman, "Convective and diffusive transport in drug delivery," in *Cancer Targeted Drug Delivery*, pp. 573–606, Springer, 2013.

[57] Y. Chahibi, M. Pierobon, S. O. Song, and I. Akyildiz, "A molecular communication system model for particulate drug delivery systems," *Biomedical Engineering, IEEE Transactions on*, vol. 60, pp. 3468–3483, Dec 2013.

[58] I. F. Akyildiz, F. Fekri, R. Sivakumar, C. R. Forest, and B. K. Hammer, "Monaco: fundamentals of molecular nano-communication networks," *Wireless Communications, IEEE*, vol. 19, no. 5, pp. 12–18, 2012.

[59] T. Zhou, L. Chen, and K. Aihara, "Molecular communication through stochastic synchronization induced by extracellular fluctuations," *Phys. Rev. Lett.*, vol. 95, p. 178103, Oct 2005.

[60] M. Pierobon and I. Akyildiz, "A statistical-physical model of interference in diffusion-based molecular nanonetworks," *Communications, IEEE Transactions on*, vol. 62, pp. 2085–2095, June 2014.

[61] D. M. Roden and A. L. George Jr, "The genetic basis of variability in drug responses," *Nature Reviews Drug Discovery*, vol. 1, no. 1, pp. 37–44, 2002.

[62] M. Fernandez and S. Williams, "Closed-form expression for the poisson-binomial probability density function," *Aerospace and Electronic Systems, IEEE Transactions on*, vol. 46, no. 2, pp. 803–817, 2010.

[63] M. Fernandez and S. Williams, "Closed-form expression for the poisson-binomial probability density function," *Aerospace and Electronic Systems, IEEE Transactions on*, vol. 46, no. 2, pp. 803–817, 2010.

[64] J. Marijnissen and L. Gradón, *Nanoparticles in medicine and environment: Inhalation and health effects*. Biomedical and Life Sciences, Springer, 2009.

[65] H. Brenner, "A general theory of taylor dispersion phenomena.," *PhysicoChem. Hydrodyn.*, vol. 1, 2012.

[66] L. Le Cam, "An approximation theorem for the poisson binomial distribution.," *Pacific Journal of Mathematics*, vol. 10, no. 4, pp. 1181–1197, 1960.

[67] J. M. Tarbell, "Shear stress and the endothelial transport barrier," *Cardiovascular research*, vol. 87, no. 2, pp. 320–330, 2010.

[68] P. Decuzzi and M. Ferrari, "Design maps for nanoparticles targeting the diseased microvasculature," *Biomaterials*, vol. 29, no. 3, pp. 377–384, 2008.

[69] J. W. Piper, R. A. Swerlick, and C. Zhu, "Determining force dependence of two-dimensional receptor-ligand binding affinity by centrifugation," *Biophysical journal*, vol. 74, no. 1, pp. 492–513, 1998.

[70] P. Decuzzi and M. Ferrari, "The adhesive strength of non-spherical particles mediated by specific interactions," *Biomaterials*, vol. 27, no. 30, pp. 5307–5314, 2006.

[71] P. V. Stroev, P. R. Hoskins, and W. J. Easson, "Distribution of wall shear rate throughout the arterial tree: a case study," *Atherosclerosis*, vol. 191, no. 2, pp. 276–280, 2007.

[72] R. Beaudouin, S. Micallef, and C. Brochot, "A stochastic whole-body physiologically based pharmacokinetic model to assess the impact of inter-individual variability on tissue dosimetry over the human lifespan," *Regulatory Toxicology and Pharmacology*, vol. 57, no. 1, pp. 103–116, 2010.

[73] C. W. Gardiner, *Stochastic methods*. Springer Berlin, 2009.

[74] G. Lindgren, *Stationary Stochastic Processes: Theory and Applications*. Chapman & Hall/CRC Texts in Statistical Science, Taylor & Francis, 2012.

[75] T. M. Cover and J. A. Thomas, *Elements of information theory*. John Wiley & Sons, 2012.

[76] S. Haas and J. Shapiro, "Capacity of the multiple-input, multiple-output poisson channel," *Stochastic Theory and Control*, pp. 155–168, 2002.

[77] M. Davis, "Capacity and cutoff rate for poisson-type channels," *Information Theory, IEEE Transactions on*, vol. 26, no. 6, pp. 710–715, 1980.

[78] Y. Chahibi, M. Pierobon, and S. O. Song, "Molecular communication model of nanoparticle-body interactions in particulate drug delivery systems," in *Signals, Systems and Computers, 2013 Asilomar Conference on*, pp. 1051–1055, IEEE, 2013.

[79] W. Coffey, Y. Kalmykov, and J. Waldron, *The Langevin Equation: With Applications to Stochastic Problems in Physics, Chemistry, and Electrical Engineering*. World Scientific Series in Contemporary Chemical Physics, World Scientific, 2004.

[80] M. N. V. R. Kumar, *Handbook of Particulate Drug Delivery*. American Scientific Publishers, 2011.

[81] A. M. Alkilany, L. B. Thompson, S. P. Boulos, P. N. Sisco, and C. J. Murphy, "Gold nanorods: their potential for photothermal therapeutics and drug delivery, tempered by the complexity of their biological interactions," *Advanced drug delivery reviews*, vol. 64, no. 2, pp. 190–199, 2012.

[82] S. Willmann, K. Höhn, A. Edginton, M. Sevestre, J. Solodenko, W. Weiss, J. Lippert, and W. Schmitt, "Development of a physiology-based whole-body population model for assessing the influence of individual variability on the pharmacokinetics of drugs," *Journal of pharmacokinetics and pharmacodynamics*, vol. 34, no. 3, pp. 401–431, 2007.

[83] P. D. Marcato, "Pharmacokinetics and pharmacodynamics of nanomaterials," in *Nanotoxicology*, pp. 97–110, Springer, 2014.

[84] D. Li, C. Emond, G. Johanson, and O. Jolliet, "Using a pbpk model to study the influence of different characteristics of nanoparticles on their biodistribution," in *Journal of Physics: Conference Series*, vol. 429, p. 012019, IOP Publishing, 2013.

[85] V. P. Chauhan, T. Stylianopoulos, Y. Boucher, and R. K. Jain, "Delivery of molecular and nanoscale medicine to tumors: transport barriers and strategies," *Annual review of chemical and biomolecular engineering*, vol. 2, pp. 281–298, 2011.

[86] K. Avgoustakis, A. Beletsi, Z. Panagi, P. Klepetsanis, A. Karydas, and D. Ithakissios, "Plga–mpeg nanoparticles of cisplatin: in vitro nanoparticle degradation, in vitro drug release and in vivo drug residence in blood properties," *Journal of Controlled Release*, vol. 79, no. 1, pp. 123–135, 2002.

[87] C. D. Walkey, J. B. Olsen, H. Guo, A. Emili, and W. C. Chan, "Nanoparticle size and surface chemistry determine serum protein adsorption and macrophage uptake," *Journal of the American Chemical Society*, vol. 134, no. 4, pp. 2139–2147, 2012.

[88] R. R. Biswas and P. N. Sen, "Taylor dispersion with absorbing boundaries: A stochastic approach," *Physical review letters*, vol. 98, no. 16, p. 164501, 2007.

[89] M. Levesque, O. Bénichou, R. Voituriez, and B. Rotenberg, "Taylor dispersion with adsorption and desorption," *Physical Review E*, vol. 86, no. 3, p. 036316, 2012.

[90] G. McVeigh *et al.*, "Evaluation of mechanical arterial properties: clinical, experimental and therapeutic aspects," *Clinical Science*, vol. 102, pp. 51–67, 2002.

[91] B. Syeda, M. Gottsauner-Wolf, S. Denk, P. Pichler, A. Khorsand, and D. Glogar, "Arterial compliance: a diagnostic marker for atherosclerotic plaque burden?," *American journal of hypertension*, vol. 16, no. 5, pp. 356–362, 2003.

[92] J. DiPiro and A. S. of Health-System Pharmacists, *Concepts in Clinical Pharmacokinetics*. American Society of Health-System Pharmacists, 2010.

[93] F. Gentile, M. Ferrari, and P. Decuzzi, "The transport of nanoparticles in blood vessels: The effect of vessel permeability and blood rheology," *Annals of biomedical engineering*, vol. 36, no. 2, pp. 254–261, 2008.

[94] J. Ottesen, M. Olufsen, and J. Larsen, *Applied Mathematical Models in Human Physiology*. Monographs on Mathematical Modeling and Computation, Society for Industrial and Applied Mathematics, 2004.

[95] V. Balakotaiah and H.-C. Chang, "Dispersion of chemical solutes in chromatographs and reactors," *Philosophical Transactions of the Royal Society of London. Series A: Physical and Engineering Sciences*, vol. 351, no. 1695, pp. 39–75, 1995.

[96] G. A. Hughes, "Nanostructure-mediated drug delivery," *Nanomedicine: nanotechnology, biology and medicine*, vol. 1, no. 1, pp. 22–30, 2005.

[97] B. H. Devkota and J. Imberger, "Lagrangian modeling of advection-diffusion transport in open channel flow," *Water resources research*, vol. 45, no. 12, 2009.

[98] S. Wang, L. Xie, and C. Zhang, "H 2 optimal inverse of periodic fir digital filters," *Signal Processing, IEEE Transactions on*, vol. 48, no. 9, pp. 2696–2700, 2000.

[99] L. A. Zadeh and C. A. Deoser, *Linear system theory*. Robert E. Krieger Publishing Company, 1976.

[100] Y. Chahibi and I. Akyildiz, "Molecular communication noise and capacity analysis for particulate drug delivery systems," *Communications, IEEE Transactions on*, vol. 62, Nov 2014.

[101] I. F. Akyildiz, M. Pierobon, S. Balasubramaniam, and Y. Koucheryavy, "Internet of bionanothings," *Communications Magazine, IEEE*, 2015.

[102] L. M. Weiner, J. C. Murray, and C. W. Shuptrine, "Antibody-based immunotherapy of cancer," *Cell*, vol. 148, no. 6, pp. 1081–1084, 2012.

[103] M. Pierobon and I. F. Akyildiz, "Diffusion-based noise analysis for molecular communication in nanonetworks," *Signal Processing, IEEE Transactions on*, vol. 59, no. 6, pp. 2532–2547, 2011.

[104] A. C. Chan and P. J. Carter, "Therapeutic antibodies for autoimmunity and inflammation," *Nature Reviews Immunology*, vol. 10, no. 5, pp. 301–316, 2010.

[105] L. G. Presta, "Molecular engineering and design of therapeutic antibodies," *Current opinion in immunology*, vol. 20, no. 4, pp. 460–470, 2008.

[106] H. Brenner, "Coupling between the translational and rotational brownian motions of rigid particles of arbitrary shape: Ii. general theory," *Journal of colloid and interface science*, vol. 23, no. 3, pp. 407–436, 1967.

[107] D. Brune and S. Kim, "Predicting protein diffusion coefficients.," *Proceedings of the National Academy of Sciences*, vol. 90, no. 9, pp. 3835–3839, 1993.

[108] A. Chauvière, L. Preziosi, and C. Verdier, *Cell Mechanics: From Single Scale-Based Models to Multiscale Modeling*. Chapman & Hall/CRC Mathematical and Computational Biology, Taylor & Francis, 2010.

[109] D. Savéry and G. Cloutier, "Effect of red cell clustering and anisotropy on ultrasound blood backscatter: a monte carlo study," *Ultrasonics, Ferroelectrics and Frequency Control, IEEE Transactions on*, vol. 52, no. 1, pp. 94–103, 2005.

[110] Y. Chahibi and I. Akyildiz, "Molecular communication noise and capacity analysis for particulate drug delivery systems," *Communications, IEEE Transactions on*, vol. 62, Nov 2014.

[111] M. Kim, R. J. Gillies, and K. A. Rejniak, "Current advances in mathematical modeling of anti-cancer drug penetration into tumor tissues," *Frontiers in oncology*, vol. 3, 2013.

[112] A. M. Berezhkovskii and A. T. Skvortsov, "Aris-taylor dispersion with drift and diffusion of particles on the tube wall," *The Journal of chemical physics*, vol. 139, no. 8, p. 084101, 2013.

[113] A. Gutmanas, Y. Alhroub, G. M. Battle, J. M. Berrisford, E. Bochet, M. J. Conroy, J. M. Dana, M. A. F. Montecelo, G. van Ginkel, S. P. Gore, *et al.*, "Pdbe: Protein data bank in europe," *Nucleic acids research*, vol. 42, no. D1, pp. D285–D291, 2014.

[114] S. Venkataraman, J. L. Hedrick, Z. Y. Ong, C. Yang, P. L. R. Ee, P. T. Hammond, and Y. Y. Yang, "The effects of polymeric nanostructure shape on drug delivery," *Advanced drug delivery reviews*, vol. 63, no. 14, pp. 1228–1246, 2011.

[115] J. A. Champion, Y. K. Katare, and S. Mitragotri, "Particle shape: a new design parameter for micro-and nanoscale drug delivery carriers," *Journal of Controlled Release*, vol. 121, no. 1, pp. 3–9, 2007.

[116] Y. Geng, P. Dalhaimer, S. Cai, R. Tsai, M. Tewari, T. Minko, and D. E. Discher, "Shape effects of filaments versus spherical particles in flow and drug delivery," *Nature Nanotechnology*, vol. 2, no. 4, pp. 249–255, 2007.

[117] M. X. Fernandes and J. G. de la Torre, "Brownian dynamics simulation of rigid particles of arbitrary shape in external fields," *Biophysical journal*, vol. 83, no. 6, pp. 3039–3048, 2002.

[118] X. Sun, T. Lin, and J. D. Gezelter, "Langevin dynamics for rigid bodies of arbitrary shape," *The Journal of chemical physics*, vol. 128, no. 23, p. 234107, 2008.

[119] J. G. de la Torre and V. A. Bloomfield, "Hydrodynamic properties of complex, rigid, biological macromolecules: theory and applications," *Quarterly reviews of biophysics*, vol. 14, no. 01, pp. 81–139, 1981.

[120] M. Matyka, A. Khalili, and Z. Koza, "Tortuosity-porosity relation in porous media flow," *Physical Review E*, vol. 78, no. 2, p. 026306, 2008.

[121] S. Ramanujan, A. Pluen, T. D. McKee, E. B. Brown, Y. Boucher, and R. K. Jain, "Diffusion and convection in collagen gels: implications for transport in the tumor interstitium," *Biophysical journal*, vol. 83, no. 3, pp. 1650–1660, 2002.

[122] E. Syková, T. Mazel, L. Vargová, I. Voříšek, and Š. Prokopová-Kubinová, "Extracellular space diffusion and pathological states," *Progress in brain research*, vol. 125, pp. 155–178, 2000.

[123] K. Whang, T. K. Goldstick, and K. E. Healy, "A biodegradable polymer scaffold for delivery of osteotropic factors," *Biomaterials*, vol. 21, no. 24, pp. 2545–2551, 2000.

[124] A. Onufriev, D. Bashford, and D. A. Case, "Modification of the generalized born model suitable for macromolecules," *The Journal of Physical Chemistry B*, vol. 104, no. 15, pp. 3712–3720, 2000.

[125] V. Lafont, M. Schaefer, R. H. Stote, D. Altschuh, and A. Dejaegere, "Protein–protein recognition and interaction hot spots in an antigen–antibody complex: free energy decomposition identifies efficient amino acids," *Proteins: Structure, Function, and Bioinformatics*, vol. 67, no. 2, pp. 418–434, 2007.

[126] W. C. Still, A. Tempczyk, R. C. Hawley, and T. Hendrickson, "Semianalytical treatment of solvation for molecular mechanics and dynamics," *Journal of the American Chemical Society*, vol. 112, no. 16, pp. 6127–6129, 1990.

[127] H. Hamaker, "The londonvan der waals attraction between spherical particles," *physica*, vol. 4, no. 10, pp. 1058–1072, 1937.

[128] L. Hu and R. J. Hansen, "Issues, challenges, and opportunities in model-based drug development for monoclonal antibodies," *Journal of pharmaceutical sciences*, vol. 102, no. 9, pp. 2898–2908, 2013.

[129] J.-F. Mao and Z.-F. Li, "Analysis of the time response of nonuniform multiconductor transmission lines with a method of equivalent cascaded network chain," *Microwave Theory and Techniques, IEEE Transactions on*, vol. 40, pp. 948 –954, may 1992.

[130] J. E. Gentle, *Matrix Algebra: Theory, Computations, and Applications in Statistics*. Springer, 2007.

[131] M. Pierobon and I. F. Akyildiz, "A physical end-to-end model for molecular communication in nanonetworks," *IEEE Journal on Selected Areas in Communications (JSAC)*, vol. 28, pp. 602–611, May 2010.

[132] S. Abadal and I. Akyildiz, "Bio-inspired synchronization for nanocommunication networks," in *Global Telecommunications Conference (GLOBECOM 2011), 2011 IEEE*, pp. 1 –5, dec. 2011.

[133] I. F. Akyildiz, F. Brunetti, and C. Blázquez, "Nanonetworks: A new communication paradigm," *Computer Networks*, vol. 52, no. 12, pp. 2260–2279, 2008.

[134] I. F. Akyildiz, J. M. Jornet, and M. Pierobon, "Nanonetworks: A new frontier in communications," *Communications of the ACMs*, vol. 54, pp. 84–89, November 2011.

[135] R. Aris, "On the dispersion of a solute in a fluid flowing through a tube," *Proceedings of the Royal Society of London. Series A. Mathematical and Physical Sciences*, vol. 235, no. 1200, pp. 67–77, 1956.

[136] R. Aris, "On the dispersion of a solute in a fluid flowing through a tube," *Proceedings of the Royal Society of London. Series A. Mathematical and Physical Sciences*, vol. 235, no. 1200, pp. 67–77, 1956.

[137] C. E. Ashley, E. C. Carnes, G. K. Phillips, D. Padilla, P. N. Durfee, P. A. Brown, T. N. Hanna, J. Liu, B. Phillips, M. B. Carter, *et al.*, "The targeted delivery of multicomponent cargos to cancer cells by nanoporous particle-supported lipid bilayers," *Nature materials*, vol. 10, no. 5, pp. 389–397, 2011.

[138] P. J. Aston, G. Derks, A. Raji, B. M. Agoram, and P. H. van der Graaf, "Mathematical analysis of the pharmacokinetic–pharmacodynamic (pkpd) behaviour of monoclonal antibodies: Predicting¡ i¿ in vivo¡/i¿ potency," *Journal of theoretical biology*, vol. 281, no. 1, pp. 113–121, 2011.

[139] B. Atakan, O. B. Akan, and S. Balasubramaniam, "Body area nanonetworks with molecular communications in nanomedicine," *Communications Magazine, IEEE*, vol. 50, no. 1, pp. 28–34, 2012.

[140] Y. H. Bae and K. Park, "Targeted drug delivery to tumors: myths, reality and possibility," *Journal of Controlled Release*, vol. 153, no. 3, p. 198, 2011.

[141] G. Batchelor, *An introduction to Fluid Mechanics*. Cambridge Mathematical Library, 2000.

[142] D. A. Beard and J. B. Bassingthwaighte, "Advection and diffusion of substances in biological tissues with complex vascular networks," *Annals of biomedical engineering*, vol. 28, no. 3, pp. 253–268, 2000.

[143] K. Binder and D. Heermann, *Monte Carlo Simulation in Statistical Physics*. Graduate Texts in Physics, Springer, 2010.

[144] D. Bolster, M. Dentz, and T. L. Borgne, "Solute dispersion in channels with periodically varying apertures," *Physics of Fluids*, vol. 21, no. 5, p. 056601, 2009.

[145] H. Brenner, "Macrotransport processes: Brownian tracers as stochastic averagers in effective-medium theories of heterogeneous media," *Journal of Statistical Physics*, vol. 62, pp. 1095–1119, 1991.

[146] P. C. Bressloff and J. M. Newby, "Stochastic models of intracellular transport," *Reviews of Modern Physics*, vol. 85, no. 1, p. 135, 2013.

[147] K. E. Caputo and D. A. Hammer, "Effect of microvillus deformability on leukocyte adhesion explored using adhesive dynamics simulations," *Biophysical journal*, vol. 89, no. 1, pp. 187–200, 2005.

[148] C. Caro, T. Pedley, R. Schroter, W. Seed, and K. Parker, *The Mechanics of the Circulation*. Cambridge University Press, 2011.

[149] S. Chakraborty, "On the use of the kolmogorov-landau approach in deriving various correlation functions in two-dimensional incompressible turbulence," *Physics of Fluids*, vol. 19, no. 8, 2007.

[150] A. J. Chorin, *Vorticity and turbulence*, vol. 103. Springer, 1994.

[151] S. Curry and R. Whelpton, *Drug Disposition and Pharmacokinetics: From Principles to Applications*. Wiley, 2011.

[152] M. E. Davis, "Fighting cancer with nanoparticle medicinesthe nanoscale matters," *MRS bulletin*, vol. 37, no. 09, pp. 828–835, 2012.

[153] P. Decuzzi, F. Causa, M. Ferrari, and P. Netti, "The effective dispersion of nanovectors within the tumor microvasculature," *Annals of Biomedical Engineering*, vol. 34, pp. 633–641, 2006.

[154] R. Deng, S. Iyer, F.-P. Theil, D. L. Mortensen, P. J. Fielder, and S. Prabhu, "Projecting human pharmacokinetics of therapeutic antibodies from nonclinical data," *What have we learned*, pp. 61–66, 2011.

[155] L. H. Dill and H. Brenner, "A general theory of taylor dispersion phenomena. vi. langevin methods," *Journal of Colloid and Interface Science*, vol. 93, no. 2, pp. 343–365, 1983.

[156] M. Liu, J. K. Nicholson, J. A. Parkinson, and J. C. Lindon, "Measurement of biomolecular diffusion coefficients in blood plasma using two-dimensional 1h1h diffusion-edited total-correlation nmr spectroscopy," *Analytical Chemistry*, vol. 69, no. 8, pp. 1504–1509, 1997. PMID: 9109350.

[157] R. L. Fournier, *Basic transport phenomena in biomedical engineering*. CRC Press, 2011.

[158] H. B. Frieboes, M. Wu, J. Lowengrub, P. Decuzzi, and V. Cristini, "A computational model for predicting nanoparticle accumulation in tumor vasculature," *PloS one*, vol. 8, no. 2, p. e56876, 2013.

[159] A. Guha, "Transport and deposition of particles in turbulent and laminar flow," *Annu. Rev. Fluid Mech.*, vol. 40, pp. 311–341, 2008.

[160] J. Hallett, J. Mills, J. Earnshaw, J. Reekers, and T. Rooke, *Comprehensive Vascular and Endovascular Surgery*. Mosby/Elsevier, 2009.

[161] M. Hazewinkel, *Encyclopaedia of mathematics: an updated and annotated translation of the Soviet "Mathematical encyclopaedia"*. Encyclopaedia of Mathematics: An Updated and Annotated Translation of the Soviet "Mathematical Encyclopaedia", Reidel, 1994.

[162] R. J. Ho and J. Chien, "Trends in translational medicine and drug targeting and delivery: new insights on an old concepttargeted drug delivery with antibody–drug conjugates for cancers," *Journal of pharmaceutical sciences*, vol. 103, no. 1, pp. 71–77, 2014.

[163] S. Huang, Q. Li, and J. Wu, "A general inflow turbulence generator for large eddy simulation," *Journal of Wind Engineering and Industrial Aerodynamics*, vol. 98, no. 1011, pp. 600 – 617, 2010.

[164] I. F. Akyildiz, F. Brunetti, and C. Blazquez, "Nanonetworks: a new communication paradigm at molecular level," *Computer Networks (Elsevier) Journal*, vol. 52, pp. 2260–2279, August 2008.

[165] D. J. Irvine, "Drug delivery: One nanoparticle, one kill," *Nature Materials*, vol. 10, no. 5, pp. 342–343, 2011.

[166] R. K. Jain and T. Stylianopoulos, "Delivering nanomedicine to solid tumors," *Nature reviews clinical oncology*, vol. 7, no. 11, pp. 653–664, 2010.

[167] M. Kac, "On distributions of certain wiener functionals," *Trans. Amer. Math. Soc*, vol. 65, no. 1, pp. 1–13, 1949.

[168] P. P. Karmali and D. Simberg, "Interactions of nanoparticles with plasma proteins: implication on clearance and toxicity of drug delivery systems," *Expert Opinion on Drug Delivery*, vol. 8, no. 3, pp. 343–357, 2011.

[169] N. Khlebtsov and L. Dykman, "Biodistribution and toxicity of engineered gold nanoparticles: a review of in vitro and in vivo studies," *Chemical Society Reviews*, vol. 40, no. 3, pp. 1647–1671, 2011.

[170] M. Kojić, N. Filipović, B. Stojanović, and N. Kojić, *Computer Modeling in Bioengineering: Theoretical Background, Examples and Software*. John Wiley & Sons, 2008.

[171] C. Korn and U. Schwarz, "Mean first passage times for bond formation for a brownian particle in linear shear flow above a wall," *The Journal of chemical physics*, vol. 126, no. 9, p. 095103, 2007.

[172] M. Long, H. Zhao, K.-S. Huang, and C. Zhu, "Kinetic measurements of cell surface e-selectin/carbohydrate ligand interactions," *Annals of biomedical engineering*, vol. 29, no. 11, pp. 935–946, 2001.

[173] L. Parcerisa and I. F. Akyildiz, "Molecular communication options for long range nanonetworks," *Computer Networks (Elsevier) Journal*, vol. 53, pp. 2753 – 2766, August 2009.

[174] H. Maeda, "Macromolecular therapeutics in cancer treatment: the epr effect and beyond," *Journal of Controlled Release*, 2012.

[175] M. Gregori and I. F. Akyildiz, "A new nanonetwork architecture using flagellated bacteria and catalytic nanomotors," *IEEE Journal on Selected Areas in Communications (JSAC)*, vol. 28, pp. 602–611, May 2010.

[176] S. M. McCormick, J. T. Seil, D. S. Smith, F. Tan, and F. Loth, "Transitional flow in a cylindrical flow chamber for studies at the cellular level," *Cardiovascular engineering and technology*, vol. 3, no. 4, pp. 439–449, 2012.

[177] J. W. MEHL, J. L. ONCLEY, and R. SIMHA, "Viscosity and the shape of protein molecules," *Science*, vol. 92, no. 2380, pp. 132–133, 1940.

[178] F. Miller, A. Vandome, and M. John, *Bilinear Interpolation*. VDM Publishing, 2010.

[179] M. Moore, A. Enomoto, T. Nakano, R. Egashira, T. Suda, A. Kayasuga, H. Kojima, H. Sakakibara, and K. Oiwa, "A design of a molecular communication system for nanomachines using molecular motors," in *Proc. of Fourth Annual IEEE International Conference on Pervasive Computing and Communications Workshops*, pp. 6–12, March 2006.

[180] T. Nakano, T. Suda, M. Moore, R. Egashira, A. Enomoto, and K. Arima, "Molecular communication for nanomachines using intercellular calcium signaling," in *Nanotechnology, 2005. 5th IEEE Conference on*, pp. 478–481, IEEE, 2005.

[181] D. L. Nelson and M. M. Cox, *Lehninger Principles of Biochemistry*, ch. 12.2, pp. 425–429. W. H. Freeman, 2005.

[182] I. Ordás, D. R. Mould, B. G. Feagan, and W. J. Sandborn, "Anti-tnf monoclonal antibodies in inflammatory bowel disease: pharmacokinetics-based dosing paradigms," *Clinical Pharmacology & Therapeutics*, vol. 91, no. 4, pp. 635–646, 2012.

[183] M. Pierobon and I. F. Akyildiz, "Diffusion-based noise analysis for molecular communication in nanonetworks," *IEEE Transactions on Signal Processing*, vol. 59, pp. 2532–2547, June 2011.

[184] M. Pierobon and I. F. Akyildiz, "Information capacity of diffusion-based molecular communication in nanonetworks," in *in Proc. of IEEE International Conference on Computer Communication, INFOCOM 2011, Miniconference*, April 2011.

[185] M. Pierobon and I. F. Akyildiz, "Noise analysis in ligand-binding reception for molecular communication in nanonetworks," *IEEE Transactions on Signal Processing*, vol. 59, pp. 4168–4182, September 2011.

[186] A. Z. Wang, R. Langer, and O. C. Farokhzad, "Nanoparticle delivery of cancer drugs," *Annu. Rev. Med.*, vol. 63, pp. 185–198, 2012.

[187] S. Pope, *Turbulent Flows*. Cambridge University Press, 2000.

[188] S. B. Pope, "Simple models of turbulent flows," *Physics of Fluids*, vol. 23, no. 1, p. 011301, 2011.

[189] M. Protter and C. Morrey, *A First Course in Real Analysis*. Undergraduate Texts in Mathematics, Springer-Verlag, 1991.

[190] Z. M. Qian, H. Li, H. Sun, and K. Ho, "Targeted drug delivery via the transferrin receptor-mediated endocytosis pathway," *Pharmacological reviews*, vol. 54, no. 4, pp. 561–587, 2002.

[191] N. J. Quinlan and P. N. Dooley, "Models of flow-induced loading on blood cells in laminar and turbulent flow, with application to cardiovascular device flow," *Annals of biomedical engineering*, vol. 35, no. 8, pp. 1347–1356, 2007.

[192] S. T. Reddy, D. A. Berk, R. K. Jain, and M. A. Swartz, "A sensitive in vivo model for quantifying interstitial convective transport of injected macromolecules and nanoparticles," *Journal of applied physiology*, vol. 101, no. 4, pp. 1162–1169, 2006.

[193] P. Ruenraroengsak, J. M. Cook, and A. T. Florence, "Nanosystem drug targeting: facing up to complex realities," *Journal of Controlled Release*, vol. 141, no. 3, pp. 265–276, 2010.

[194] R. Schiestel, *Modeling and Simulation of Turbulent Flows*. ISTE, Wiley, 2010.

[195] J. Seifter, A. Ratner, and D. Sloane, *Concepts in Medical Physiology*. Lippincott Williams & Wilkins, 2005.

[196] C. W. Shuptrine and L. M. Weiner, "Bifunctional antibodies: Preclinical and clinical applications," in *Advances in Tumor Immunology and Immunotherapy*, pp. 183–211, Springer, 2014.

[197] S. A. Socolofsky and G. H. Jirka, *Special Topics in Mixing and Transport Processes in the Environment*. Engineering Lectures, Coastal and Ocean Engineering Division, 5th Edition, 2005.

[198] G. I. Taylor, "Dispersion of soluble matter in solvent flowing slowly through a tube," in *Proc. Roy. Soc. A.*, p. 186203, 1953.

[199] G. M. Thurber and R. Weissleder, "A systems approach for tumor pharmacokinetics," *PloS one*, vol. 6, no. 9, p. e24696, 2011.

[200] V. J. Venditto and F. C. Szoka Jr, "Cancer nanomedicines: So many papers and so few drugs!," *Advanced Drug Delivery Reviews*, 2012.

[201] A. Vikhansky and W. Wang, "Taylor dispersion in finite-length capillaries," *Chemical Engineering Science*, vol. 66, no. 4, pp. 642 – 649, 2011.

[202] J. L. Vivero-Escoto, I. I. Slowing, B. G. Trewyn, and V. S.-Y. Lin, "Mesoporous silica nanoparticles for intracellular controlled drug delivery," *Small*, vol. 6, no. 18, pp. 1952–1967, 2010.

[203] B. Younis and S. Berger, "A turbulence model for pulsatile arterial flows.," *Journal of biomechanical engineering*, vol. 126, no. 5, pp. 578–584, 2004.

[204] Z. Zeng, Y. Yin, K.-M. Jan, and D. S. Rumschitzki, "Macromolecular transport in heart valves. ii. theoretical models," *American Journal of Physiology-Heart and Circulatory Physiology*, vol. 292, no. 6, pp. H2671–H2686, 2007.

[205] Z. Zhang and C. Kleinstreuer, "Laminar-to-turbulent fluid–nanoparticle dynamics simulations: Model comparisons and nanoparticle-deposition applications," *International Journal for Numerical Methods in Biomedical Engineering*, vol. 27, no. 12, pp. 1930–1950, 2011.

[206] L. Zhao, E. Y. Shang, and C. G. Sahajwalla, "Application of pharmacokinetics–pharmacodynamics/clinical response modeling and simulation for biologics drug development," *Journal of pharmaceutical sciences*, vol. 101, no. 12, pp. 4367–4382, 2012.

[207] "Comsol multiphysics," 2013.

VITA

Youssef Chahibi received the M.S. degree from the Georgia Institute of Technology, Atlanta, USA, in 2012, and the Diplôme d'Ingénieur in Telecommunications and Networks from Institut National Polytechnique de Toulouse, France, in 2011. During 2011, he was a physical-layer Engineer at Alcatel-Lucent, Antwerp, Belgium. In Summer 2014, he was a guest research scholar at the Nano Communication Center (NCC) at Tampere University of Technology, and during 2015, he was a fellow of the Research Council of Norway at the Norwegian University of Science and Technology (NTNU) in Trondheim, Norway. His research interests include nanoscale biologically-inspired communications, and drug delivery systems. He joined the BWN lab of the School of Electrical and Computer Engineering, Georgia Institute of Technology, Atlanta, as a Ph.D. student in January 2012. His research interests are in nanoscale biologically-inspired communications and drug delivery systems.

SUMMARY